1-12-1998

An experimental study of micro-end-milling operations

Tug Tacku Arkan
Florida International University

FLORIDA INTERNATIONAL UNIVERSITY

Miami, Florida

AN EXPERIMENTAL STUDY OF MICRO-END-MILLING

OPERATIONS

A thesis submitted in partial satisfaction of the

requirements for the degree of
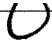
MASTER OF SCIENCE

IN
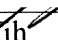
MECHANICAL ENGINEERING

by

Tug Tacku Arkan

1998

To: ___Dean Gordon Hopkins___
      College of Engineering and Design

This thesis, written by Tug Tacku Arkan, and entitled An Experimental Study of Micro-End-Milling Operations, having been approved in respect to style and intellectual content, is referred to you for judgement.

We have read this thesis and recommend that it be approved.

_____
Sabri Tosunoglu

_____
Tachung Yih

_____
Ibrahim Tansel, Major Professor

Date of Defense: January 12, 1998

The thesis of Tug Tacku Arkan is approved.

_____
Dean Gordon Hopkins
College of Engineering and Design

_____
Dr. Richard L. Campbell
Dean of Graduate Studies

Florida International University, 1998

ii

ACKNOWLEDGEMENTS

ABSTRACT OF THE THESIS

AN EXPERIMENTAL STUDY OF MICRO-END-MILLING OPERATIONS

by

Tug Tacku Arkan

Florida International University, 1998

Miami, Florida

Professor Ibrahim Tansel, Major Professor

Cutting tools less than 2mm diameter can be considered as micro-tool. Micro-tools are used in variety of applications where precision and accuracy are indispensable. In micro-machining operations, a small amount of material is removed and very small cutting forces are created. The small cross sectional area of the micro-tools drastically reduces their strength and makes their useful life short and unpredictable; so cutting parameters should be selected carefully to avoid premature tool breakage. The main objective of this study is to develop new techniques to select the optimal cutting conditions with minimum number of experiments and to evaluate the tool wear in machining operations. Several experimental setups were prepared and used to investigate the characteristics of cutting force and AE signals during the micro-end-milling of different materials including steel, aluminum and graphite electrodes. The proposed optimal cutting condition selection method required fewer experiments than conventional approaches and avoided premature tool breakage. The developed tool wear monitoring technique estimated the used tool life with $\pm 10\%$ accuracy from the machining data collected during the end-milling of non-metal materials.

TABLE OF CONTENTS

List of Figures

List of Tables

Chapter I

Introduction

Cutting tool less than 2mm diameter can be considered as micro-tool. Micro-tools are used in variety of applications where precision and accuracy are indispensable. Today many products use complex parts. Even the manufacturers of common consumer products aim to miniaturize their products to increase their profit margin and market share. Micro-tools have been finding many new applications in these market conditions. Conventional cutting tools have been used in metal cutting operations for a longtime and machine operators know their behavior on different workpieces as steel, aluminum, and some non-metals. In addition, databases are available to find the optimum cutting conditions easily. The small cross sectional area of the micro-tools drastically reduces their strength and makes their useful life short and unpredictable. Also very limited machinability data is available on micro-tools.

Due to the facts stated above, the need of on-line or off-line monitoring of micro-tools during micro machining operations is indispensable for better product quality with less work time, less expense. To maximize the productivity and product quality, best cutting conditions have to be selected and used in the micro-machining operations. Different parameters can be monitored during machining operations to obtain the optimum conditions. Cutting forces can be measured during cutting operations and can be used by using various techniques to estimate and prevent premature tool breakage. Tool life (wear) and cutting forces relationships can be analyzed by using acoustic emission (AE) techniques.

In conventional machining operations, machinability of a material is evaluated based on the following three factors:

1. Surface finish and integrity

2. Tool life

3. Force and power requirements

Thus good machinability indicates good surface finish and integrity, long tool life and low force and power requirements. However, in micro machining, the main goal is to avoid premature breakage.

The objectives of this study are the following:

1. To develop a new experimental procedure to select the optimal cutting conditions for machining of different materials including metals (steel, aluminum) and non-metals (electric discharge machining electrodes) experimentally.

2. To investigate the relationship between the wear of carbide tools and cutting force.

3. To evaluate feasibility of computational tools (neural networks), to estimate tool wear from the characteristics of experimental cutting force data.

4. To propose a new method to estimate tool wear in industrial applications. The method is developed to require a low cost hardware, to use a reliable and simple computer program.

Chapter II

Theoretical Background

The modeling end-milling operations, cutting forces, acoustic emission (AE) generation, neural networks (Backpropagation, PNN), wavelet transformations and dynamic response of structures will be briefly introduced in this section.

II.1. Modeling End-Milling Operations

Several researchers [1, 2, 3] have developed deterministic models for the simulation of cutting forces in end milling. An accurate model of cutting forces in milling is indispensable in the machinability analysis and the prediction of tool life. In milling, a cutting edge will create two components of force while cutting. These are called as tangential and radial forces. Tlusty and MacNeil [1], modeled the dynamics of cutting forces in end milling, for a steady state cutting, at a constant depth of cut and width. In this model, the instantaneous cutting force at cutting angle is assumed to be proportional to the chip thickness. The instantaneous tangential cutting force in end milling can be approximated by:

$$F_T = k \, b \, h \qquad\qquad (2.1)$$

Where, b is the axial depth of cut; k is the cutting force coefficient that depends on the material of the workpiece, geometry of the tool and average chip thickness; h is the instantaneous chip thickness at angle ϕ, as shown below:

$$h = S_t \sin \phi \qquad (2.2)$$

where, S_t is the feed rate per tooth.

In this model, the radial component of cutting force is assumed to be 30% of the tangential component:

$$F_R = 0.3\, F_T \qquad (2.3)$$

The total resultant cutting force is assumed to be the equivalent of the sum of the components over the differential rotation angles, $d\phi$.

$$dF_T = K\, S_t \sin \phi \qquad (2.4)$$

$$dF_R = 0.3\, K\, S_t \sin \phi \qquad (2.5)$$

where, dy is the differential cutting edge.

The differential components of the cutting force on two fixed perpendicular directions are:

$$dF_x = -\, dF_T \cos \phi - dF_R \sin \phi \qquad (2.6)$$

$$dF_y = -\, dF_T \sin \phi - dF_R \cos \phi \qquad (2.7)$$

For the case of non-helical teeth, the cutting forces may be represented by:

4

$$F_x = -F_T (\cos\phi + 0.3\sin\phi) \qquad (2.8)$$

$$F_y = -F_T (-\sin\phi + 0.3\cos\phi) \qquad (2.9)$$

where F_t is the tangential force.

Tlusty and Ismail [4] improved this model to study chatter in end milling. This model allowed for tool deflection in both the *x* and *y* directions. The tangential cutting force in equation 2.1 is modified to include the displacement,

$$F_T = K_b (h - Z + Z \min) \qquad (2.10)$$

Where, Z is the displacement of the tool normal to the machined surface. Z_{min} lowest undulation left behind in the preceding cuts at angle, ϕ. The *Fx* and *Fy* components of the cutting force excite vibrations in the *X* and *Y* directions.

Models of cutting forces, which include the influence of cutter offset (run-out) on the cutting force [5, 6] have also been developed. The effects of cutter offset can be included by adding a term when determining the normal *z* displacement, which adjusts for the eccentricity,

$$Z = x\sin\phi + y\cos\phi + t_{ec} \qquad (2.11)$$

5

where t_{ec} adjusts for the eccentricity. For a four flute end mill, the first and third, and the second and fourth flute values of t_{ec} average one. For a six flute end mill, the first and fourth, second and fifth, and third and sixth flute values of t_{ec} average one.

II.2. Acoustic Emission Generation

During the machining operations, a series of spherical elastic stress waves are generated by the rapid release of strain energy within the material. These waves travel until they reach the surface of the material, where they can be detected with piezoelectric transducers in intimate contact with the body and transformed into an electrical signal for processing and analysis purposes. This release of strain energy can be due to a material undergoing deformation, fracture or a combination of both factors.

The sources of acoustic emission during peripheral milling [7], are the following:

1. Plastic deformation in the shear zone near the cutting edges of the cutting teeth.

2. Rubbing between the rake faces of the cutting teeth and chips.

3. Rubbing between the flank faces of the cutting teeth and the workpiece.

4. Rubbing between the flank faces of the end teeth of the cutter and the machined workpiece surface.

6. Chip breakage (less important).

5. Entanglement (less important).

During a cutting operation [8], dislocation in primary shear zone and the sliding friction in the secondary shear zone primarily generate acoustic emission. As the cutting tool wears,

additional frictional action between the tool flank and the workpiece also creates acoustic emission. The portion of AE that is attributed to friction on the wear land becomes more important when flank / workpiece contact area increases as a result of tool wear. Acoustic emission generated from shearing and friction exhibit different signal characteristics since the mechanisms by which AE is produced in these occasions are fundamentally different. As a result, the signal characteristics of AE are expected to change when tool wear-land progresses.

The relationship between the AE signal and tool wear is not as direct or as simple as the relationship between the cutting force and cutting edge condition (tool wear). The major advantage of using AE to monitor tool wear is that the frequency range of the AE signal is much higher than that of the machine vibrations and environmental noises. Therefore, a relatively, uncontaminated signal can be easily obtained by the use of a high-pass filter. AE can be measured by simply mounting a piezoelectric transducer on tool holder. In addition, the characteristics of the AE signal are independent of cutting direction. However, due to its high frequency nature and the sensitivity to micro-structural behavior of material, acoustic emission signals often have to be treated with additional signal processing schemes so that the most useful information can be extracted.

Many studies have been carried out to study the acoustic emission during metal cutting and different ways to process the signals have been experimented. Table 1 illustrates these different approaches.

Table 1. Different approaches in the study of the acoustic emission for Tool Wear Analysis

Document	Process	Signal processing method	Year
▪ Zheng, L., Luo, Z. B., Wu, Y., et al., "Research and Development on Synthetic Cutting Tool Monitoring with AE Signal," Transactions of NAMRI/SME, 1990. [9]	All processes	Signal amplified band-pass filtered between 1000 kHz and 1 MHz. Ring count, envelope, spectral and correlation analyses were used.	1990
▪ Koning, W., Kutzner K., Shehl, U., "Tool Monitoring of Small Drills With Acoustic Emission," International Journal of Machine Tools Manufacture Vol. 32, No. 4, pp. 487-493, Pergamon Press, Great Britain, 1992. [10]	Drilling	Band-pass filtered signal, rectified, and low pass filtered. The original high frequency is converted to low frequency. RMS analyzed	1992
▪ Vajpayee S., Sampath, A., "Acoustic Emission as an Indirect Parameter for Tools Monitoring," Proceedings of Manufacturing International '88, Symposium on Product and Process Design, Vol. 1, Atlanta, Georgia, 1988. [11]	Turning	Transducer with resonance of 200 kHz, signal amplified and filtered at 100kHz high-pass, 2MHz low-pass and a pulse counter. Count and count rate analyzed.	1988
▪ Liu M., Liang, S. Y., "Analytical Modeling of Acoustic Emission for Monitoring of Peripheral Milling Process," International Journal of Machine Tools Manufacture, Vol. 31, No. 4, pp. 589-606, Pergamon Press. 1991. [12]	Peripheral milling	An analytical model relating the acoustic emission energy content to the cutting parameters is developed.	1991

• Liu, M., Liang, S. Y., "Monitoring of Peripheral Milling Using Acoustic Emission," Transactions of NAMRI/SME, 1990. [13]	Peripheral milling	Bridgeport vertical milling machine. A wide band (0.1-1.0 MHz) transducer followed by an amplifier. TMS was analyzed.	1 9 9 0
• Klaiber, J. R., Dornfeld, D. A., Liu, J. J., "Acoustic Emission Feedback for Diamond Turning," Transactions of NAMRI/SME, 1990. [14]	Diamond turning	Signal amplified and sent to RMS voltage filter. RMS analyzed.	1 9 9 0
• Liu, J. J., Dornfeld, D. A., "Monitoring of Micro-machining Process Using Acoustic Emission," Transactions of NAMRI/SME. Vol. XX, 1992. [15]	Micro-machining simulated by end milling with very small feed and high spindle speed	A piezoelectric transducer with resonance frequencies at 125 kHz and 375 kHz was used. The signal was pre-amplified high-pass filtered at 50 kHz, then amplified, stored and finally digitized at 2 MHz sampling rate. Analyzed with power spectrum estimation, zero crossing rate, and kurtosis of the signal.	1 9 9 2
• Diniz, A. E., Liu, J. J., Dornfeld, D. A., "Correlating Tool Life, Tool, Wear and Surface Roughness by Monitoring Acoustic Emission in Finish Turning," Wear No. 152, pp. 395-407, 1992. [16]	Turning (finishing)	Signal pre-amplified, high-passed, amplified, recorded, digitized and band-passed at 50-500 kHz and at 200-300kHz, RMS. Analyzed the frequency spectrum.	1 9 9 2
• Hutton, D. V., "A Non-contact Acoustic Emission Sensing System For Rotating-Cutter Machining Process," Experimental Techniques, Nov/Dec, 1991. [17]	Rotating tools	Proposes a chamber, surrounding the spindle, filled with a liquid, which links the spindle with the acoustic emission sensor	1 9 9 1
• Osuri, R. H., Chatterjee, S., Chandrashekhar, S., "On-Line Condition Monitoring of Tools Wear in End Milling Using Acoustic Emission," International Journal of Research, Vol. 29, No. 7, pp. 1339-1353, 1991. [18]	End Milling	Bridgeport vertical milling machine. The signal was amplified, high passed at 20 kHz and recorded. RMS analyzed.	1 9 9 1

• Rangwala, S., Dornfeld, D., "A Study of Acoustic Emission Generated During Orthogonal Metal Cutting - 1:Energy Analysis," International Journal of Mechanical Science Vol. 33, No. 6 pp. 471-487, Pergamon Press, Great Britain, 1991. [19]	Orthogonal metal cutting	The signal was amplified and recorded. The RMS was analyzed.	1991
• Tansel, I.N., Bao, W.Y., Medardo, E.T., Arkan, T.T, " Detection of Tool Breakage in Micro-End-Milling Operations by Monitoring Acoustic Emission," Technical Conference Paper, NAMRI, SME [28]	End - Milling	The tool breakage mechanism of micro-end mills, wear-induced stress, is explained by evaluating the thrust direction cutting force characteristics.	1997
• Rangwala, S., Dornfeld, D., "A Study of Acoustic Emission Generated During Orthogonal Metal Cutting - 2:Spectral Analysis," International Journal of Mechanical Sciences, Vol. 33, No. 6, pp. 489-499, Great Britain 1991. [20]	Orthogonal cutting	The signal was amplified and recorded, low-pass filtered and sampled at 5 MHz. Was analyzed the RMS distribution in the signal power spectrum.	1991
• Liang, S. Y., Dornfeld, D. A., "Tool Wear Detection Using Time Series Analysis of Acoustic Emission," Journal of Engineering for Industry, Vol. 111, pp. 199-205, August 1989. [21]	Turning	Signal amplified, high-passed at 50 kHz, sent to a RMS meter, modulated to remove the D.C. component and digitized at 5 kHz. AR time-series modeling of the acoustic emission RMS signal has been implemented.	1989
• Carolan, T.A., Hand, D.P., Barton J.S., "Assessment of Tool Wear in Milling Using Acoustic Emission Detected by a Fiber-Optic Interferometer," Journal of Manufacturing Science and Engineering, 1996, Vol. 118, Transaction of the ASME [31]	Milling	It describes the use of a robust fiber optic interferometer for the in-process measurement of AE during face milling of steel to provide tool wear information via analysis of the rms. AE signal	1996

▪ Principe, J.C., Yoon, T., "A New Algorithm for the Detection of Tool Breakage in Milling," Int. Journal of Machine Tools & Manufacturing, Vol. 31 No. 4 pp. 443-454, Great Britain, 1991 [32]	Milling	A novel signal processing system is presented for the detection of tool breakage using the displacement signal (RORPA). The algorithm extracts information from consecutive revolutions to decrease dependencies on runout conditions and ideal noise by creating a more robust signal. 1991
▪ Emel, E., Kannatey-Asibu, E. Jr., "Acoustic Emission and Sensor Fusion for Monitoring the Cutting Process," International Journal of Mechanical Sciences, Vol. 31, No. 11/12, pp. 795-809, Great Britain, 1989. [22]	Turning	Three force components measured with a dynamometer, amplified, digitized at 2kHz and low-pass filtered at 1kHz. The AE and the force signal are used to monitor the cutting process. 1989

II.3. Neural Networks

A directed graph is a geometrical object consisting of a set of points (called nodes or neurons) along with a set of directed line segments (called links) between them. A neural network is a parallel-distributed information processing structure in the form of a directed graph, with the following sub-definitions and restrictions: [33]

1. The nodes of the graph are called processing elements.

2. The links of the graph are called connections. Each connection functions as an instantaneous unidirectional signal-conduction path.

3. Each processing element can receive any number of incoming connections (also called input connections).

4. Each processing element can have any number of outgoing connections, but the signal in all of these must be the same. In effect, each processing element has a single output connection that can branch of fan out into copies to form multiple output connections, each of which carries the same identical signal (the processing element output signal).

5. Processing elements can have local memory.

6. Each processing element possesses a transfer function which can use (and alter) local memory, can use input signals, and which produces the processing element's output signal. The only inputs that allowed to the transfer function are the values stored in the processing element's local memory and the current values of the input signals in the connections received by the processing element. The only outputs allowed from the transfer function are values to be

stored in the processing element's local memory and the processing element's output.

Transfer functions can operate continuously or episodically. If they operate episodically, there must be an input called "activate" that causes the processing element's transfer function to operate on the current input signals and local memory values and to produce an updated output signal (and possibly modify local memory values). Continuous processing elements are always operating. The "activate" input arrives via a connection from a scheduling processing element that is a part of the network.

7. Input signals to a neural network from outside the network arrive via connections, which originate the outside world. Outputs from the network to the outside world are connections that leave the network.

Neural networks can be classified in information domain as:

1. Time independent information (mapping problem)

2. Time dependent information (prediction problem)

3. Self learning information (induction and deduction problem)

4. Others (creation problem)

In this section, Backpropagation (BP) and Probabilistic Neural Networks (PNN) will be introduced.

II.3.1. Backpropagation Neural Networks (BP)

The backpropagation is the well known and the most commonly used neural network. Figure 1 presents the structure of BP. Each link between the neurons represents a weight and a simple (most commonly sigmoid) function. The user selects the number of hidden layers and hidden neurons. BP can be used for mapping or characterization. The backward propagation neural network is a kind of construction model. Construction methods base on the biology theory. It tries to build a physical brain model to imitate the think or behavior of a human being. During the training process, the weights of neurons are adjusted. At the beginning weights are selected randomly.

In this study, "Neurashell" is used. The network has two drawbacks. First the user should have knowledge and experience to select the number of hidden layers and number of neurons in each layer. Second, training of the original algorithm is extremely slow. BP is a very effective method when the characteristics of large number of training data are represented with a small network.
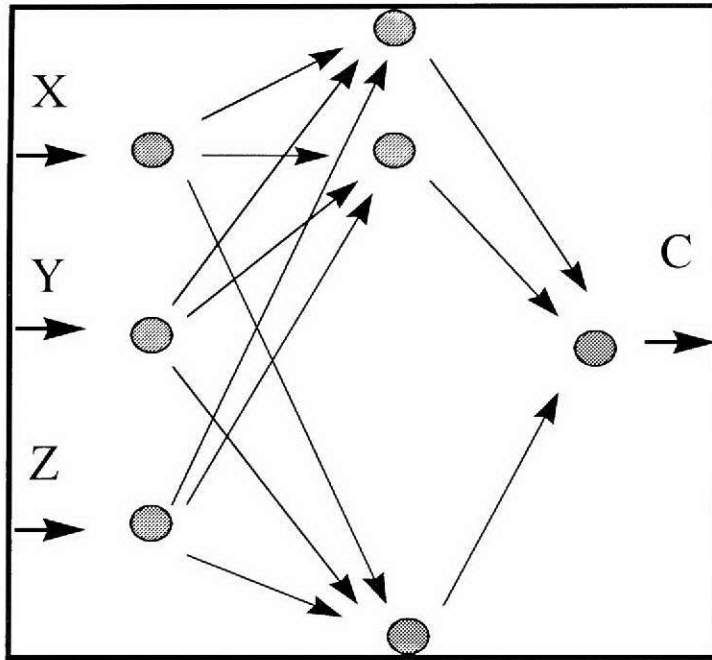
Figure 1. Backpropagation type of neural network

II.3.2. Probabilistic Neural Networks (PNN)

Probabilistic neural networks are based on the distribution theory and Bayes' theorem. It is a statistical model and it assumes that general information is obeyed a normal distribution and uses the Bayes' theorem to assume the prior probabilities, PNN optimizes the distribution model factors (mean and standard deviation) by using judge the post probabilities. There are two problems in this kind of model. First one is the time independent information problem and the other is normal distribution. It is difficult process in small sample information cases and non-normal distribution information cases. Figure 2 represents the structure of a PNN. For each training case, one neuron is assigned to the pattern layer. Pattern layer neurons create an output according to the distance between the input and the training case they represent. There is one summation neuron

for each class. In this type of neural networks, training is very fast compared to BP, however, the size of the network could be too large, if there are too many training cases. In PNN, for each training case, one neuron is assigned to the pattern layer. Pattern layer neurons create an output according to the distance between the input and the training case they represent. There is one summation neuron for each class.

There are two kinds of PNN used in this study PNN Basic and PNN SEPVAR [25]. The PNN Basic is the simplest probabilistic neural network. One sigma is used to cover all variables. Training is the fastest of all PNN models, but quality is usually lowest. The PNN Sepvar uses a separate sigma for each variable. During the training phase, this model is identical to the Basic (single sigma model).
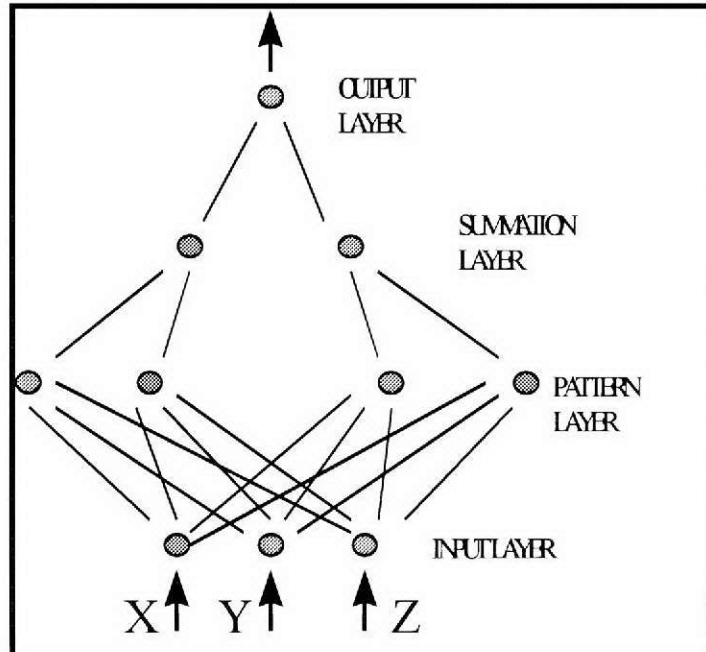
Figure 2. PNN type of neural network

II.4. Wavelet Transformations

The wavelet transformation analysis is based on particular curves called wavelets. In the recent years, new families of orthonormal basis functions have been discovered that lead to transformations, which can translate a time-domain function into a representation that is localized not only in frequency, but in time as well (39).

There are two basic functions that form the core of the wavelet transformation. The scaling function $\Phi(t)$, (also called dilation function or fundamental recursion) and the basic (or primary wavelet) $\Psi_{i,j}(t)$ shown below:

$$\Phi(t) = \sum_{j \in Z} a_j \Phi(2t - j) \tag{2.12}$$

$$\Psi_{i,j}(t) = \sum_{j \in Z} (-1^j) a_{j+1} \Phi(2t + j) \tag{2.13}$$

Where the parameter j controls the compression-expansion in time scale and amplitude, and k controls the translation of the function in time. The set of fundamental functions defined by $\Phi(t)$ and $\Psi_{i,j}(t)$ is a system of scaled and translated wavelets.

This orthonormal basis of functions, called wavelets, can be combined to represent any given signal $f(t)$ by translating and scaling a custom designed mother wave (40, 41). The original $f(t)$ function can be calculated according to the following expression:

$$f(t) = \sum_{n=-\infty}^{\infty} c(n) \Phi_n(t) + \sum_{i=0}^{\infty} \sum_{j=-\infty}^{\infty} d(i,j) \Psi_{i,j}(t) \tag{2.14}$$

17

Where the coefficients $c(n)$ and $d(i,j)$ can be calculated by using the following expressions

$$c(n) = \int f(t)\Phi_n(t)dt$$
$$d(i,j) = \int f(t)\Psi_{ij}(t)dt$$

(2.15)

Here the $c(n)$ are the approximation coefficients. They represent the approximation of the original signal f(t), with a resolution of one point per every 2^n points of the original signal. The $d(i,j)$ coefficients are called the detail coefficients of the wavelet transform. They represent details of the original signal at different levels of resolution.

It can be said that, the wavelet transformation is the process of determining the values of the $c(n)$ and $d(i,j)$ coefficients, for a given $f(t)$ and a chosen wavelet system (39) 1992).

II.5. Static and Dynamic Characteristics of Micro-Tools

The relationship between the cutting force and tool displacement can be represented with a simple coefficient (static) or a transfer function (dynamic) depending on the considered frequency range. This relationship is important to evaluate the accuracy of cutting and tool breakage probability. The static relationship can be obtained easily by using least squares method. Frequency and time-domain techniques can be used effectively to obtain the dynamic characteristics. Frequency-domain techniques may perfect their frequency response estimation by averaging the spectrums of incoming data many times if the data set is long enough (5,000 or more). Frequency-domain identification techniques have been widely used today for the experimental investigation of the dynamic characteristics of planes, buildings, machine tools, and many other systems thanks to dedicated Fast Fourier Transformation (FFT) hardware of the real-time analyzers. However, the resolution and accuracy of frequency-domain methods are limited if the data sequence is short (less than 500 points). For short data sequences time-domain methods work effectively without lowering resolution, having leakage-related errors, and having noise-related fluctuations. It is possible to estimate the dynamic characteristics from the estimated parameters of these methods. Autoregressive Vector (ARV) models have been used on simulated and experimental data.

The Recursive Multichannel Maximum Entropy Method (RMMEM) is a fast ARV model estimation technique and has been used for the estimation of the frequency response of the metal cutting process, structural dynamics, and unified transfer functions (which represent both cutting and structural dynamics) of machining operations. The RMMEM starts from a first-order model and estimates the parameters of all the ARV models up to

desired highest order. The main advantages of the RMMEM are its computational speed and acceptable accuracy (less than 10% frequency response estimation error for a 3-degrees-of-freedom [DOF] system).

The Autoregressive model of a one-output system is written as:

$$y(i) = \sum_{k=1}^{n} \phi_k \, y(i\text{-}k) \,, \tag{2.16}$$

where the y(i) is the output of a system, and n is the order of the Autoregressive (AR) model. Burg has proposed the Maximum Entropy Method (MEM) for the estimation of the ϕ_k AR parameters by minimizing the forward and backward prediction errors.

For multi-input systems, Autoregressive Vector (ARV) models can be used to identify multi- input and multi-output systems. The ARV model of a system with one output and several inputs can be written as:

$$\underline{u(i)} = \sum_{k=1}^{n} \underline{\phi_k} \, \underline{u(i\text{-}k)} \,, \tag{2.17}$$

where,

$\underline{u(i)} = [y(i), x_1(i), x_2(i), \ldots\ldots x_m(i)]^T$

$\underline{\phi_k}$: parameters, (m+1) * (m+1) matrix

$y(i)$: output

$x_1(i), x_2(i), \ldots\ldots x_m(i)$: 1st, 2nd ... mth inputs

m : number of inputs

n : order of the model

Or for a one-input/one-output system, the same model can be written as:

$$\begin{vmatrix} y(i) \\ x_1(i) \end{vmatrix} = \sum_{k=1}^{n} \begin{vmatrix} \phi_{k11} & \phi_{k12} \\ \phi_{k21} & \phi_{k22} \end{vmatrix} \begin{vmatrix} y(i-k) \\ x_1(i-k) \end{vmatrix} \tag{2.18}$$

If the input $[x_1(i)]$ and the output $[y(i)]$ of a system are known, the ϕ_k parameter matrices can be estimated for various approaches.

The RMMEM was used to obtain the frequency response (dynamic behavior) of micro-tools in this study.

II.6. On-line Monitoring of Tool Condition during Cutting Operations

Tool condition monitoring is based on tool wear measuring during cutting operation. Tool wear measuring techniques fall into two categories: direct and indirect. The direct method which is also called off-line monitoring involves optical measurement of wear, such as by periodically observing changes in tool profile. This is the most common and reliable technique and is done using a microscope. This procedure, however, requires that cutting operation be stopped which is not suitable for industrial applications. Indirect methods, which are also called on-line methods, to measure the wear involve the correlation of wear with process variables such as forces, AE, power, temperature rise, surface finish, and vibrations. Since the direct observation methods interrupt the machining operation, increase the cost; implementing on-line methods for

21

monitoring the tool wear, is more attractive. [37]. Table 2 listed below summarizes the general techniques used for tool condition monitoring for machining operations.

II.6.1. Wear – Cutting Force Relationship in Micro-Machining Operations

[Tool Breakage Mechanism and Wear Induced Stress (WIS) Relation]

Conventional tools wear out gradually and the quality of surface finish deteriorates. It is beneficial to estimate wear and to change these tools before the surface quality and accuracy become unacceptable. On the other hand, the life of micro-tools is very short and unpredictable. Touching them with a prop similar to conventional tool inspection methods cannot be used to inspect the condition of these tiny tools. In previous studies, chip clogging was observed as the main cause of tool breakage in micro-drilling operations for some materials [36]. Tool breakage mechanism can be investigated during machining of different workpiece materials by evaluating the cutting force data.

Various changes occur on cutting tool, while they are used for machining operations. Some of these changes are loss of tool material, deposition of small workpiece particles on tool surfaces and change of tool geometry with deflection. Microscopic damages at the cutting edges, gradually developing dullness, filling of the empty spaces around the cutting edges with deposition of small particles can be also be considered as wear. The relation between these changes (wear) and the related stress variation at the tool shaft was called Wear Induced Stress (WIS). The WIS causes tool failure as a result of excessive stress beyond the strength of shaft or fatigue depending on the magnitude of the cutting force.

If a chip clogging occurs, cutting forces and stresses increase beyond the endurance limit of the tool and breakage will occur in a few rotations. In such a case, a sharp increase is expected at the cutting force. Tool wear does not have any influence on the breakage mechanism. Breakage is very unpredictable and fast. It is almost impossible to predict chip clogging ahead of time.

WIS causes fatigue-related breakage if the cutting force and stress (at the tool shaft) increase for a while as a result of tool wear, but they stay at a constant level. The stress is below the endurance limit of the shaft, but it is above the normal level. The tool will not be broken immediately. It will be deflected in the opposite direction to the feed while it is rotating. This means that the stress and strain distribution will be periodically change at the tool shaft and create fatigue. The increase of cutting force in the feed direction beyond the normal force range will indicate the existence of WIS. The tool will eventually break with fatigue.

The breakage happens very quickly if the wear related problems are extensive and the cutting force continuously increases beyond the strength of the tool. For example, if the cutting edges of the tool are partially damaged or deposition of workpiece particles filled the tiny groves (or build-up edge is created), metal removal rate decreases. In this case, the cutting edges cannot remove enough material to open satisfactory space for the central section (shaft) of the tool. The workpiece starts to push the shaft of the tool against the workpiece and it deflects. The workpiece will push the tool a little more at each rotation and a linear increase is expected at the absolute value of the static part of the feed direction force until the tool breaks. The main reason of breakage in this case is the excessive stress beyond the endurance limit of the tool. [26, 27, 28, 29]

Table 2. Tool wear-sensing methods

	Procedure	Measurement	Transducer
Direct	Optical [7, 32]	Shape or position of cutting edge	TV camera, optical transducer
	Wear particles and radioactivity	Particle size and concentration	Spectrophotometer, scintillator
	Tool/work junction resistance	Changes of junction resistance	Voltmeter
	Workpiece size	Dimension of workpiece	Micrometer, optical, pneumatic, ultrasonic, electromagnetic transducers
	Tool/work distance	Distance of workpiece and tool or tool holder	Micrometer, pneumatic gauge, displacement transducer
Indirect	Cutting force [1, 6]	Changes of cutting force	Dynamometer, strain gauges
	Acoustic emission [20]	Stress wave energy	AE transducer
	Sound	Acoustic waves	Microphone
	Light reflection	Reflection by cutting edge	Phototransistor
	Vibration [34]	Vibration of tools and/or tool posts	Accelerometer
	Temperature [35]	Variation of cutting temperature on tool	Thermocouple, pyrometer
	Power input [36]	Power or current consumption of spindle or feed motor	Ampere meter, dynamometer
	Roughness of machined surface	Changes in surface roughness of workpiece	Mechanical stylus, optical transducer

Chapter III

Selection of Cutting Conditions and Monitoring of Tool Wear for

Industrial Applications

In this chapter, a new machinability test and wear estimation methods are proposed for micro-tools. This new analysis technique requires less experiment and it is accurate.

III.1. A New Method for Machinability Analysis

In conventional milling operations, the main goal is to reduce the cost, to improve the quality and to increase the productivity. Various databases, machinability handbooks and experienced operators are available to select optimal tool conditions in conventional cutting operations with bigger then ¼ inch diameter tools. In the case of micro machining, the main goal is to prevent the premature tool breakage. The life of micro tools is very unpredictable. Since the machinability handbooks are prepared with other goals, they cannot be used directly for micro-machining applications.

A new method is proposed to select optimal conditions to machine graphite electrodes used in electric discharge machining, special injection molding steel and aluminum workpieces, with High Speed Steel (HSS) and Carbide cutting tools from 0.020 – 0.0625 inches diameter. The architecture and process flow diagram of the proposed method is presented in Figure 3 and 4. Experiments were repeated until the most aggressive cutting conditions, which have static cutting force below the critical values observed with static test. Then tool life is evaluated with a new micro-tool.
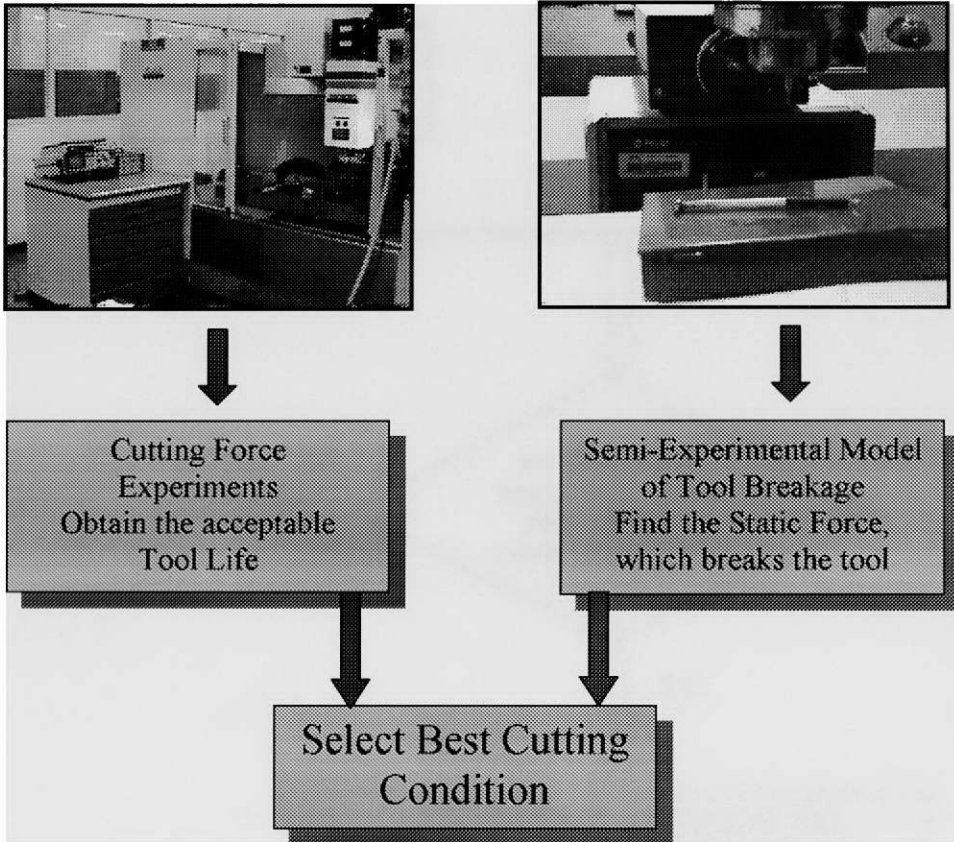
Figure 3. Proposed Machinability Method

Figure 4. Flow Diagram of the New Machinability Method

SELECT MORE
SEVERE CUTTING
CONDITIONS

SELECT LESS
SEVERE CUTTING
CONDITIONS

STATIC TEST
FIND THE BENDING
FORCE WHICH BREAKS
THE TOOL

PERFORM EXPERIMENT
MEASURE CUTTING
FORCE

NO

EVALUATE IF
TOOL MAY HAVE
PREMATURE
TOOL BREAKAGE

YES

PERFORM EXPERIMENT AT THE
SELECTED CUTTING CONDITION UNTIL
TOOL IS BROKEN

TOOL LIFE
ACCEPTIBLE

YES

NO

STOP
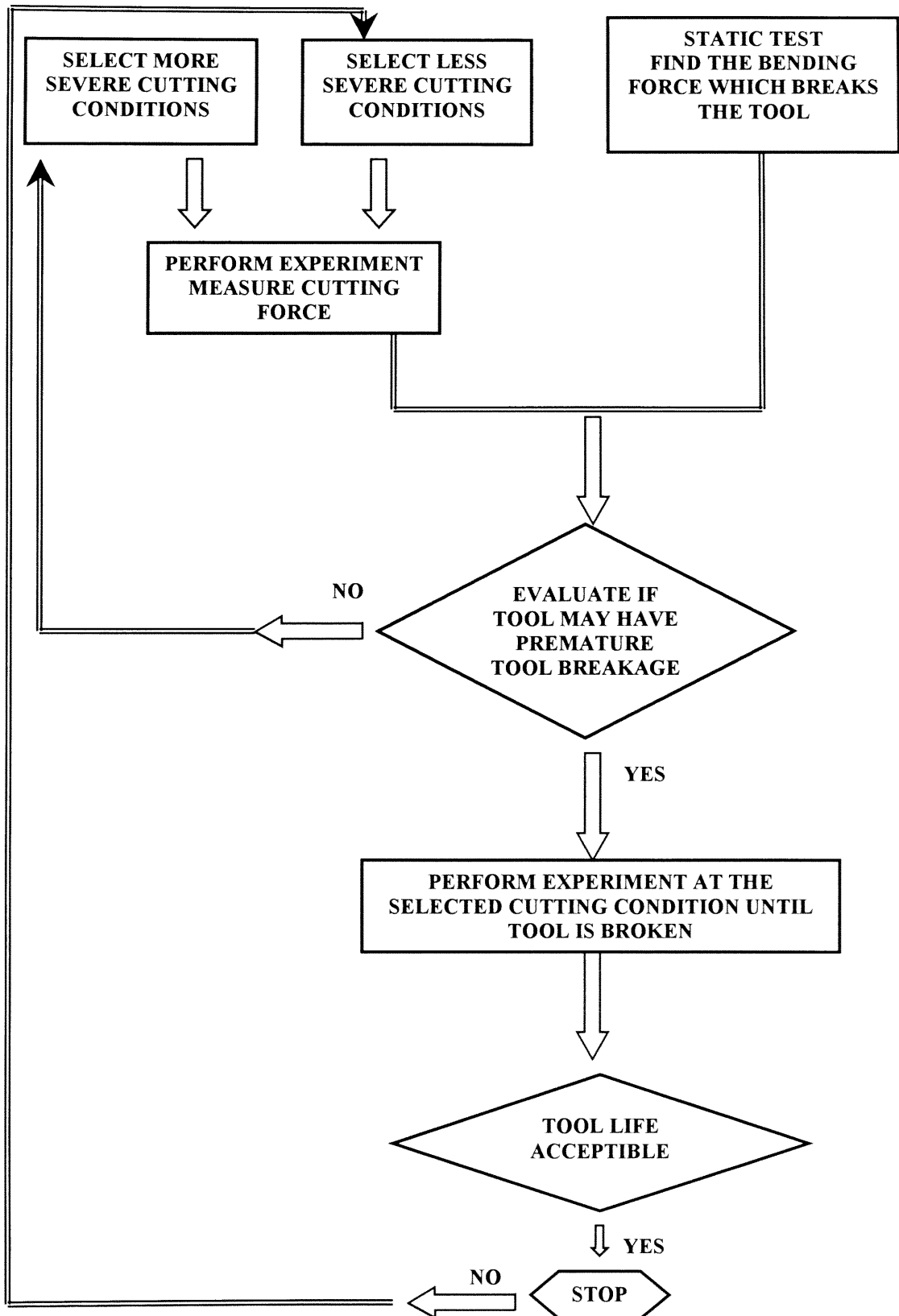
III.2. Studied Static and Dynamic Behaviors of Micro-Tools

The new machinability method required the testing of the static maximum allowable bending force. For this reasons a series of experiments were performed. HSS and Carbide end-mills were deflected with a bending force to obtain the stiffness of the tools. All workpiece–tools combinations were tested to evaluate the effect of workpiece hardness on tool deflection. High-Speed Steel and Carbide tools have very different material proprieties and stiffness. The main goal of the static test realized was to obtain the allowable maximum bending force, which can be applied to the tool.

A series of impact tests also were conducted to study the dynamic behavior of the tools. The goal was to find the natural frequency of the micro-tools. The results obtained from the static and dynamic behavior of the tools were used for the developed new machinability method. Static and dynamic experiments were performed on a Bridgeport Milling Machine. Tool was not rotating in these experiments. Figure 5 presents the experimental setup.
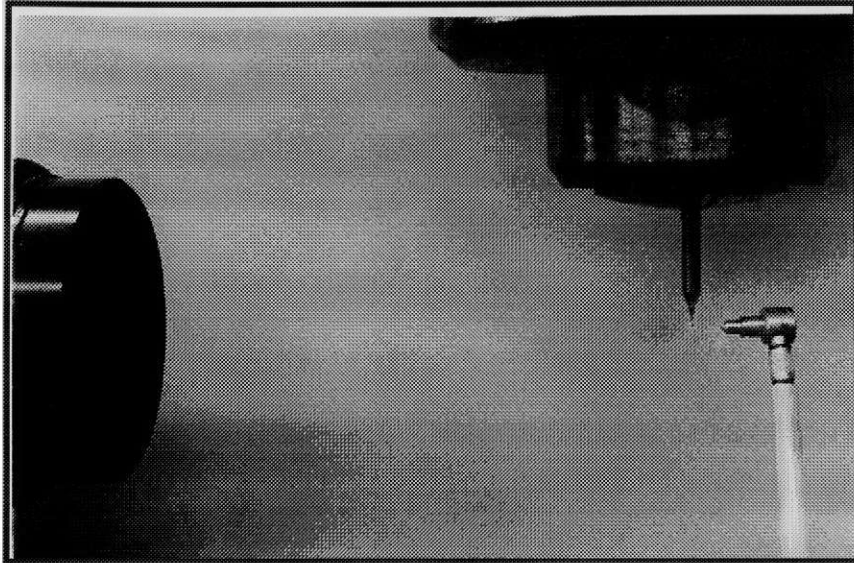
Figure 5. Laser Vibrometer and the Impact Hammer during the Dynamic Behavior
Study Experiment

III.3. Development of an Estimation Method for Tool Wear Monitoring [Estimation of Wear by Using Neural Networks (N^2PTI)]

Micro-end mills with less than 2-mm diameter have a short and unpredictable tool life [30]. However, it is possible to use these tools for hours when non-metal materials such as plastics and electrodes are machined by using conservative cutting conditions. After a long machining operation, micro-tools wear out, lose material, and their dimensions change. The quality of the surface finish deteriorates, burr is created, and the dimensional accuracy of the manufactured parts is ruined when the tool is very badly worn out. The Neural Network based Periodic Tool Inspector (N^2PTI) is introduced in this section. The N^2PTI requires the tool to cut a test piece, which is attached to a

dynamometer. The variation of the feed and thrust direction cutting force is measured while the test piece is cut. Neural networks estimate the tool's wear from these two inputs. (Figure 6) The performances of three different networks are discussed in this section.

The N^2PTI was developed with the following goals:

- To have the cutting force signal of micro machining with an acceptable S/N ratio. Typically the cutting forces are very small when the electrodes and plastic materials are cut. The inertia forces are almost equal or larger than the cutting forces. The Signal-to-Noise (S/N) ratio of the cutting force readings is very low. The material of the test piece and the cutting conditions can be selected to have the cutting forces at least two or three times larger than the inertia forces.

- To have a low cost, reliable system convenient for industrial applications: The characteristics of the cutting forces continuously change during the machining of a workpiece if the metal removal rate and machining parameters change. The N^2PTI uses a test piece and cuts the material exactly at the same cutting conditions. In this test, the characteristics of the cutting forces are only affected by the tool wear. The encoding and interpretation of the signal becomes much simpler and the cost of the system is reduced.

```
┌─────────────────┐                ┌─────────────────┐          ┌──────────┐
│ Thrust Direction│                │    NN Model     │          │  Tool    │
│  Cutting Force  │  ──────▶        │ Backpropagation │ ──────▶  │  Life    │
└─────────────────┘                │      PNN        │          └──────────┘
┌─────────────────┐                │                 │
│  Feed Direction │  ──────▶       └─────────────────┘
│  Cutting Force  │
└─────────────────┘
```
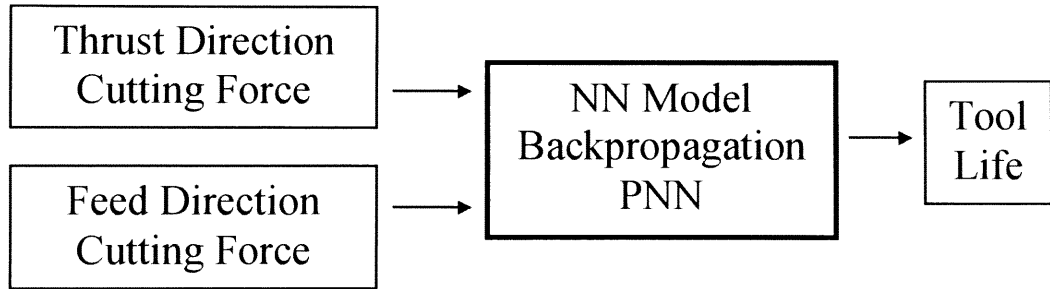
Figure 6.   Neural Network Training Model

The operation of the N^2PTI is outlined in Figure 7. The N^2PTI evaluates the tool wear with periodic intervals. The workpiece is attached to the table of the milling machine. A test piece is installed on a dynamometer, which is attached to the table next to workpiece. The user prepares the part program to cut the workpiece and periodically move the tool to the test piece to cut a slot on it. The feed and thrust direction cutting forces are measured while the test piece is cut. The difference of the measured average maximum and minimum cutting forces are given to the neural network. In the rest of the study this difference will be called variation. The neural network is run first during the training, and later in the testing mode. During the training mode two inputs (feed and thrust direction cutting force variation) and one output (the tool life) are given to the network. The network establishes a model between the inputs and the outputs. In the testing mode only

two inputs are given to the network. The network estimates the tool life by inspecting the variation of the feed and thrust direction cutting force variations.
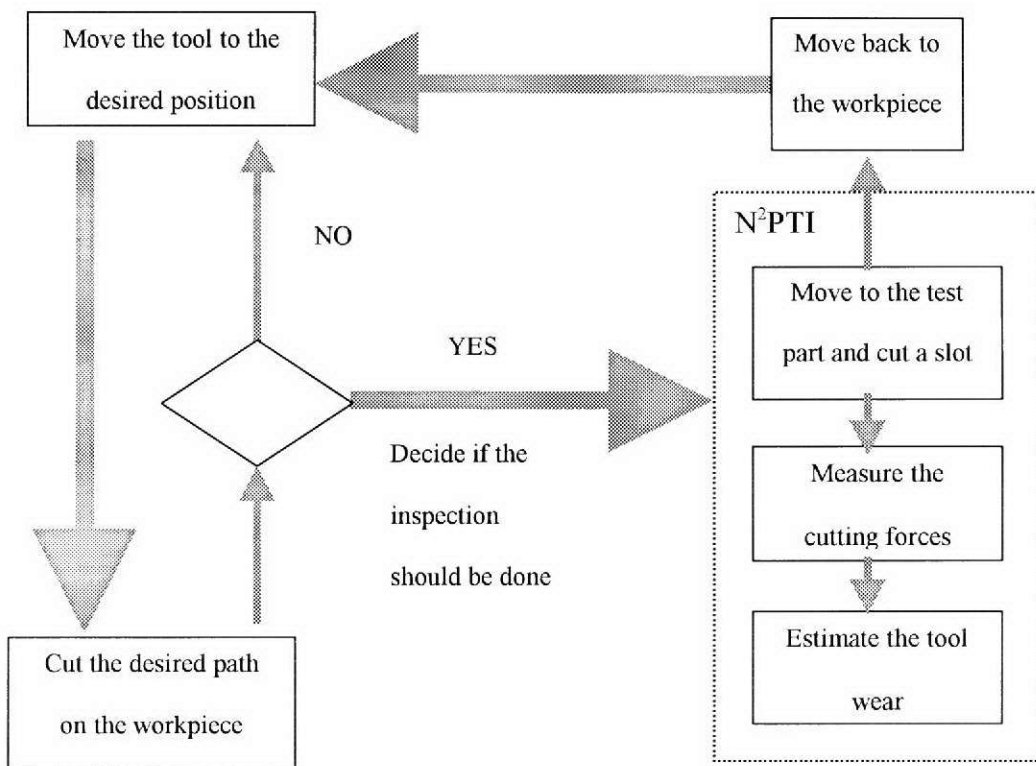
Figure 7. Operation of N^2PTI

III.4. Improvement of the Neural Network based Periodic Tool Inspector

Neural Network Based Tool Inspector was designed to work with the amplitude of the cutting forces. The network was trained with the amplitude of the cutting forces in *X (Thrust)* and *Y (Feed)* directions. The N^2PTI could work for only at the specific spindle speed, feed rate and depth of cut. To improve the capability of the N^2PTI, a new approach is proposed. The new approach estimates the tool wear by evaluating the relationship between the *X* and *Y* direction cutting forces and eliminates the dependence of the method to constant depth of cut. The new procedure can work with two different techniques to select the parameters for the neural network training:

Segmental Averaging:

The new procedure first finds the maximum cutting force for each period which corresponds to one revolution. The data is averaged for a certain number of points (up to the spindle speed and sampling frequency of the digital oscilloscope) between the maximum value of the first period and the one in the second period. After the averaging, 10 local parameters are obtained to represent the cutting forces in each direction. The parameters are normalized, by dividing them by the maximum parameter. After normalization, all the parameters are between 1 and 0.

Wavelet Transformation:

To obtain the local parameters that will represent the data profile better, wavelet transformation is also used. Data is given to wavelet and 64 coefficients are chosen for transformation. Data can only be given as number of 2^n to wavelet. 2048 and 1024 data points are used for the analysis. After wavelet transformation, 64 coefficients, which represent best the original signal, are obtained and the inverse wavelet transformation is

taken. Cutting force data is filtered of noise after wavelet transformation. One period is presented with 8 local parameters. The parameters are normalized by dividing them by the maximum parameter.

The parameters obtained with wavelet transformation are more precise than local avearging to represent the original collected cutting force data

Chapter IV

Experimental Set-Up and Procedures

IV.1. Cutting force - AE Data Collection for Machinability and Tool Wear Analysis

The experiments were conducted on a Fadal 3-axis CNC Machining Center. (Figure 8) This milling machine had a maximum 50,000-rpm spindle speed. The micro-tools used during the work had 1/16, 1/32 and 0.020 inches diameter. High Speed Steel (HSS) and Carbide tools were used. Three different workpiece materials were cut:

1.   Graphite Electrodes used in electric discharge machining (POCO-3, POCOEDMC-3)

2.   Aluminum

3.   Steel (NAK55 molding steel)

The tool path generation code was generated by using SmartCAM. (Production Milling Version10)

First phase of the experiments was the machinability analysis of the workpiece materials with the developed machinability test technique. Optimal cutting conditions for each tool-workpiece combination were selected with the machinability study. Second phase of the experiments was the tool wear monitoring, This phase was conducted on the specific workpieces, which were found abrasive by the first phase or reported by the users.
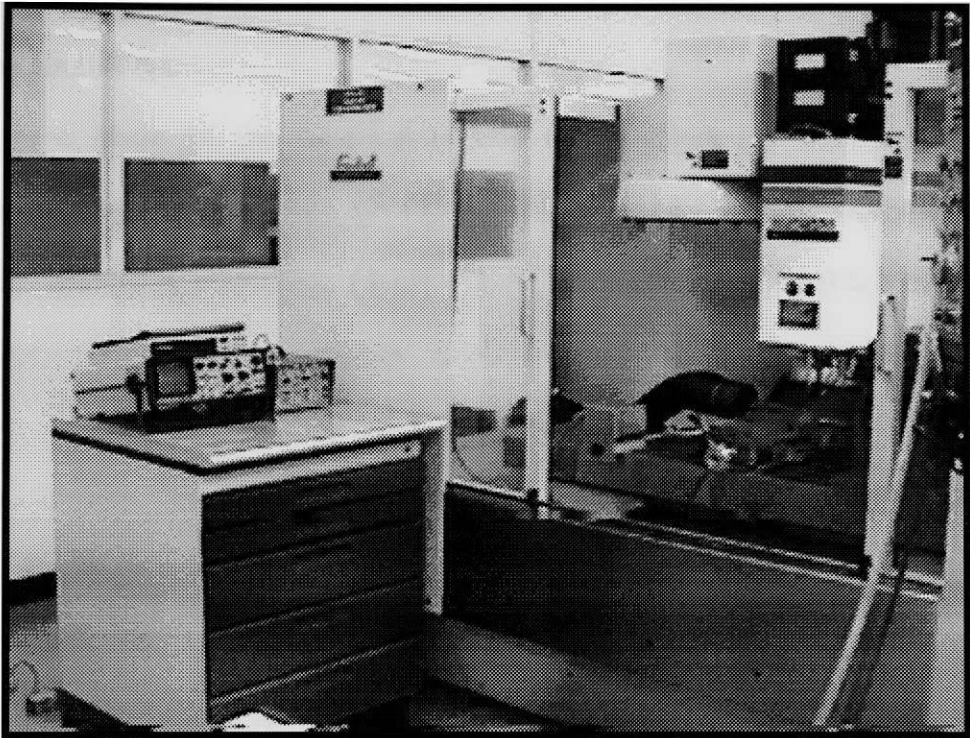
Figure 8. Experimental Setup

Cutting force data was collected with a Kistler 9257B dynamometer and Kistler three channel charge amplifier. Real time cutting force signal was digitized and recorded with a Nicolet Integra model four channel 1MS/s 12-bit digitizer and a Nicolet 310 two channels oscilloscope. Low Frequency Acoustic emission signal was collected with an AE sensor attached to the dynamometer and recorded with the same oscilloscope.

The experimental setups and procedures followed for 3 different workpiece materials are presented in the following sections:

Graphite Electrodes (POCO-3, POCOEDMC-3):

- **Machinability:**

First phase of the experiments was the machinability analysis of copper implemented electrode graphite (POCO-3). This electrode is used widely in electric discharge machining operations. Electric Discharge Machining (EDM) is a process that utilizes electrical discharges or sparks, to machine any electrically conductive workpiece material, including carbide, high alloy steels and hardened metals of many types. So POCO-3 is very suitable and highly desirable electrode graphite for EDM. During electric discharge machining very high voltages are created between the workpiece and the electrode itself. The electrode is moved toward the workpiece within an ionizing fluid allowing a discharge to occur when the gap is sufficiently small. The discharge, with the aid of dielectric fluid, melts and removes metal from the workpiece. During each energy discharge stock is removed from the end and sides of the electrode as well as from the workpiece. Under normal operating conditions the stock removed from the workpiece exceeds that removed from the electrode, but the ratio of wear is different for each material. By knowing the wear ratios, it is possible to manufacture electrodes to the exact size and quantity required for a particular job. Preparation of electrodes for EDM is a very time consuming and difficult machining process due to the complexity of molds and required precision.

POCO-3 is very abrasive and very conductive copper implemented carbon graphite. The machinability analysis of POCO-3 was conducted with HSS end-mills with 0.0625 and 0.020 inch diameter. The workpiece (3 x 4 x 1 inches) dimensions was clamped on the dynamometer. The dynamometer was hold by a vise that is bolted on the

linear table of the milling machine. Dynamometer was connected to the charge amplifier, which amplifies the cutting force signal. BNC cables connected the amplifier to digital oscilloscope. Thrust (X) and feed (Y) direction forces were recorded. Climb milling operation was performed. (Figure 9) 50 % overlapping was used in face milling of the graphite. Test conditions were listed in Table 3. Optimal cutting conditions were found after a series of experiments and used it the rest of the study.

- **Tool Wear:**

    Second phase of the experiments with electrode was conducted on POCO EDMC-3. Since POCO EDMC-3 is much more abrasive than POCO-3, it was used for wear analysis.
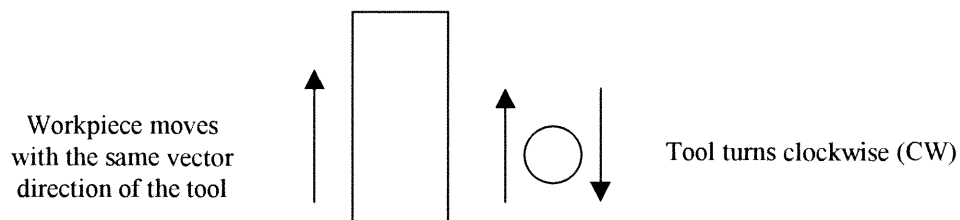
Figure 9. Climb Milling

Table 3. Test Conditions for POCO-3 Machinability

Tool type	HSS 2 Flutes End-Mill	HSS 2 Flutes End-Mill
Tool diameter	0.0625 inch	0.020 inch
Spindle speed	15,000 rpm	15,000 rpm
Feed rate	30, 65, 100 ipm	20, 70, 120 ipm
Depth of cut	0.0625, 0.1, 0.15 inch	0.01, 0.03, 0.05 inch
Workpiece	POCO – 3	POCO – 3

The main purpose of this second phase work was to measure the tool wear while POCO EDMC-3 was machined. The graphite workpiece was climb milled with certain amount of passes on the face of the POCO EDMC-3 and then a slot was cut on the aluminum workpiece to record the cutting force of the tool. This process was repeated periodically until the tool got worn out. The overlapping on the graphite machining was 50 %. 0.0625 and 0.030 inches diameter Carbide two flute end-mills were used. The experiment was done with a brand new tool. Different cutting parameters were used on the abrasive POCO EDMC-3 and aluminum test piece. The dimensions of the POCO EDMC-3 workpiece was (3.75 x 8 x 1). The dimensions of the aluminum test piece was (0.5 x 4 x 0.2). The experimental setup is presented in Figure 10. Numerical control tool path generation of the experiment for the CNC machining center was prepared with SmartCAM (Production Milling Version 10). The cutting parameters were listed for two different diameters sized carbide end-mill in Table 4.

Table 4. Test Conditions in POCO EDMC-3 - Tool Wear Experiments

Tool type	Carbide 2 Flutes End-Mill	Carbide 2 Flutes End-Mill
Tool diameter	0.0625 inch	0.030 inch
Spindle speed	15,000 rpm	15,000 rpm
Feed rate	5 ipm (electrode) 2.5 ipm (Aluminum)	5, 7 ipm (Electrode) 1.25, 2.5 (Aluminum)
Depth of cut	0.015 inch (Both same)	0.015 (Electrode) 0.0075 (Aluminum)
Workpiece	POCO EDMC – 3 Aluminum	POCO EDMC – 3 Aluminum
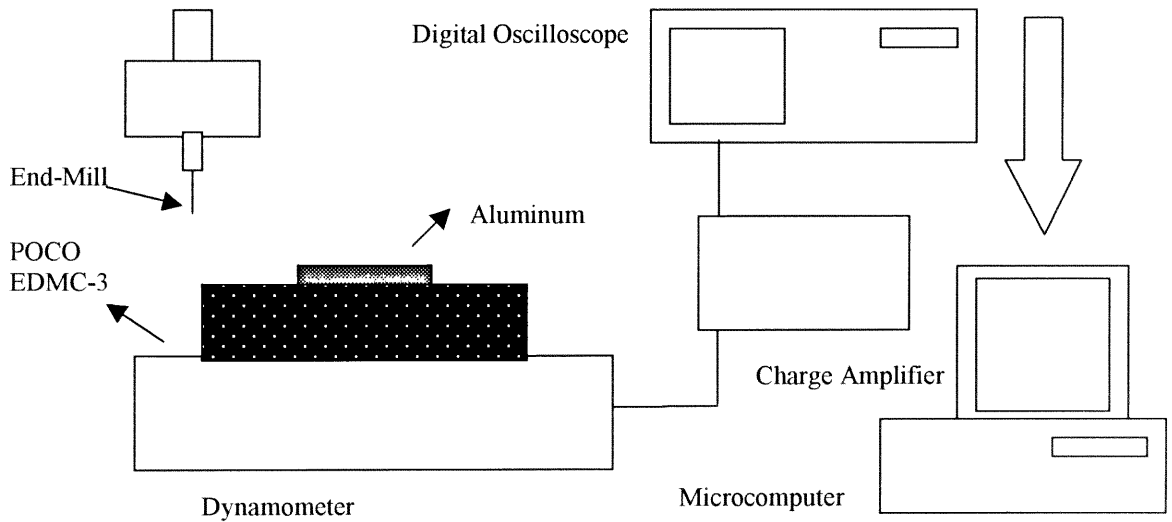
Figure 10.   The diagram of the experimental set-up for Tool Wear on POCO EDMC-3

Aluminum:

The aluminum workpiece machinability and tool wear experiments were realized within the same data collecting instruments but with different cutting tools and cutting parameters. Cutting force data on aluminum workpiece was larger than the electrode graphite and easier to monitor. For the first stage on these experiments, different cutting conditions were chosen and applied within the face milling of aluminum workpiece. Optimal cutting conditions were obtained and several experiments were repeated to analyze the machinability of aluminum with carbide 0.0625 and 0.03125 inches diameter two flute micro-end-mills. The workpiece dimensions were (3 x 4 x 1 inches). The tests were performed, by using 50 % overlapping end milling. Climb milling was used. The cutting parameters used in the experiments for machinability of the aluminum workpiece is presented in Table 5.

Table 5. Test Conditions in Aluminum Machinability Experiments

Tool type	Carbide 2 Flutes End-Mill	Carbide 2 Flutes End-Mill
Tool diameter	0.0625 inch	0.03125 inch
Spindle speed	15,000-32,000-50,00 rpm	15,000-32,000-50,00 rpm
Feed rate	15, 22.5, 30, 32, 48, 50, 64, 75, 100 ipm	9, 18, 27, 30, 60, 90 ipm
Depth of cut	0.015, 0.020, 0.030 inch	0.015, 0.020, 0.030 inch
Workpiece	Aluminum	Aluminum

Steel (NAK 55):

NAK 55 is specially developed with variety of heat treatment (age hardened, not quenched and tempered) techniques for injection molding processes. It has an excellent uniformity of hardness throughout even heavy sections. Internal stresses are minimized. The chemistry of NAK 55 was specially formulated to produce the most desired features in mold steel. It is working perfectly with machining process and EDM. [International Mold Steel, Inc. 1997 Product Catalogue]

The experiment was conducted with the same experimental setup presented above except a new digital four-channel digitizer (Figure 11). Addition to the cutting force data in feed and thrust direction (2-channel record) acoustic emission signal of the cut was also collected and recorded. (1-chnanel) The steel NAK 55 workpiece (4 x 3 x 1 inches) was clamped to the dynamometer and the acoustic emission sensor was magnetically attached to the dynamometer to ensure the closest contact. The experiment was performed with a variety of cutting parameters to find out the optimal cutting conditions as spindle speed, feed rate and depth of cut for this specific workpiece NAK 55. 50 % overlapping, climb end milling operations were performed to monitor the force variation at different stages of the tool life. Table 6 presents the cutting conditions.

Table 6. Test Conditions in NAK 55 Steel Machinability Experiments

Tool type	Carbide 2 Flutes End-Mill	Carbide 2 Flutes End-Mill
Tool diameter	0.0625 inch	0.0300 inch
Spindle speed	15,000; 30,000; 45000	15,000; 30,000; 45000
Feed rate	1.25, 2.5, 5, 7.5	1.25, 2.5, 5
Depth of cut	d/2, 3d/4, d, 1.5d	d/2, 3d/4, d, 1.5d
Workpiece	NAK 55 steel	NAK 55 steel
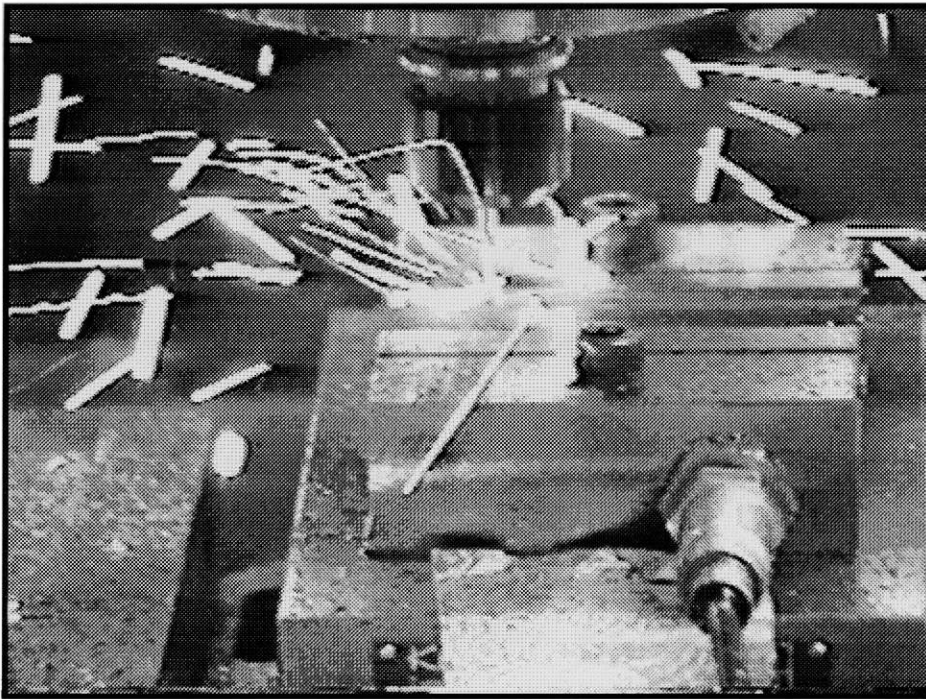
Figure 11. NAK55 Steel Workpiece Machining with 0.0625" Diameter End-Mill

IV.2. Static test

The same kind of micro tools used in the machinability experiments were used in static test. High speed steel (HSS) and carbide 0.0625, 0.03125, 0.020 inches diameter two flutes end-mills were analyzed under the static loading conditions. The tool was attached to a Bridgeport Milling machine with an end-mill holder. The workpiece was clamped to the dynamometer. The dynamometer was tightened to a vise that is fixed on the X-Y table of the milling machine. A linear displacement sensor was clamped on the vise with respect to the tool holder. The sensor supposed to measure the linear table displacement during the experiment. The sensor with its signal conditioner was connected to a Nicolet 310 digital oscilloscope. The dynamometer was connected to a charge amplifier and to the oscilloscope also. Figure 12 presents the experimental setup. Force and displacement data were collected and recorded.

Table was fed manually within the thrust direction (X direction) against the micro-tool applying a bending force to the tool itself. Tool was deflecting towards the same direction of the loading. Bending forces and linear displacements respectively were collected continuously until the tool broke down. Experiment was conducted with static conditions, spindle of the milling machine was off. Thrust direction bending force was recorded within the linear small displacement in X direction.

Experiments were repeated with different static bending moment loading to measure the stiffness of the micro-end-mill. The collected data were analyzed and manipulated to find out the stiffness coefficient of HSS and Carbide micro-tool for the

specified diameter and type. The bending moment loading limits of the tools also were measured with extreme loading conditions.
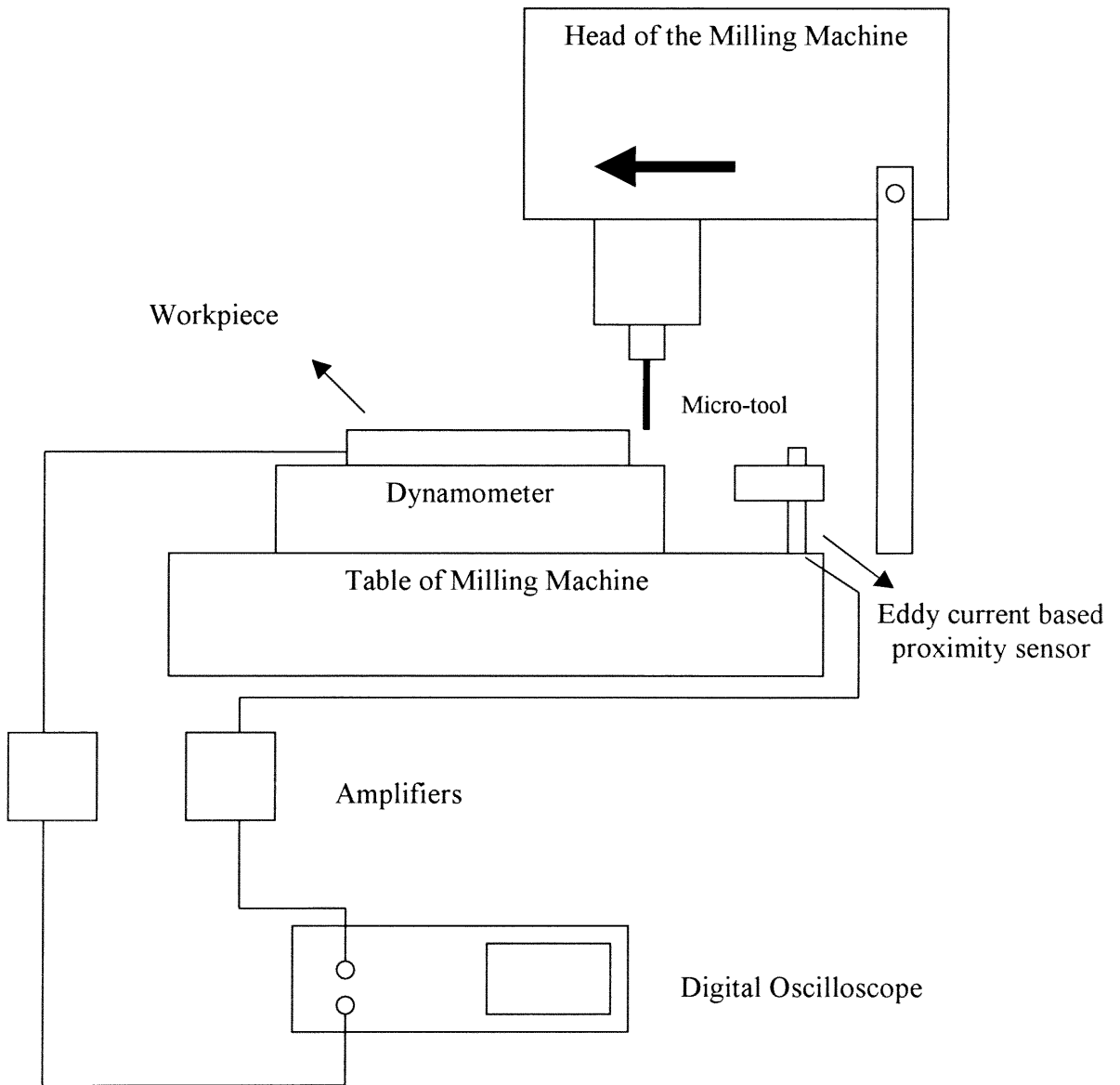
Figure 12.   Static experiment of the Micro-Tool

IV.3. Dynamic test

In order to find out the dynamic behavior of micro-tools, some experiments were conducted. HSS and Carbide 0.0625, 0.02135 and 0.020 inches diameter two flute micro end-mills were used. End-mills were connected to a Bridgeport Milling machine with a tool holder. The experimental setup is presented in Figure 13 and 14. A Polyter OFV 2500 Laser Vibrometer controller and OFV 350 Sensor Head were used to measure the vibration of the tools. As an exciter, a miniature impact-hammer used. A digital Nicolet 310 oscilloscope was used to collect and record data. Digitizer was pre-triggered to catch the input impact and the dynamic response of the tool at the same time.

The tip and the bottom of the micro end-mill were hit with the impact hammer to analyze the dynamic response. When the tool was excited, it was vibrating and the vibration was measured with a vibrometer. The vibrometer was directing a laser beam to the tip of the end-mill. Once the tip was hit with the impact hammer, the impact was digitized and recorded to the oscilloscope. The response of the tool to this excitation was a typical dynamic vibration signal. Input and output signals were recorded as 4,000 data points.

The data was studied and graphs were prepared. The dynamic characteristics of the end-mills were calculated from the variation of the output signal amplitude versus time. The natural-angular frequency and the damping factor of the tools were calculated analytically and numerically. Transfer function of the system was established with the aid of a computer program.
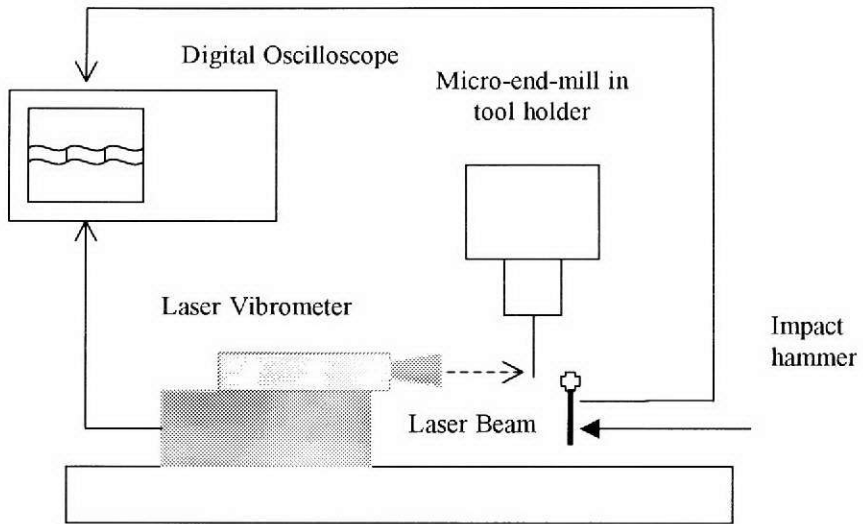
Figure 13. Dynamic Experiment of Micro-Tools
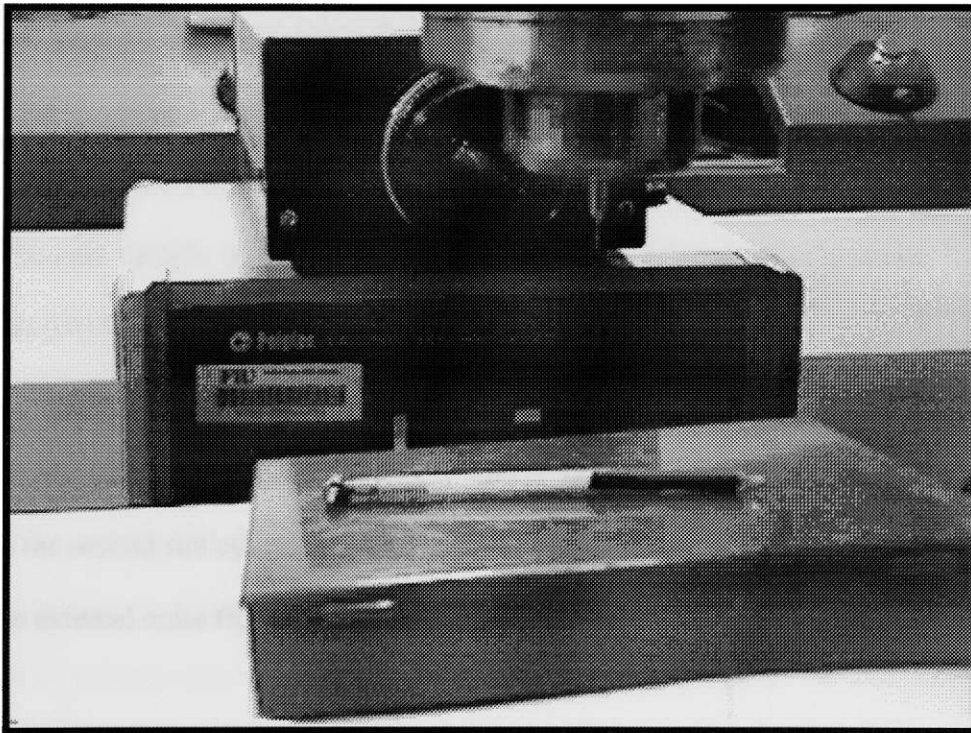
Figure 14. Experimental setup of Dynamic Test

Chapter V

Results and Discussions

In this section, the performance of the new machinability test method, characteristics of the cutting force at different tool wear levels, the accuracy of the developed neural network based tool wear estimators are discussed.

V.1. Characteristics of Cutting Force at Different Tool Wear Levels

Graphite Electrodes (POCO3, POCOEDMC-3):

A series of experiments were conducted to study the tool wear related cutting force variation during the end milling of graphite electrodes. POCO 3 and POCO EDMC-3 workpieces were used. POCOEDMC-3 was reported to be more abrasive by the users. At the first stage of the study, the optimal cutting conditions were experimentally found by using the developed procedure. Later, these cutting conditions were used to study tool wear. Table 7 shows a summary of the proposed machinability method results with 0.0625-inch diameter carbide end-mill for POCOEDMC-3. 15,000-rpm spindle speed, 5 ipm feed rate and 0.015 inches depth of cut, were used in the experiments.

Figure 15 and 16 shows the thrust and feed direction cutting force after 120 inches of tool life when POCOEDMC-3 is cut with a carbide micro-tool. This is just one pass before the second slot cut on the aluminum test piece. The small magnitude of cutting force and the external noise from the machine itself make the data very difficult to interpret.

Table 7. Results of the Proposed Machinability Method for POCOEDMC-3

Experiment	Cutting Conditions	Maximum Cutting Forces	Acceptability
1	15,000 rpm 15 ipm 0.030" doc	X - 40 N Y- 25 N	Tool is broken
2	15,000 rpm 10 ipm 0.030 doc	X - 31 N Y- 19 N	not acceptable Tool Survived
4	15, 000 rpm 5 ipm 0.015 doc	X - 20 N Y -12 N	Tool is OK Conditions are optimal
5	15,000 rpm 7.5 ipm 0.015 doc	X - 25 N Y- 16 N	Tool is OK conditions are severe

To overcome this problem, and to be able to monitor the tool wear during the machining of non-metals, an aluminum piece was used to inspect cutting force variation at different stages of tool wear. A slot was cut on the aluminum test piece. The machining operation continued on the non-metal workpiece. Periodically, aluminum test piece was cut at the same cutting conditions and cutting data was collected. The magnitude of the X and Y direction cutting forces had the tendency to increase as the tool began to wear out. Even without monitoring of the cutting force, tool wear could be estimated from the burr on the aluminum test piece. After the third and fourth slots on the test piece burr appeared and increased with tool wear. The carbide end-mill with 1/16 inches diameter gave more consistent results than 0.030 ones. The amplitude of the cutting force increased when the tool wears out.

The pictures of the slots are presented in Figure 17, 19 and 21. The variation of the cutting force at different stages of the tool wear is presented in Figure 18, 20 and 22.
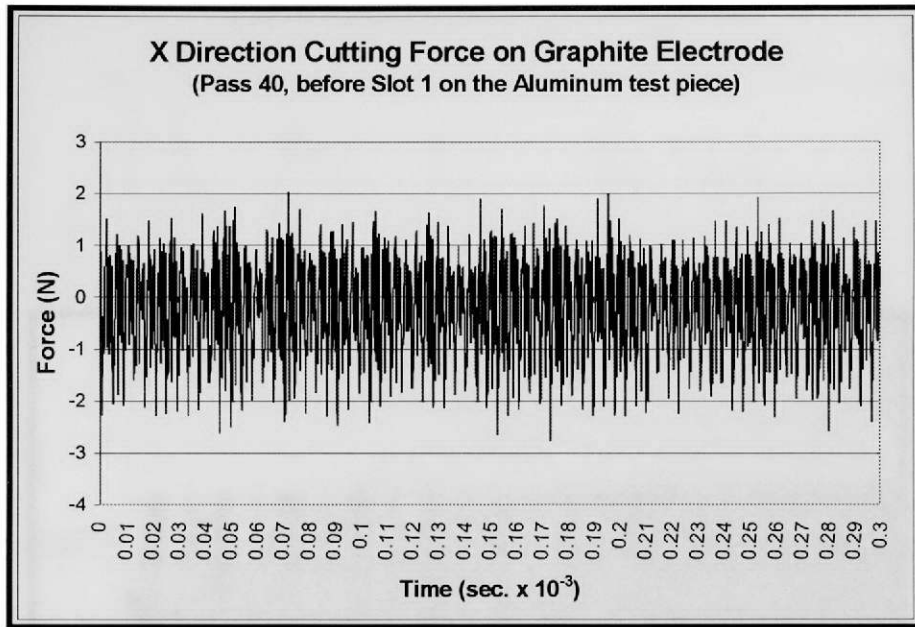
Figure 15. Thrust Direction Cutting Force on POCOEDMC-3 after 40 Pass
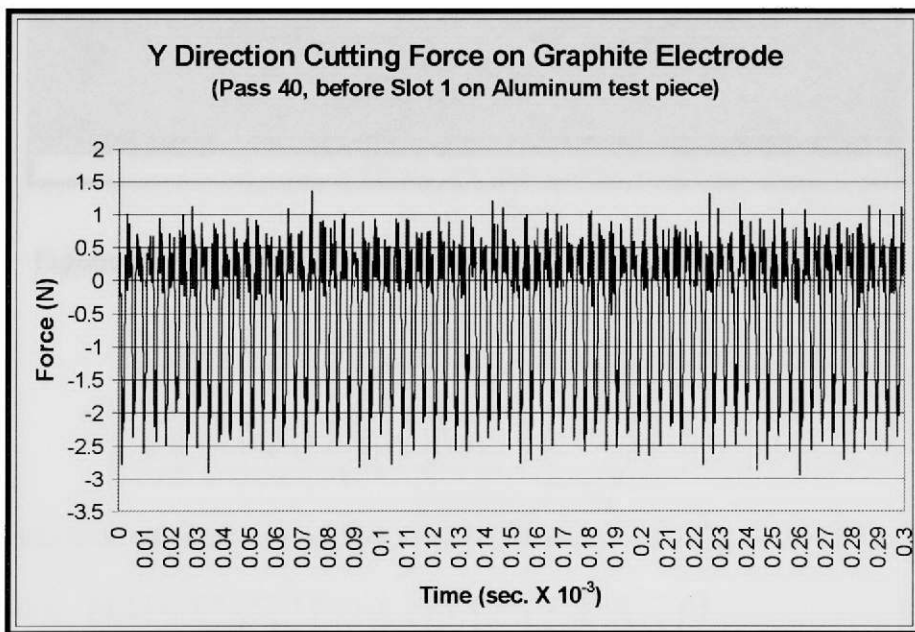
Figure 16. Feed Direction Cutting Force on POCOEDMC-3 after 40 Passes
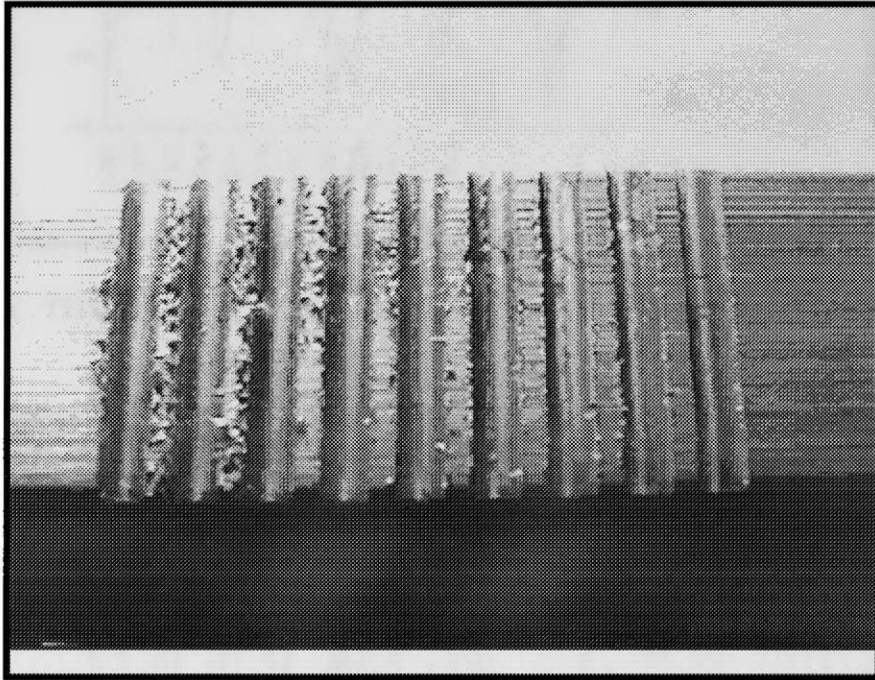
Figure 17. THE SLOTS FROM PERFECT TO WORN OUT TOOL
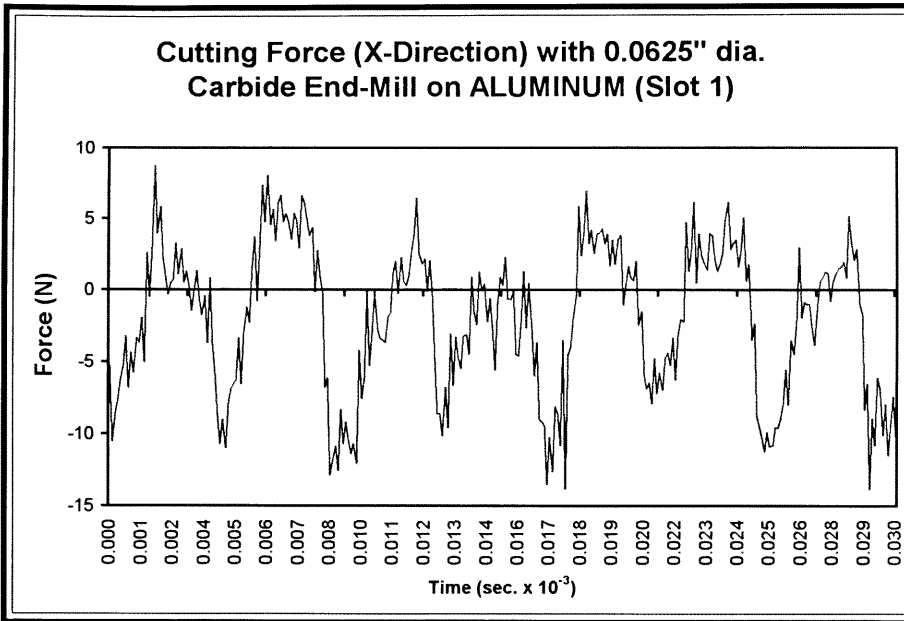
Figure 18.a. THRUST DIRECTION CUTTING FORCE OF PERFECT TOOL (SLOT1)
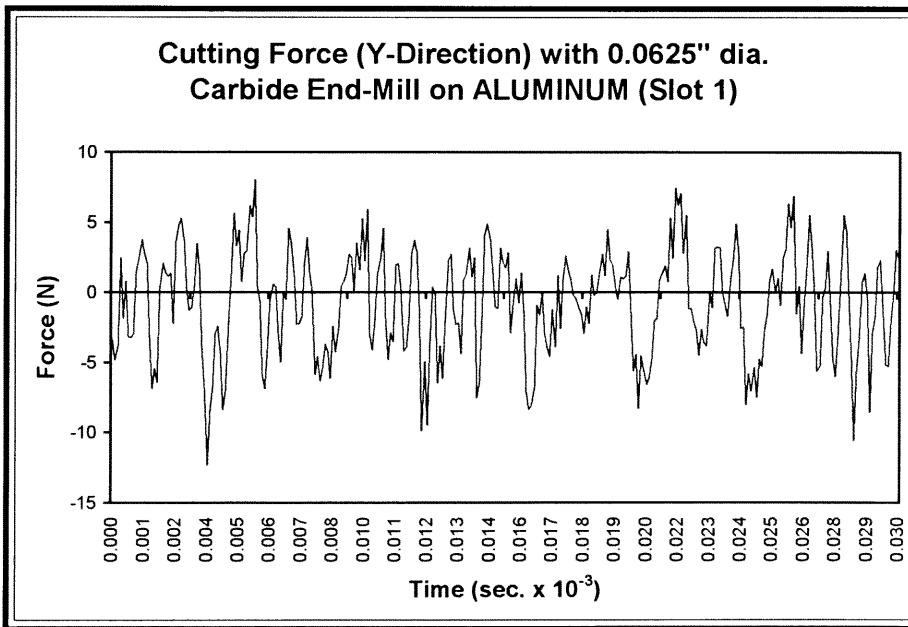
Figure 18.b. FEED DIRECTION CUTTING FORCE OF PERFECT TOOL (SLOT 1)
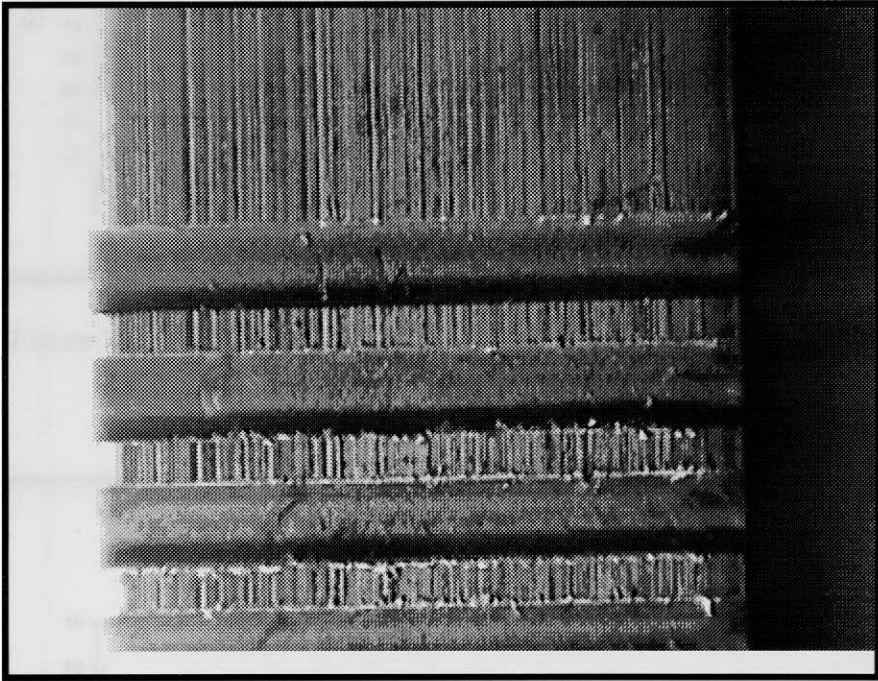
Figure 19. PICTURE OF THE SLOTS #1, #2, #3
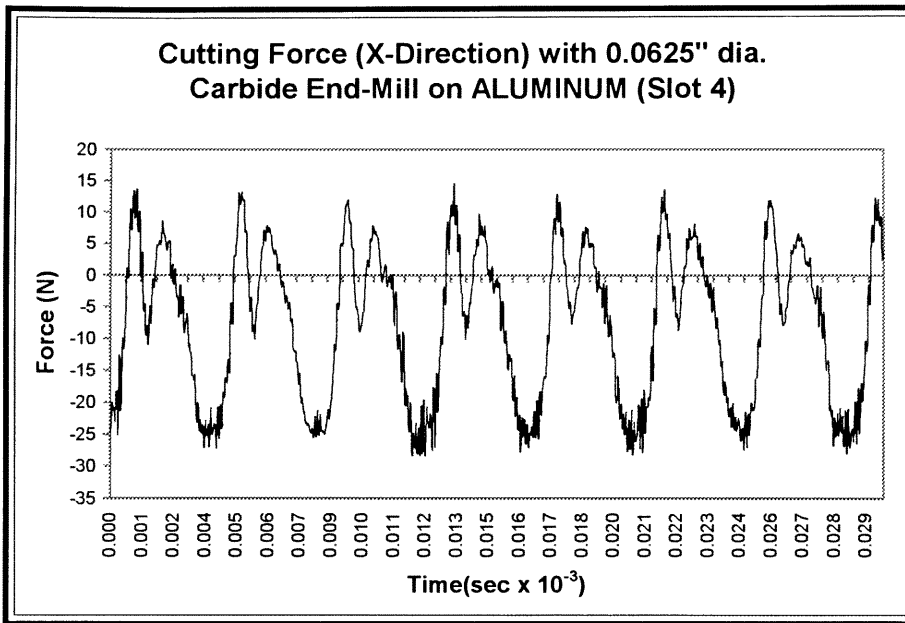
Figure 20.a. THRUST DIRECTION CUTTING FORCE OF TOOL (SLOT 4)
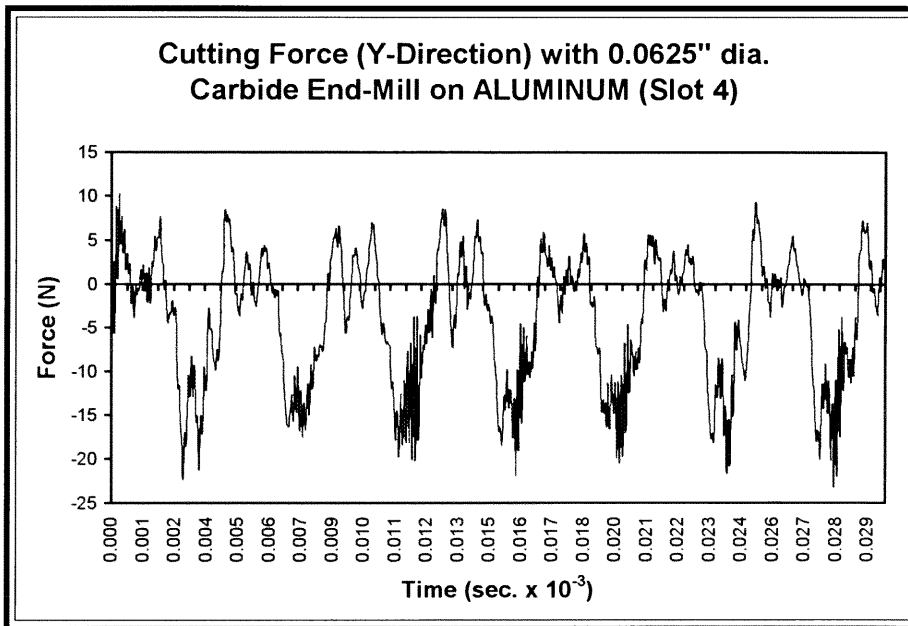
Figure 20.b. FEED DIRECTION CUTTING FORCE OF TOOL (SLOT 4)

54
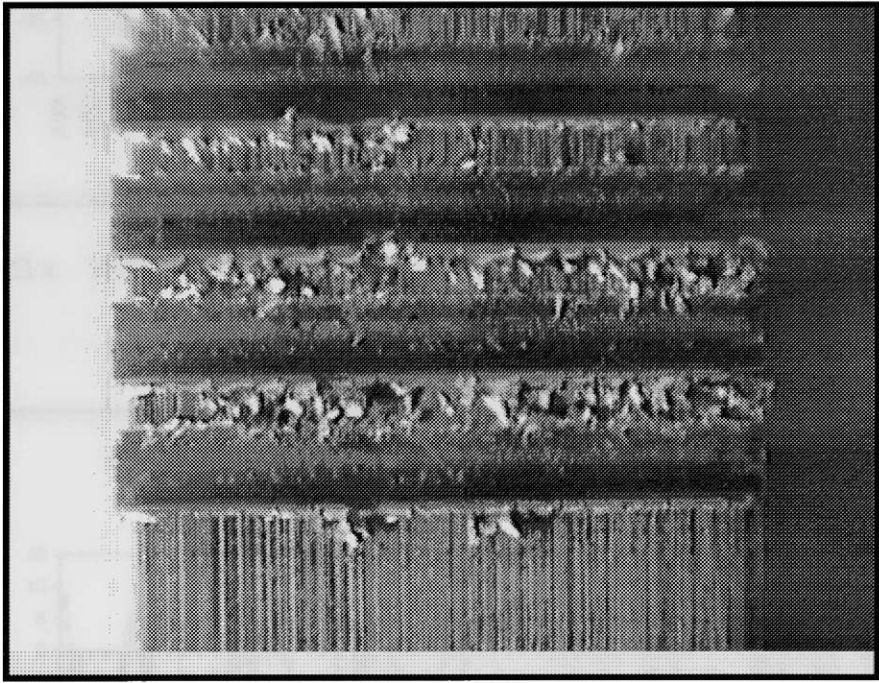
Figure 21. PICTURE OF THE SLOTS #6, #7, #8. #9
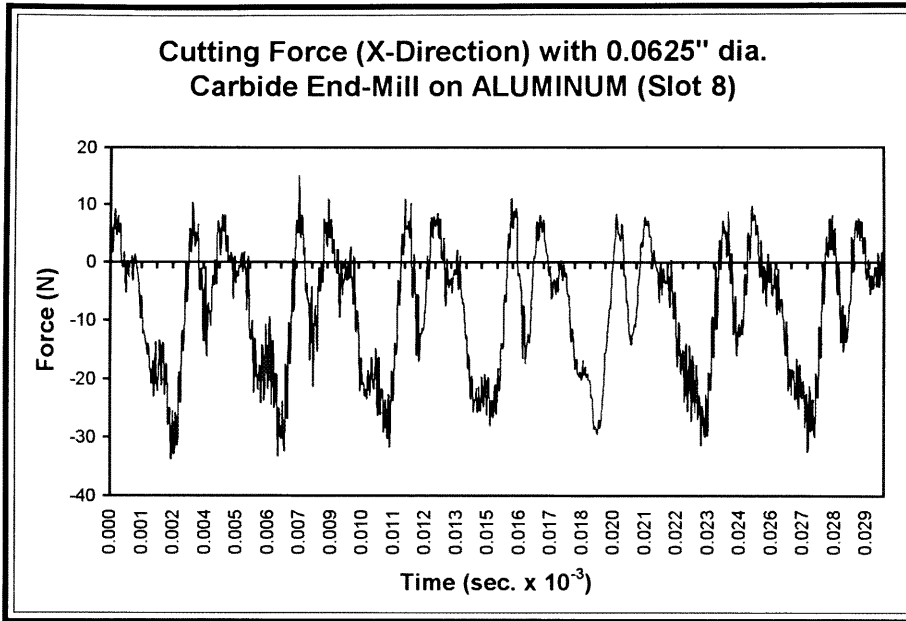
Figure 22.a. THRUST DIRECTION CUTTING FORCE OF TOOL (SLOT 8)
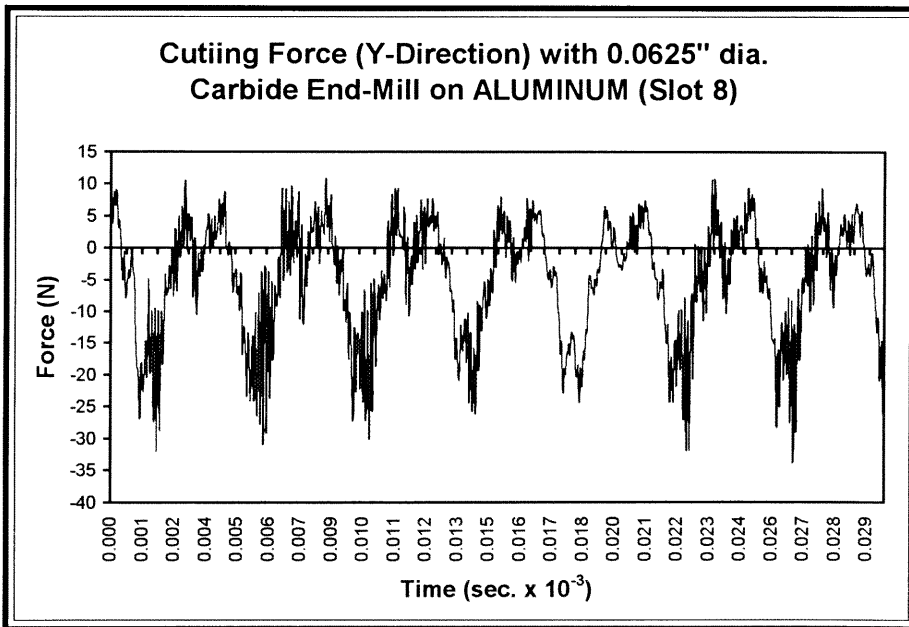
Figure 22.b. FEED DIRECTION CUTTING FORCE OF TOOL (SLOT 8)

The amplitudes of the Thrust and Feed direction cutting force variation of the 1/16 inches diameter carbide end-mill are represented in Figure 23.a. and 23.b. This cutting forces belong to ten slots cut on the aluminum test piece during the wear test of POCOEDMC-3. Cutting forces had the tendency to increase with the usage of the tool. Linear and exponential models were fitted to the data. The results were presented in Figure 24.a., 24.b., 25.a., and 25.b. The result of the study showed that linear curve fitted better than the exponential curve.

The following equation was used to represent the wear and cutting force relationship.

$$y = a + bx \tag{5.1}$$

a nad b were calculated from the following equations:

$$a = [Y] - b[X] \tag{5.2}$$

and

$$b = \frac{n\sum xy - (\sum x)(\sum y)}{n\sum x^2 - (\sum y)^2} \tag{5.3}$$

where y = wear, x = magnitude of cutting force.

The results of the curve fitting study are presented in Figure 26.a. and 26.b.
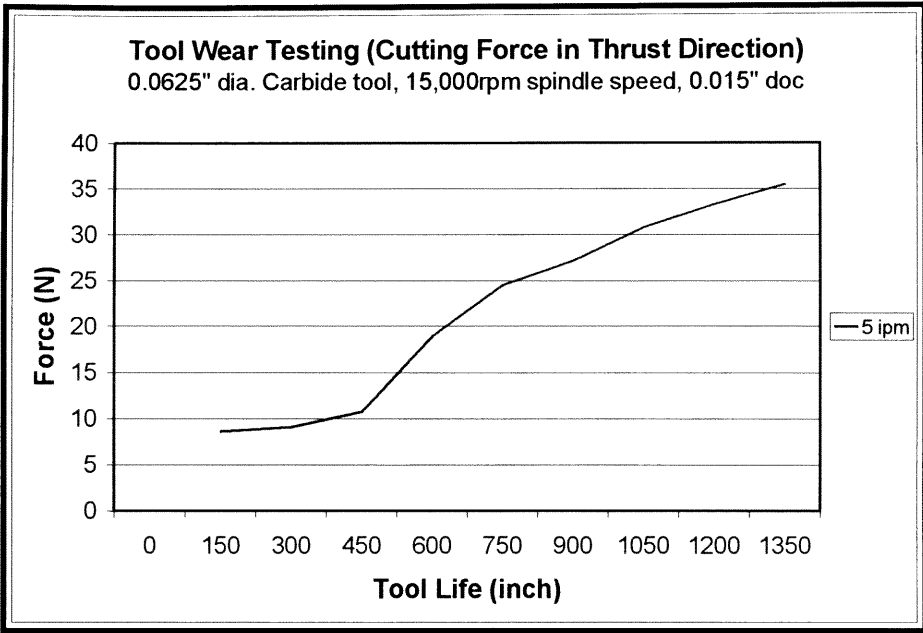
Figure 23.a.   Thrust Direction Cutting Force Variation with the Usage of the End-Mill
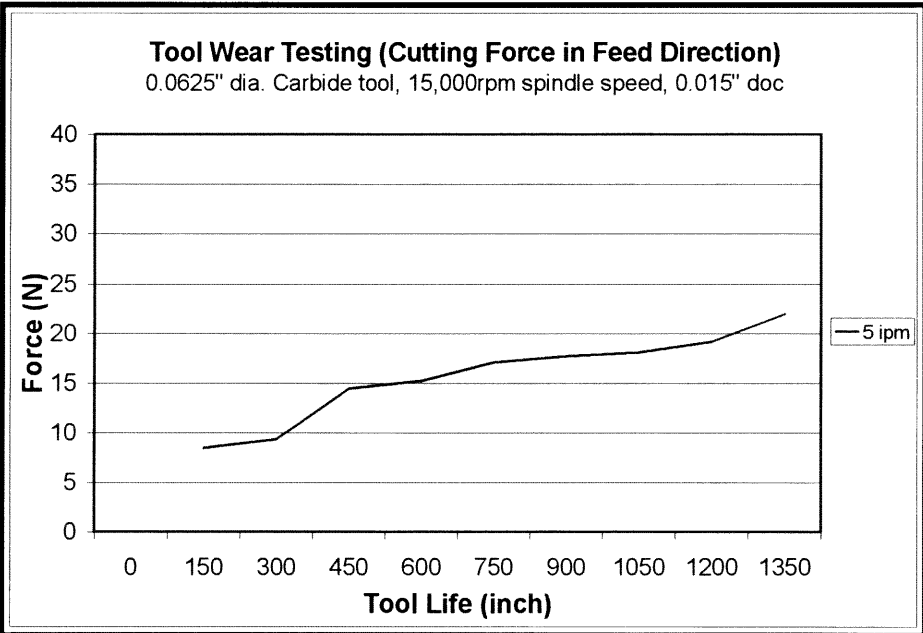
Figure 23.b.   Feed Direction Cutting Force Variation with the Usage of the End-Mill
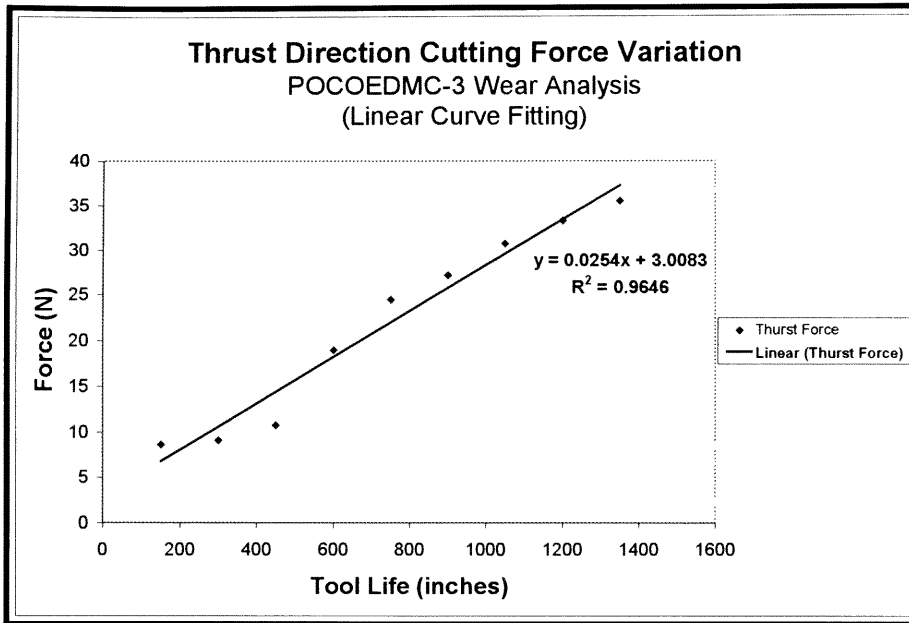
Figure 24.a.   Linear Curve Fitting to the Experimental Thrust Direction Cutting Force
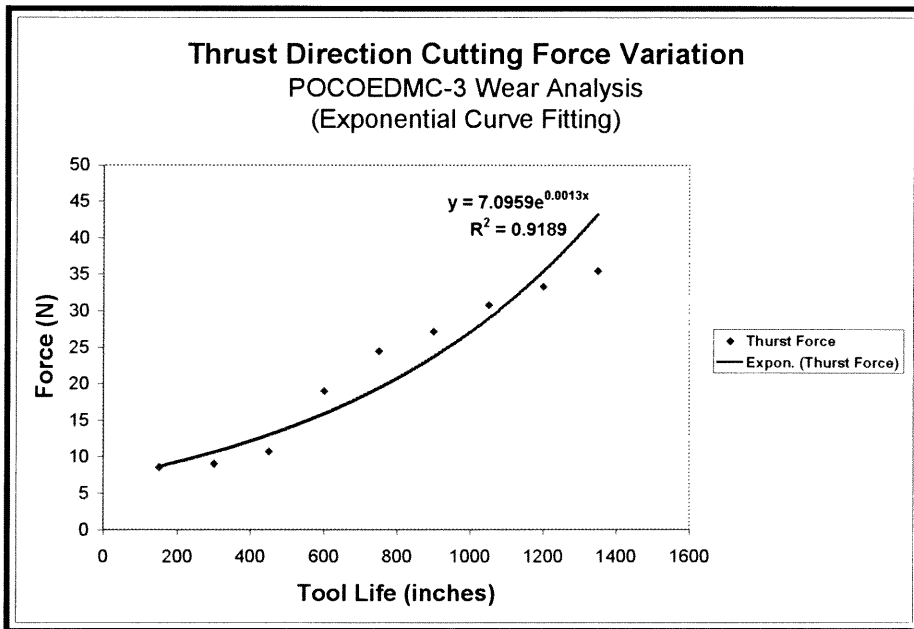
Figure 24.b.   Exponential Curve Fitting to the Experimental Thrust Direction Cutting
Force

Feed Direction Cutting Force Variation
POCOEDMC-3 Wear Analysis
(Linear Curve Fitting)

$y = 0.0104x + 7.9521$
$R^2 = 0.9208$

Force (N)

Tool Life (inches)

♦ Feed Force
— Linear (Feed Force)
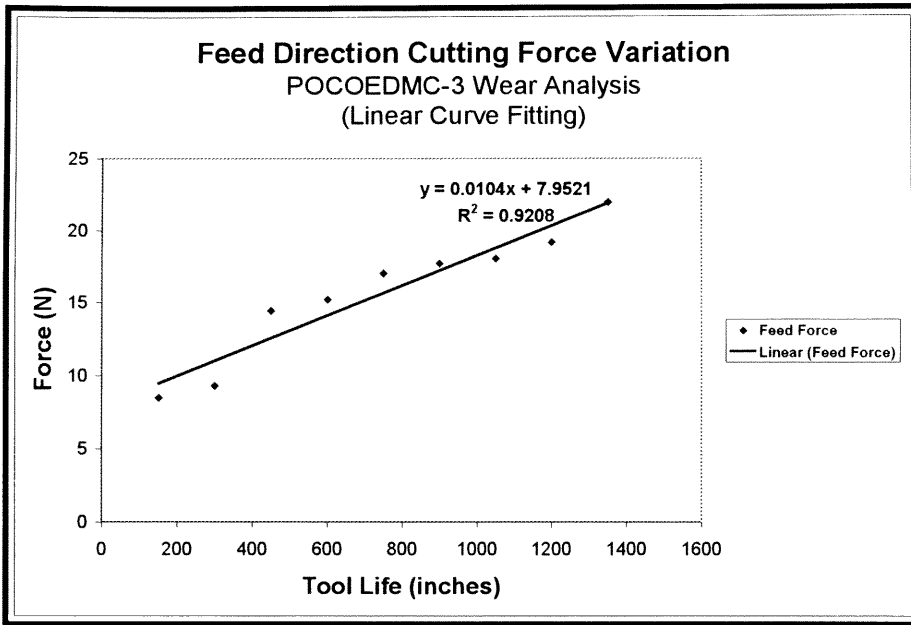
Figure 25.a.   Linear Curve Fitting to the Experimental Feed Direction Cutting Force

Feed Direction Cutting Force Variation
POCOEDMC-3 Wear Analysis
(Exponential Curve Fitting)

$y = 8.7233e^{0.0007x}$
$R^2 = 0.8594$

Force (N)

Tool Life (inches)

♦ Feed Force
— Expon. (Feed Force)
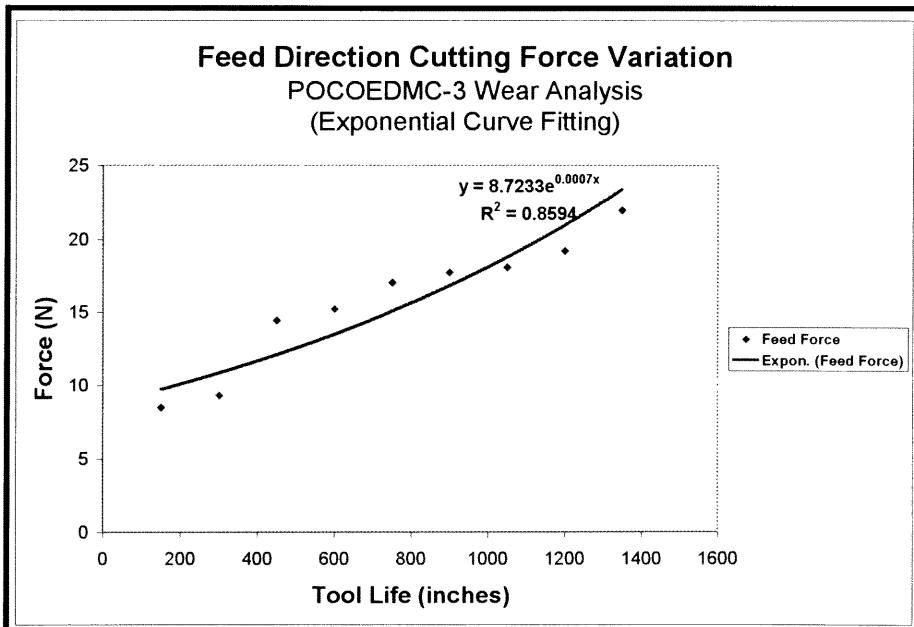
Figure 25.b.   Exponential Curve Fitting to the Experimental Feed Direction Cutting Force
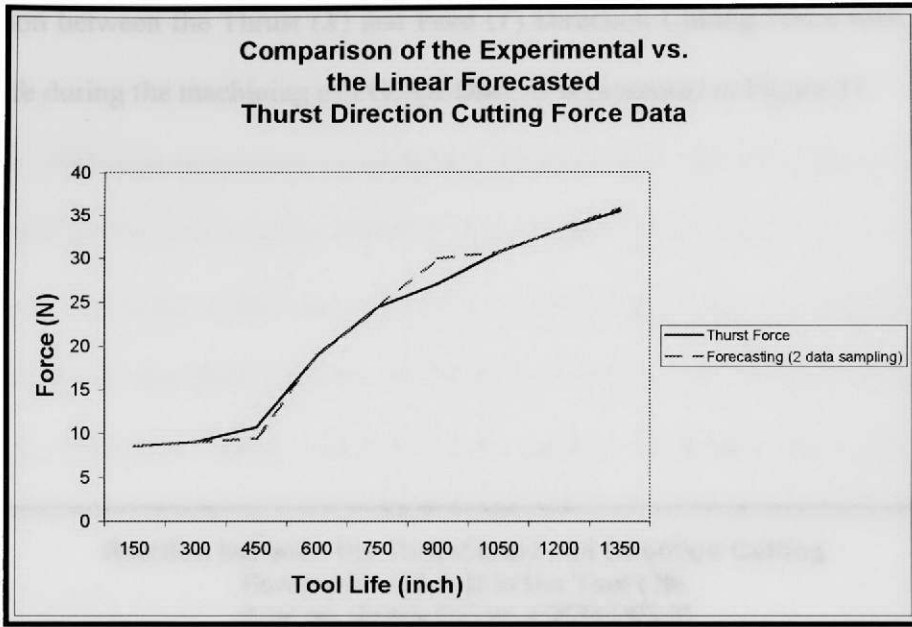
Figure 26.a. Comparison of the Experimental and the Forecasted Data for Thrust Direction
Cutting Force (POCOEDMC-3 Workpiece)
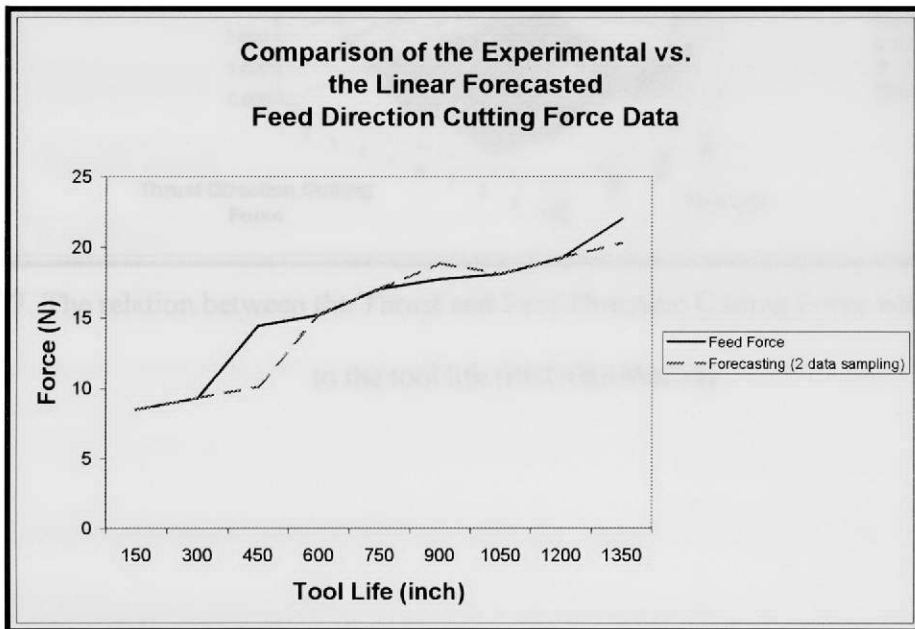
Figure 26.b. Comparison of the Experimental and the Forecasted Data for Feed Direction
Cutting Force (POCOEDMC-3 Workpiece)

The relation between the Thrust (X) and Feed (Y) Direction Cutting Force with respect to the tool life during the machining of POCOEDMC-3 is presented in Figure 27.
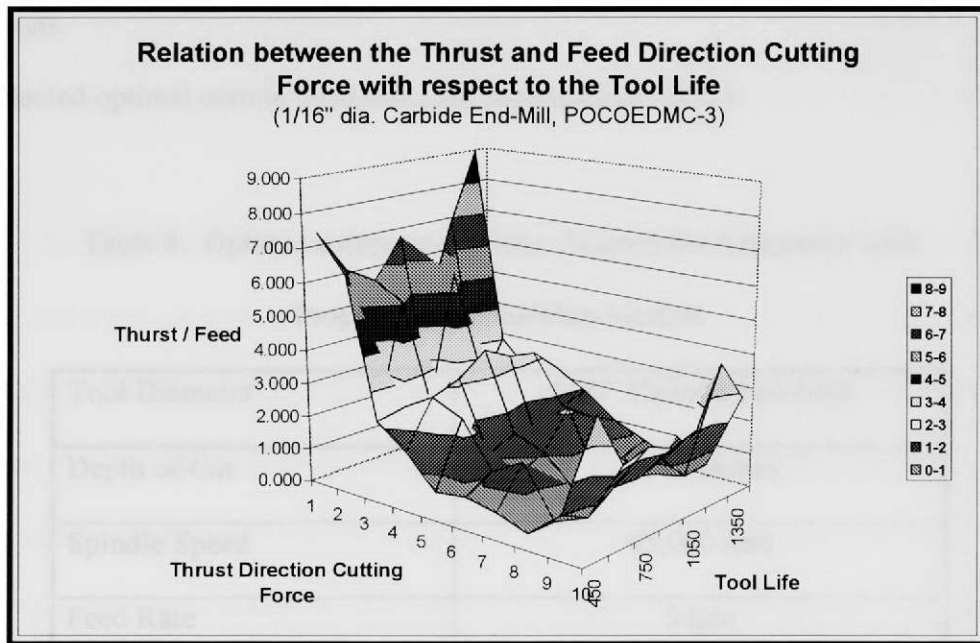
Figure 27. The relation between the Thrust and Feed Direction Cutting Force with respect to the tool life (POCOEDMC-3)

Aluminum:

The machinability and tool wear experiments were performed on aluminum workpiece. Although machining of aluminum is easier than the other harder metal with conventional cutting tools, fuzzy behavior and premature tool breakage are commonly encountered. The value of the cutting force was larger than the forces encountered during the machining of electrode graphite and easier to monitor. At the first stage on these experiments, different cutting conditions were applied to identify the optimal cutting conditions.

The selected optimal cutting conditions are presented in Table 8.

Table 8. Optimal cutting conditions obtained for Aluminum with Proposed Machinability Method

Tool Diameter	1/32" Carbide End-Mill
Depth of Cut	0.015 inches
Spindle Speed	45,000 rpm
Feed Rate	5 ipm
Tool Life obtained	156 inches

The tool wear experiments were conducted with the cutting conditions stated above. The thrust and feed direction cutting force variation with tool usage for the 1/32 inches diameter carbide end-mill was shown in Table 9.

Table 9. Cutting Forces -Tool Life Results in Tool (1/32" Carbide End-Mill)

Wear Experiment (Aluminum Workpiece)

Cutting Force in Thrust Dir. (N)	Feed Rate 5 ipm	Cutting Force in Feed Dir. (N)	Feed Rate 5 ipm
Tool Life (inch)	Force	Tool Life (inch)	Force
30	6.6	30	9.78
45	7.1	45	10.11
60	10.42	60	14.62
62	8.56	62	11.23
75	10.11	75	12.5
90	12.23	90	13.47
105	16.86	105	16.78
107	14.78	107	14.96
120	16.74	120	16.41
135	18.35	135	18.54
156	20.13	156	21.75

Thrust and Feed direction cutting force variation of the 1/32 inches diameter carbide end-mill are represented in Figure 28.a. and 28.b. As it can be seen from the graphs that cutting forces are increasing with a certain of amount usage of the tool. Within this trend, some of the cutting force data were larger than the usual ones. This phenomenon is not related with the tool wear; the reason for this instantaneous increase in the data is the chip of the aluminum workpiece stocked to the cutting edges of the tool. Aluminum is a soft material and chips are created during the machining. Cutting tool used for the experiment was carbide steel. During the test, for certain passes of the tool on the workpiece, the aluminum temperature increased and the chips got melted and stocked to the teeth of the end-mill. For most of the data, chips were released after certain amount of tool usage after the specified pass. So for these reasons, when the cutting forces are monitored larger than the usual ones, the data record was repeated after a while. The linear increment trend can be seen if these abnormalities were ignored.

Data was also studied with curve fitting analysis technique to evaluate the trend of the increase in cutting forces. Linear and exponential models were fitted to the data. The results were presented below in Figure 29.a., 29.b., 30.a., and 30.b. The interpolation method was used for the curve fitting. The result of the study showed that linear curve fitted better than the exponential curve. After the observation of the study, a linear forecasting analysis is conducted to interpret the cutting force data. Forecasting method used is based on the linear interpolation of the collected data. The equations 5.1 to 5.3 were used for forecasting. The results are shown in Figure 31.

Figure 28.a. Thrust Direction Cutting Force Variation with Tool Usage on Aluminum
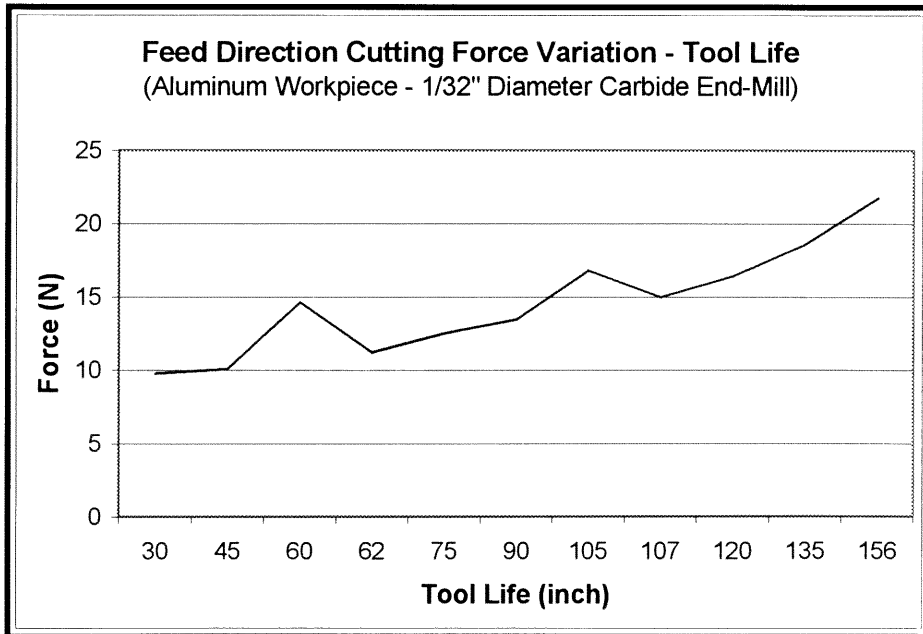
Figure 28.b. Feed Direction Cutting Force Variation with Tool Usage on Aluminum
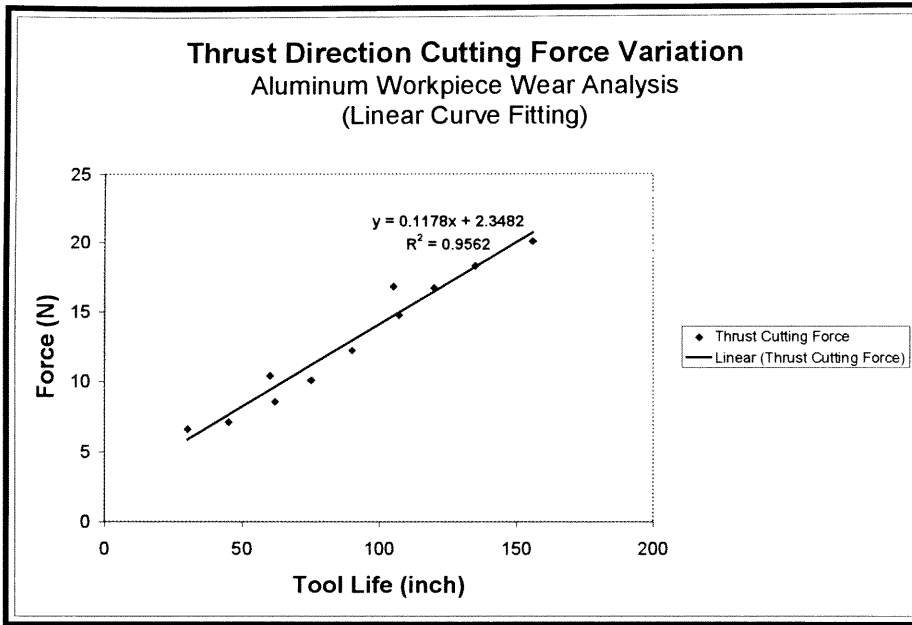
Figure 29.a. Linear Curve Fitting to the Experimental Thrust Direction Cutting Force

(Aluminum Workpiece)
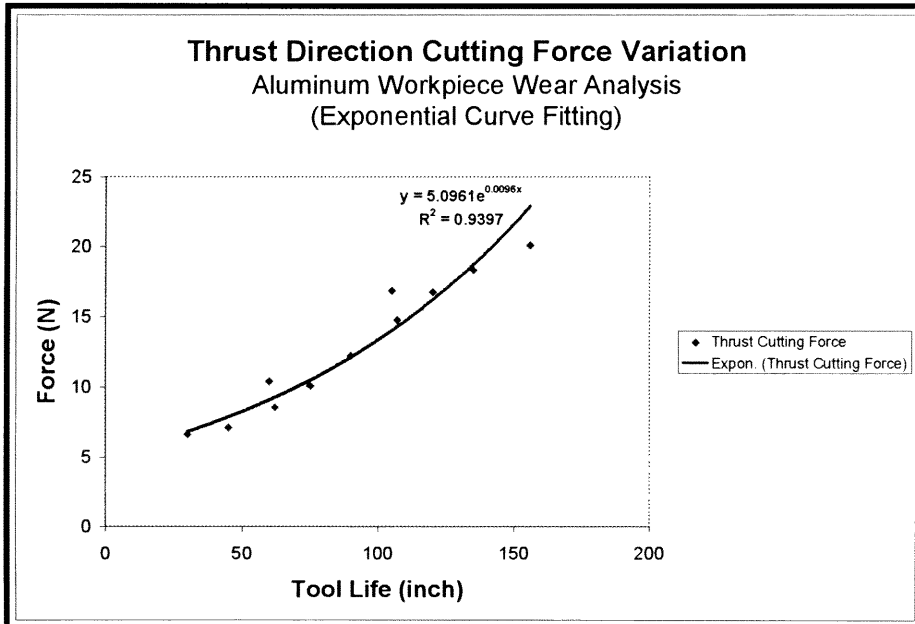
Figure 29.b. Exponential Curve Fitting to the Experimental Thrust Direction Cutting Force

(Aluminum Workpiece)
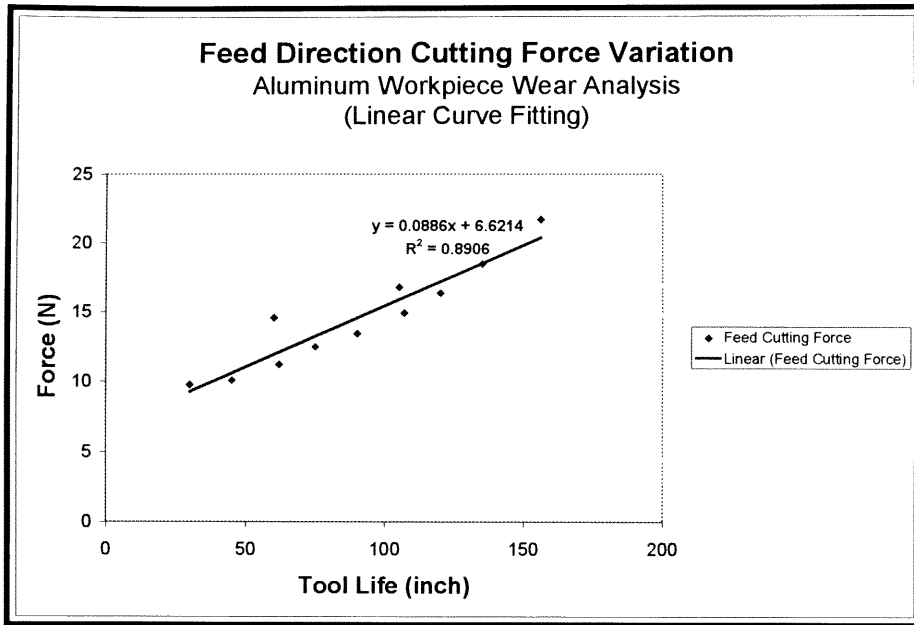
Figure 30.a. Linear Curve Fitting to the Experimental Feed Direction Cutting Force

(Aluminum Workpiece)
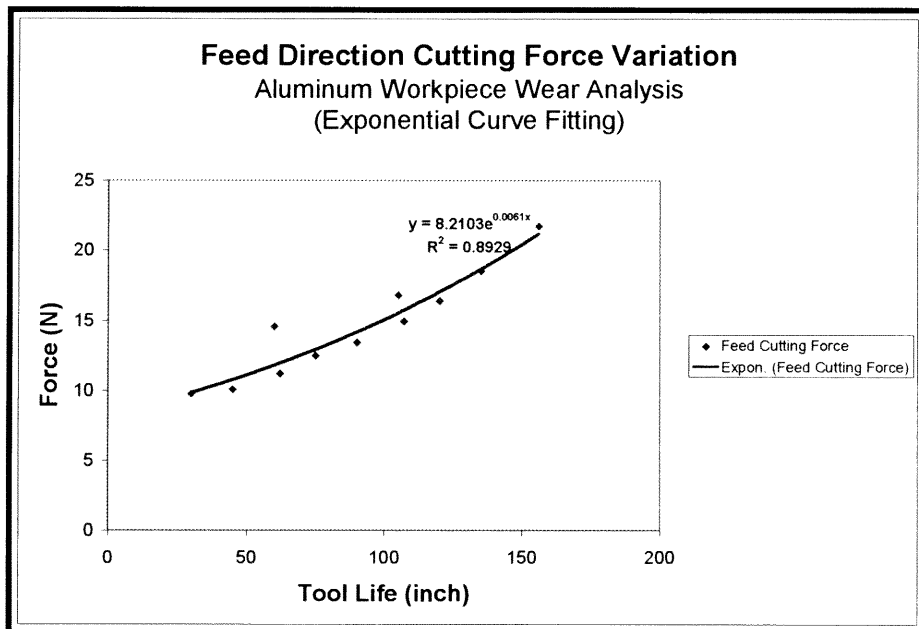
Figure 30.b. Exponential Curve Fitting to the Experimental Feed Direction Cutting Force

(Aluminum Workpiece)
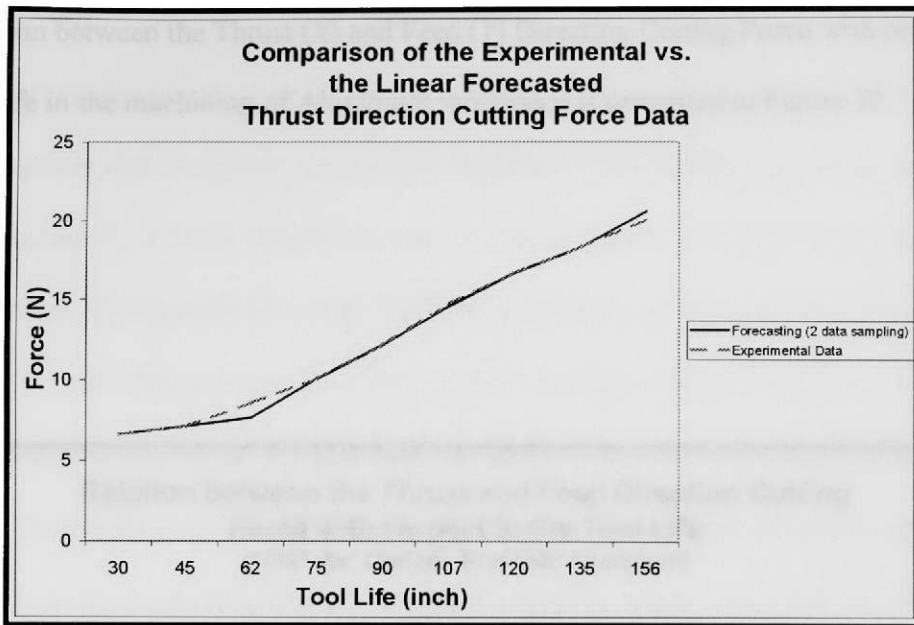
Figure 31.a. Comparison of the Experimental and the Forecasted Data for Thrust Direction Cutting Force (Aluminum Workpiece)
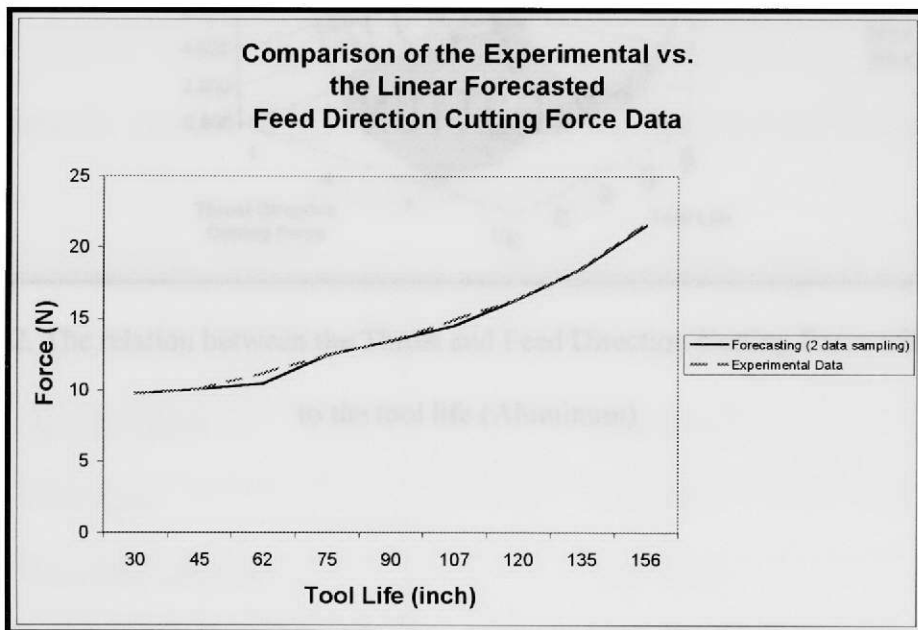
Figure 31.b. Comparison of the Experimental and the Forecasted Data for Feed Direction Cutting Force (Aluminum Workpiece)

The relation between the Thrust (*X*) and Feed (*Y*) Direction Cutting Force with respect to the tool life in the machining of Aluminum workpiece is presented in Figure 32.
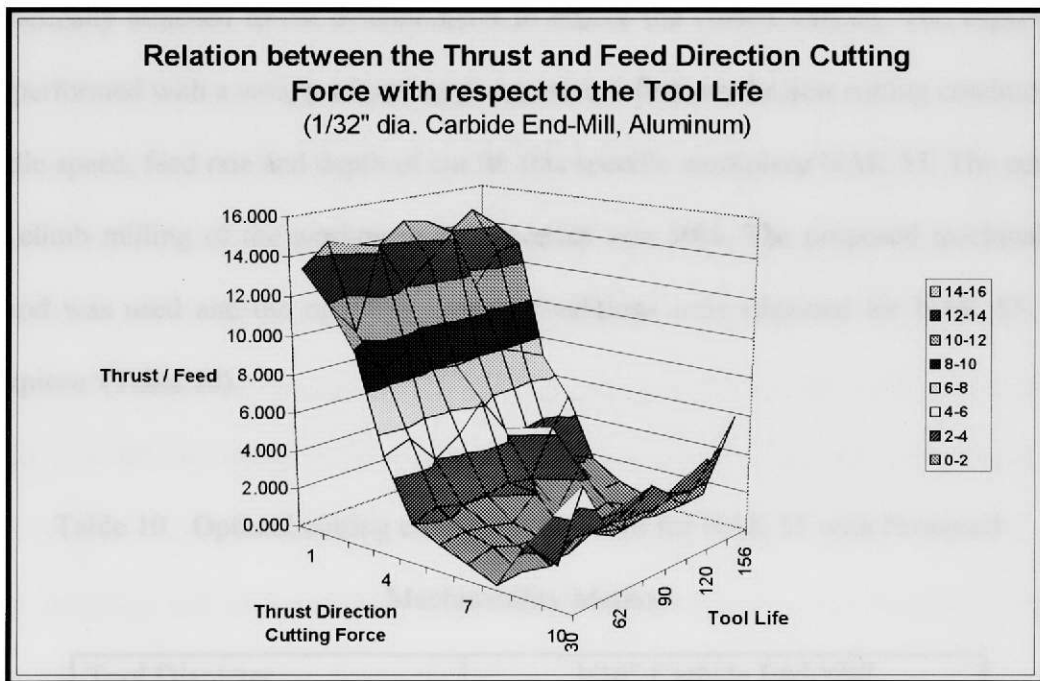
Figure 32. The relation between the Thrust and Feed Direction Cutting Force with respect to the tool life (Aluminum)

Steel (NAK 55):

The machinability of NAK 55 was studied. Carbide tools with 0.0625 and 0.030 inches diameter and two flutes were used. Addition to the cutting force data in feed and thrust direction (2-channel record) acoustic emission signal of the cut was also collected and recorded. (1-chnanel) The steel NAK 55 workpiece which has (4 x 3 x 1 inches) dimensions, was clamped to the dynamometer and the acoustic emission sensor was magnetically attached to the dynamometer to ensure the closest contact. The experiment was performed with a variety of cutting parameters to find out the best cutting conditions as spindle speed, feed rate and depth of cut for this specific workpiece NAK 55. The cut was face climb milling of the workpiece. The overlap was 50%. The proposed machinability method was used and the optimum cutting conditions were obtained for NAK 55 Steel workpiece. (Table 10).

Table 10. Optimal cutting conditions obtained for NAK 55 with Proposed Machinability Method

Tool Diameter	1/16" Carbide End-Mill
Depth of Cut	3d/4
Spindle Speed	15,000 rpm
Feed Rate	2.5 ipm
Tool Life obtained	250 inches

For 0.0625 inches diameter carbide end-mill, 15,000-rpm spindle speed, 2.5 ipm feed rate and 3d/4 depth of cut were chosen as optimized conditions and tool wear analysis was conducted with these conditions. 250 inches tool life was obtained with the optimized cutting conditions.

Cutting force variation during the micro end milling of NAK 55 did not have the same trend that graphite electrodes had. The cutting force in X and Y directions slightly fluctuated but did not increase with the usage of the tool. These results are presented in Figure 33. Table 11 presents the cutting force variation with the usage of the tool. The thrust and feed direction cutting force during the tool breakage pass on the workpiece are presented in Figure 34. Cutting forces were larger for a certain amount of tool life at the beginning of the experiment and later tool became dull and cutting force slightly decreased. The overall analysis of the data showed that the characteristics of the cutting force of the cutting tool did not change. The reason for this phenomenon is that the tool material and the workpiece material have similar material characteristics. Tool and workpiece have closer hardness and tool probably wears out the tool gradually. Tool breakage happens when an excessive bending force applied to the tool. Also the low-frequency acoustic emission signal of the machining process and its frequency domain representation were shown in Figure 35. Cutting Forces and Acoustic Emission data during the experiments had a constant trend to be stable, but when the excessive bending force passed the limits of the tool, the breakage occurred.
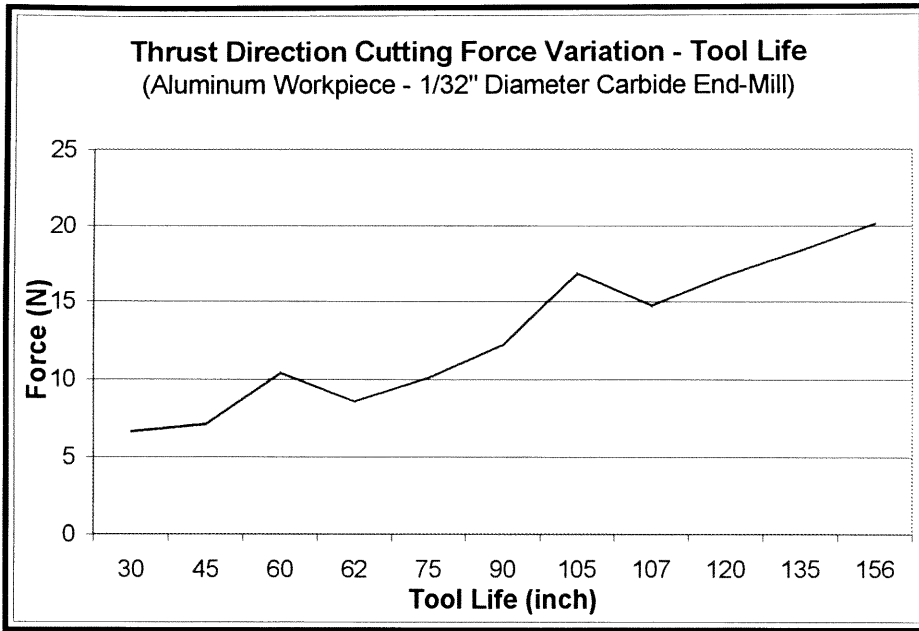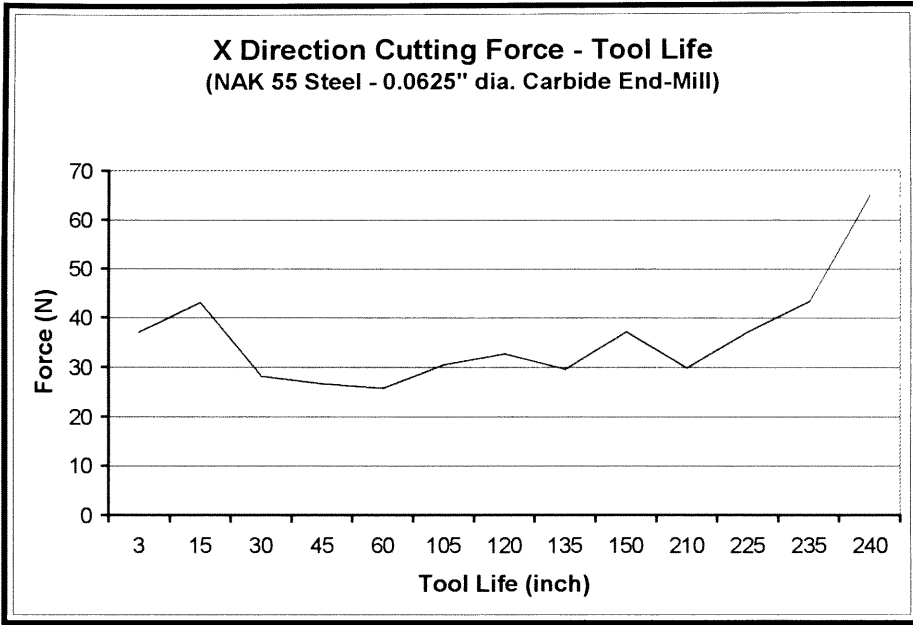
Figure 33.a. Thrust Direction Cutting Force Variation with Tool Usage on NAK 55 Steel
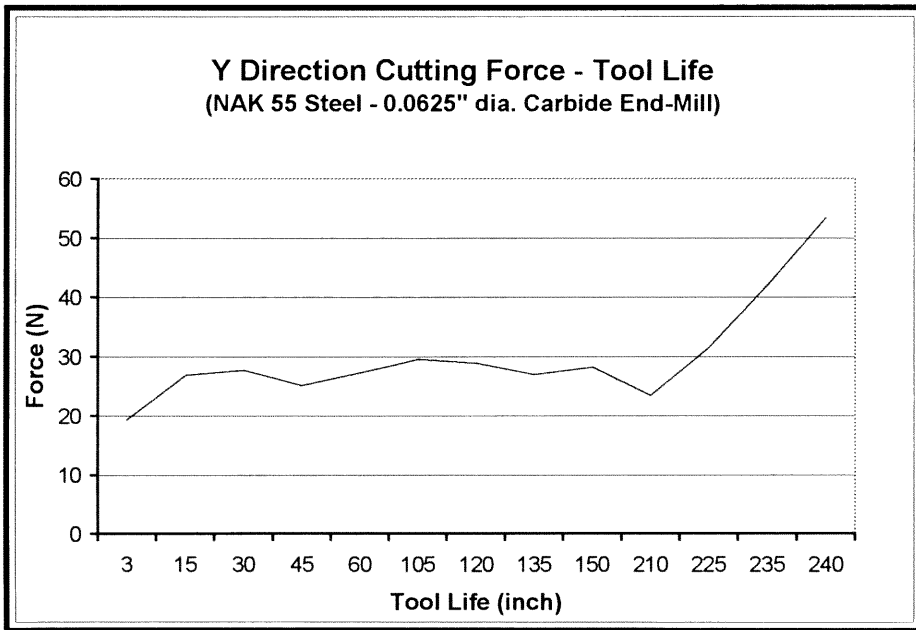
Figure 33.b. Feed Direction Cutting Force Variation with Tool Usage on NAK 55 Steel
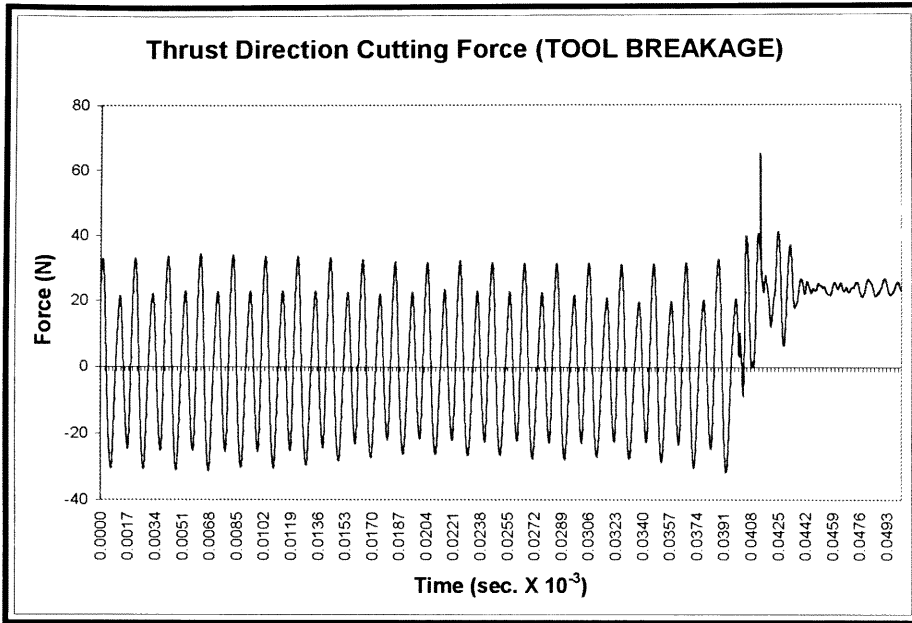
Figure 34.a. Thrust Direction Cutting Force of 1/16" Diameter Carbide End-Mill
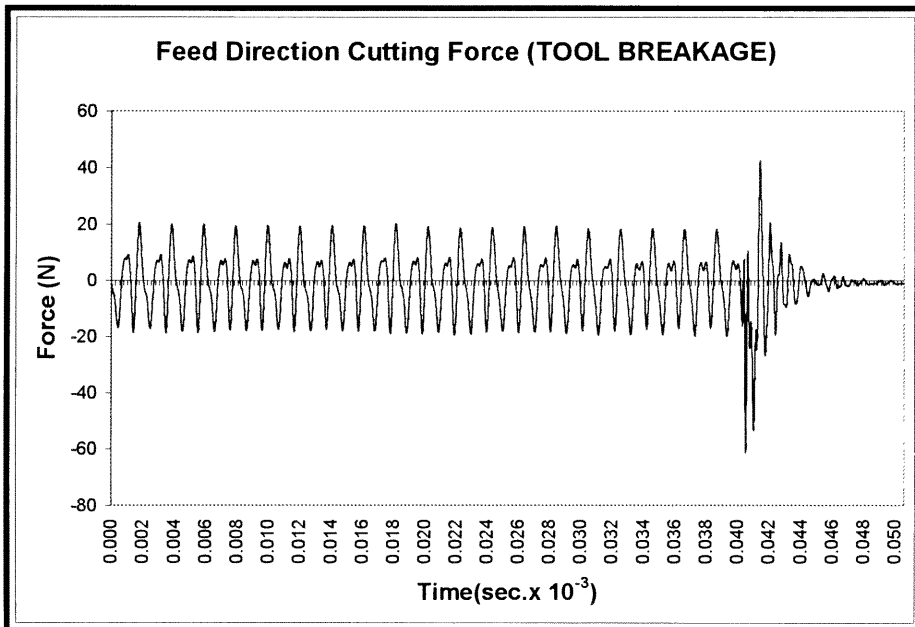
(Tool Breakage)

Figure 34.b. Feed Direction Cutting Force of 1/16" Diameter Carbide End-Mill

(Tool Breakage)

74
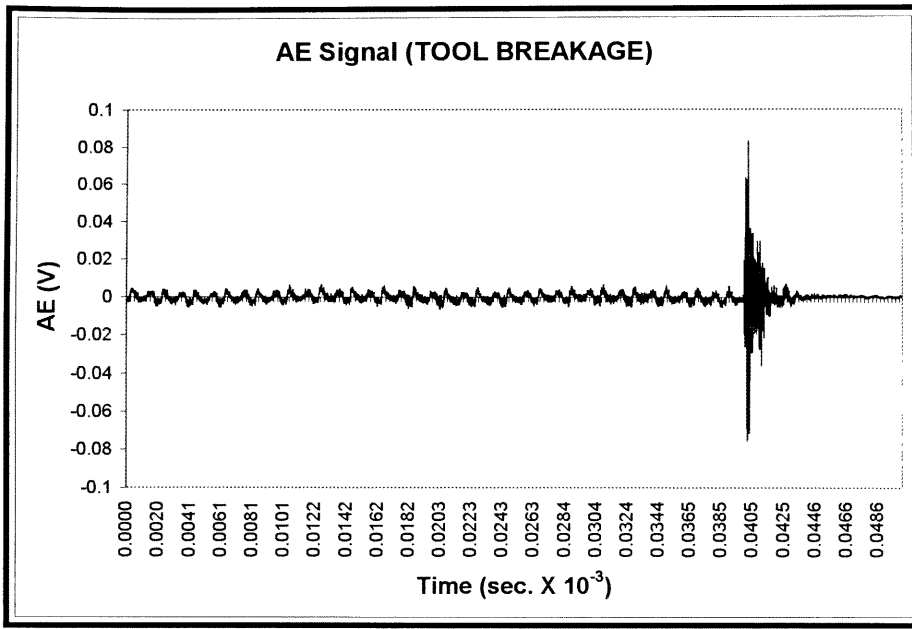
Figure 35.a. Acoustic Emission Signal of 1/16" Diameter Carbide End-Mill
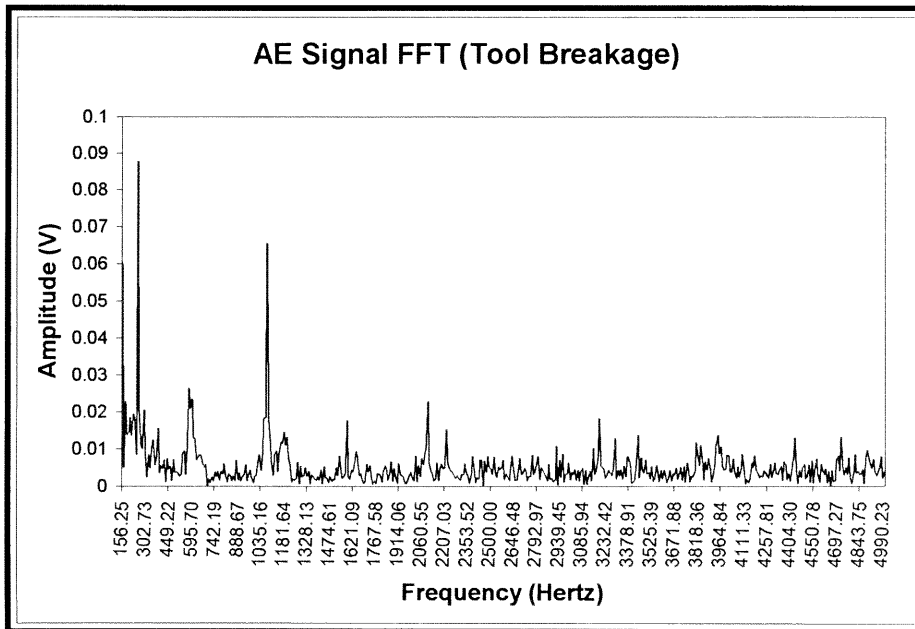
(Tool Breakage)

Figure 35.b. FFT of the Acoustic Emission Signal for 1/16" Diameter Carbide End-Mill

(Tool Breakage)

Table 11. Cutting Forces -Tool Life Results in Tool Wear Experiment (NAK 55 Steel)

Cutting Force in Thrust Dir. (N)	Feed Rate 2.5 ipm	Cutting Force in Feed Dir. (N)	Feed Rate 2.5 ipm
Tool Life (inch)	Force	Tool Life (inch)	Force
3	37.05	3	19.35
15	43.1	15	26.85
30	28.25	30	27.7
45	26.65	45	25.2
60	25.8	60	27.25
105	30.5	105	29.5
120	32.75	120	28.95
135	29.6	135	27
150	37.15	150	28.25
210	29.85	210	23.4
225	37.15	225	31.5
235	43.24	225	42
240	65	240	53.35

NAK 55 Steel workpiece cutting force data was also studied with curve fitting analysis technique to evaluate the trend of the increase in cutting forces. Linear and exponential curve fitting techniques were applied to the data. The results are presented in Figure 36.a., 36.b., 37.a., and 37.b. The result of the study showed that linear curve fitted better than the exponential curve. An approximate interpolated cutting force variation equation is obtained from this analysis.

Also, the experiment was repeated with 0.030 inches diameter carbide end-mill. The trend of the cutting force was the same.
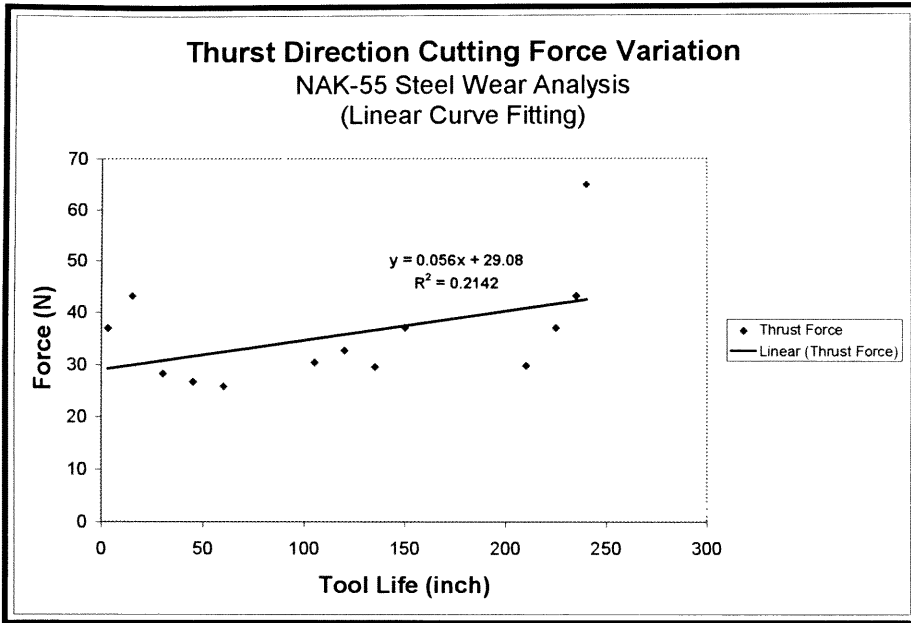
Figure 36.a. Linear Curve Fitting to the Experimental Thrust Direction Cutting Force
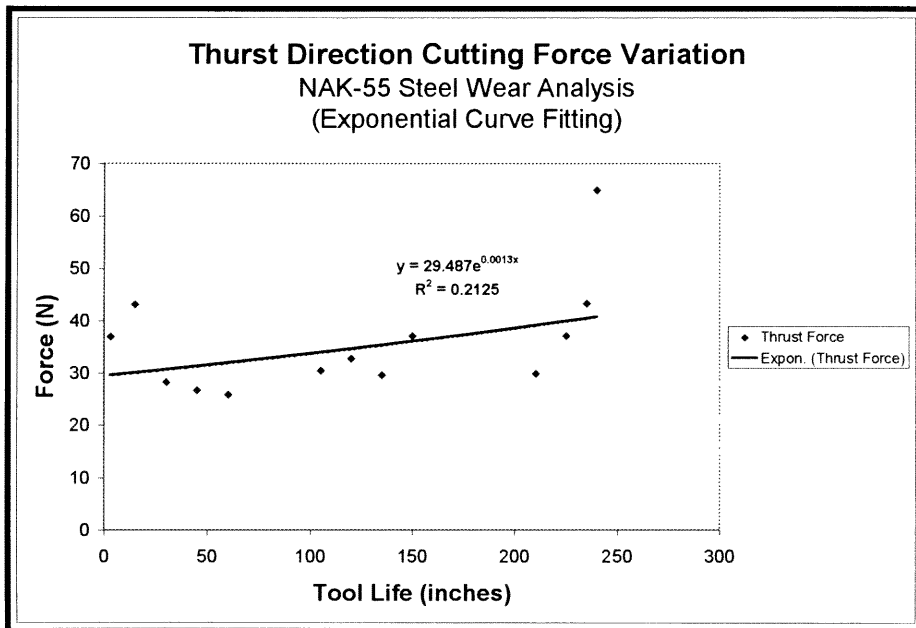
(NAK 55 Steel)

Figure 36.b. Exponential Curve Fitting to the Experimental Thrust Direction Cutting Force
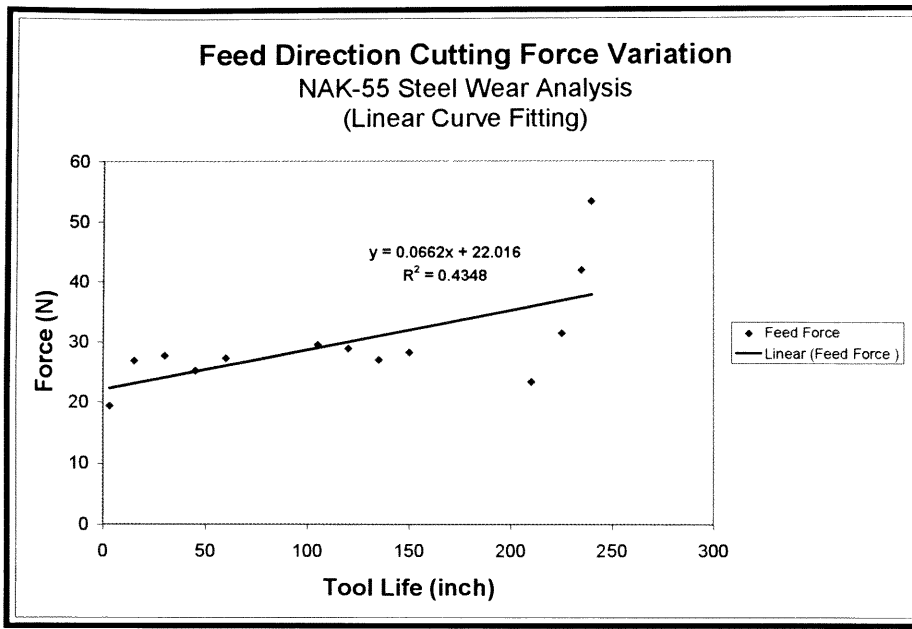
(NAK 55 Steel)

Figure 37.a. Linear Curve Fitting to the Experimental Feed Direction Cutting Force
(NAK 55 Steel)
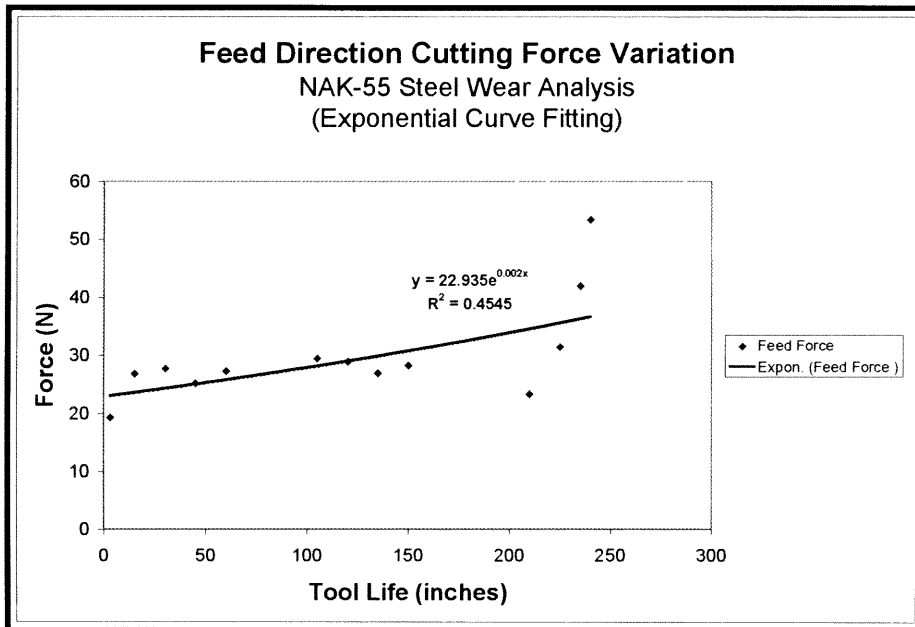
Figure 37.b. Exponential Curve Fitting to the Experimental Feed Direction Cutting Force
(NAK 55 Steel)

V.2. Performance and Reliability of the Neural Network Based Periodic Tool Inspector (N^{2}PTI)

The Neural Network based Periodic Tool Inspector (N^{2}PTI) was introduced to estimate the tool wear in end-milling operations. The proposed method is used to estimate the tool life during the micro end milling of graphite electrodes (POCOEDMC-3), aluminum and steel (NAK 55). The results are presented in the following sections.

Graphite Electrodes (POCOEDMC-3):

The N^{2}PTI requires the tool to cut a test piece, which is attached to a dynamometer. The variation of the feed and thrust direction cutting force is measured while the secondary part is cut. Neural networks estimate the tool's wear from these two inputs. Three different networks are used in this study: Backpropagation NN (ANALOG), Probabilistic NN (BASIC, SEPVAR).

The main workpiece, a POCO-EDM-C3 electrode, and an aluminum test piece are attached on a 9257B three-component Kistler dynamometer. The dynamometer is connected to a charge amplifier. The feed and thrust direction forces were digitized, by using a Nicolet 310 digital oscilloscope. Experimental setup, which was used to collect the training data, was presented in Figure 10.

A 1/16" carbide tool was used to collect the experimental data. The spindle speed was 15,000 rpm. The tool was worn by cutting POCO EDM-C3 electrode material with a 20 inch/min feed rate and 0.030 inch depth of cut. To test the tool condition, an aluminum test piece was cut at 15,000 rpm with a 5 inch/min feed rate and a 0.015-inch depth of cut. Experimental results are listed in Table 12.

The experimentally observed cutting force variation readings are presented in Figure 38 by using bubble diagrams. The size of the bubble corresponds to the tool life. The observed thrust and feed direction force variations are shown on the X and Y axes, respectively. The diagram showed that both of the cutting force variations increased while the tool wore out.

Table 12. Cutting Forces -Tool Life Results in Tool Wear Experiment (0.0625")

Cutting Force in Thrust Dir. (N)	Feed Rate 5 ipm	Cutting Force in Feed Dir. (N)	Feed Rate 5 ipm
Tool Life (inch)	Force	Tool Life (inch)	Force
150	8.6	150	8.5
300	9.05	300	9.325
450	10.725	450	14.475
600	18.95	600	15.225
750	24.5	750	17.05
900	27.15	900	17.725
1050	30.75	1050	18.1
1200	33.3	1200	19.2
1350	35.5	1350	22

TOOL USAGE - CUTTING FORCE RELATIONSHIP
(0.0625" dia Carbide End Mill - POCO EDM-C3 Workpiece)
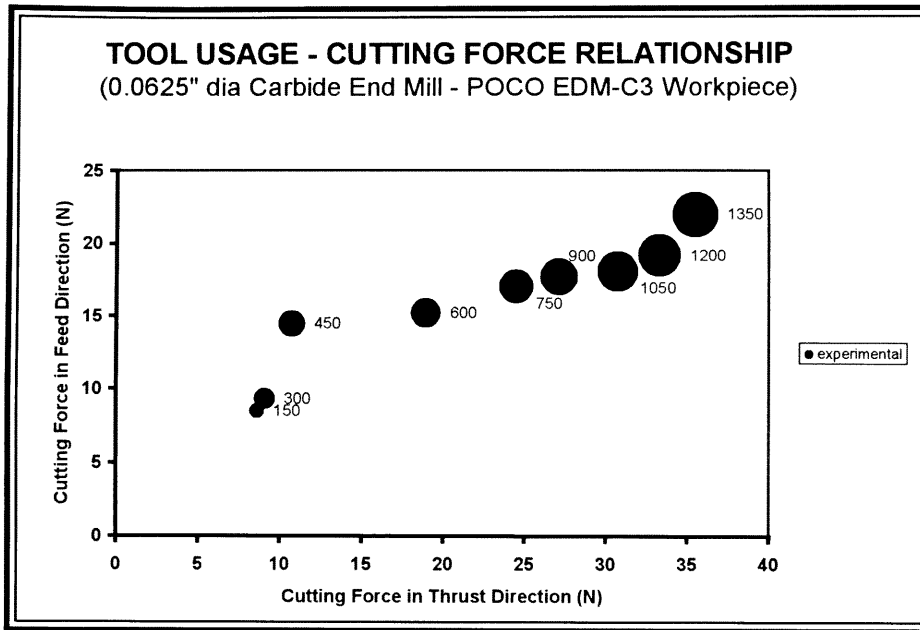
Figure 38.   Tool Usage and Cutting Force Relation – Experimental Test Results

Five cases were given to three different neural networks for training.   One of the networks was a backpropagation type neural network and the other two were Probabilistic Neural Networks (PNN).   The BASIC PNN used single sigma for both inputs.   The SEPVAR used different sigma for each input.   After the training, the neural networks estimated the tool life of the training data (Figure 39) and four other cases they have never seen before (Figure 40). The estimated results are presented in Table 13.

Figure 39.a. Estimated Results of the Training Cases with Analog BP NN

Figure 39.b. Estimated Results of the Training Cases with PNN BASIC

Figure 39.c. Estimated Results of the Training Cases with PNN SEPVAR

Figure 40.a. Estimated Results of the Test Cases with Analog BP NN

83

Figure 40.b.   Estimated Results of the Test Cases with PNN BASIC
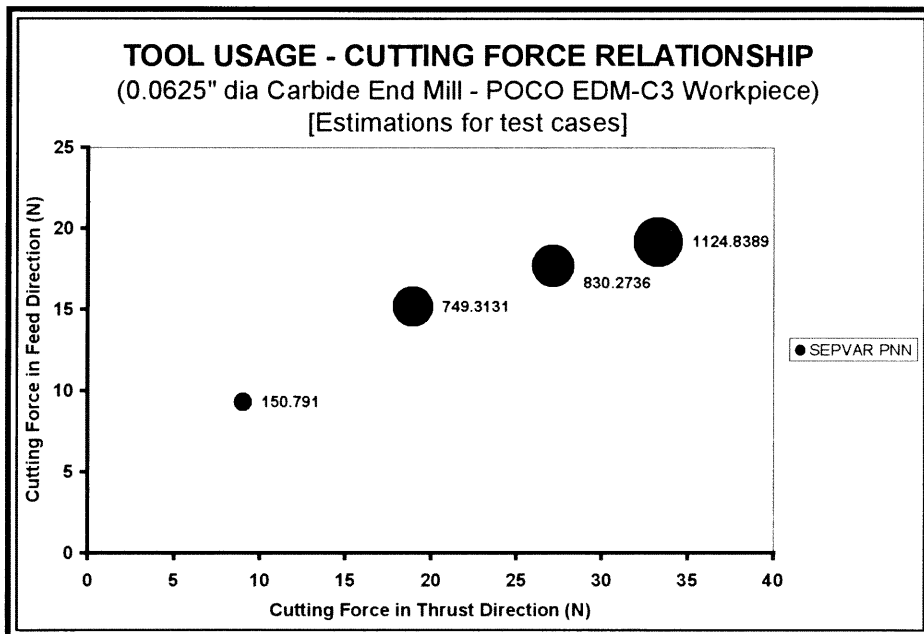
Figure 40.c.   Estimated Results of the Test Cases with PNN SEPVAR

Table 13. Comparison of the Experimental Data and Neural Network Estimation Data

X Direction Force	Y Direction Force	Experimental Tool Life	Analog BP Estimation	Basic PNN Estimation	Sepvar PNN Estimation
8.6	8.5	150	146.845	301.3526	150.0698
9.05	9.325	300	193.192	312.8789	150.791
10.725	14.475	450	406.898	386.0638	449.9302
18.95	15.225	600	545.888	645.3932	749.3131
24.5	17.05	750	757.077	878.1269	750.2033
27.15	17.725	900	876.623	957.7835	830.2736
30.75	18.1	1050	1001.48	1038.8513	1050
33.3	19.2	1200	1142.73	1092.7248	1124.8389
35.5	22	1350	1341.33	1147.0956	1349.7967

The performances of all the networks were very similar. All of them estimated the test cases with acceptable accuracy. The training process of the PNN is almost completely automated and takes much a shorter time than backpropagation. Backpropagation can create much more compact neural networks than PNN and generalizes the given information much more effectively. The performance of the used neural networks and the experimental data was compared and plotted together for training and test cases. (Figure 41)

Figure 41.a.   Estimation Accuracy Comparison of the Three Different Neural Network
with Training Case Cutting Force Data

Figure 41.b.   Estimation Accuracy Comparison of the Three Different Neural Network
with Test Case Cutting Force Data
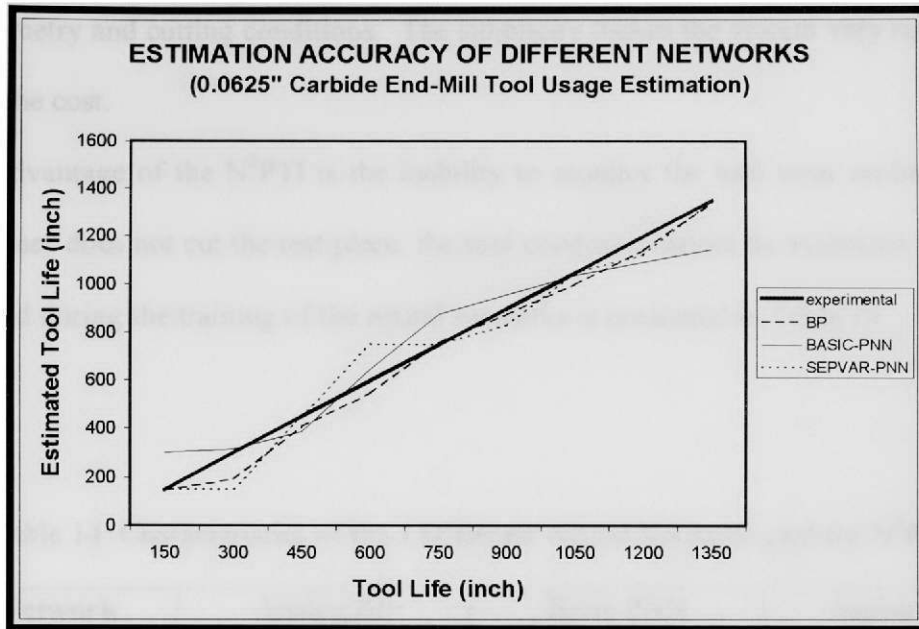
Figure 41.c.   Estimation Accuracy of the Three NN for the Tool Life

It is found that the backpropagation much more reliable in other studies when a small number of training cases were available. In this study two hidden nodes were used for the backpropagation neural network.

The proposed tool wear estimation method is primarily for the machining of non-metals. Although the proposed approach is almost inevitable during the machining of non-metals on conventional machine tools when the machine vibrations create inertia forces larger than the cutting force signals, it can be used for metals to simplify the classification of the force measurements.

The main advantages of the N^2PTI are the simplicity of the data processing and classification. Because the cutting condition is the same, the only factor, which affects the cutting force, is the tool wear. There is no force variation related to a change of the

chip geometry and cutting conditions. The simplicity makes the system very reliable and reduces the cost.

The disadvantage of the N^2PTI is the inability to monitor the tool wear on-line. If the programmer does not cut the test piece, the tool condition cannot be evaluated. The final setup used during the training of the neural networks is presented in Table 14.

Table 14. Characteristics of the 3 Different Neural Network used for N^2PTI

Neural Network	Analog BP	Basic PNN	Sepvar PNN
Input Nodes	2	2	2
Output Nodes	1	1	1
Training Cases	5	5	5
Test Cases	4	4	4
Training Time	11 seconds	1.54 seconds	1.63 seconds
Network Proprieties	2 Hidden Nodes 0.6 Learning Rate 0.9 Momentum	0.0 Sigma Low 5.0 Sigma High 5 Sigma Tries	0.003 Sigma Low 5.0 Sigma High 5 Sigma Tries

The same analysis was repeated by using a carbide end-mill with 0.030 inches diameter. The experimental results are presented in Figure 42. The N^2PTI estimated the tool wear with acceptable accuracy. The measured cutting forces were smaller than the ones recorded with the bigger tool and some deviation existed. The results are presented in Figure 43 and 44 and 45.

Figure 42.   0.030" Tool Usage and Cutting Force Relation – Experimental Test Results
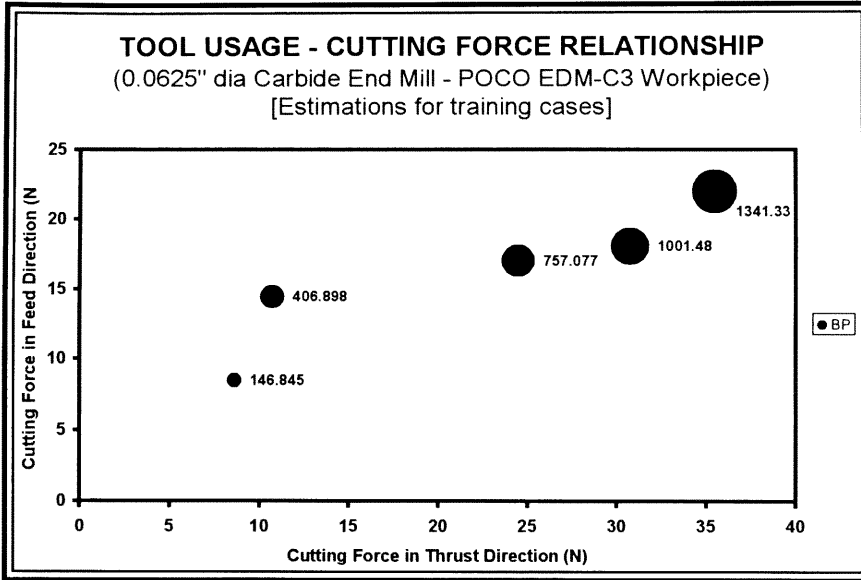

Figure 43.a.   Estimated Results of the Training Cases with Analog BP NN
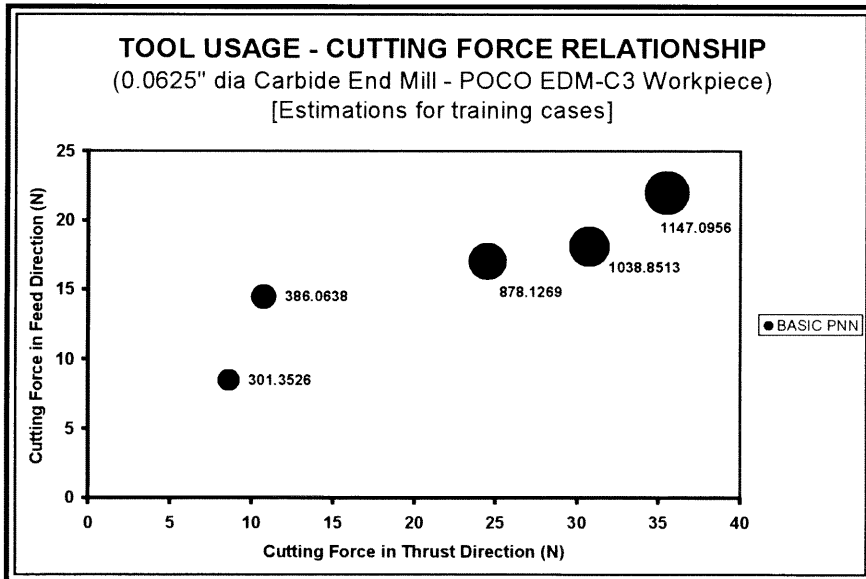
for 0.030" Tool

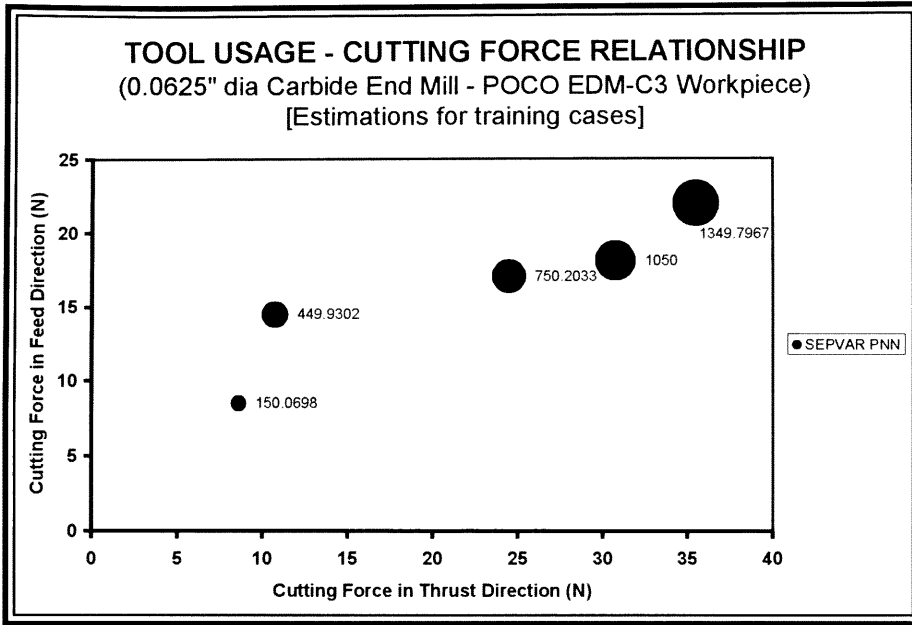Figure 43.b. Estimated Results of the Training Cases with PNN BASIC
for 0.030" Tool

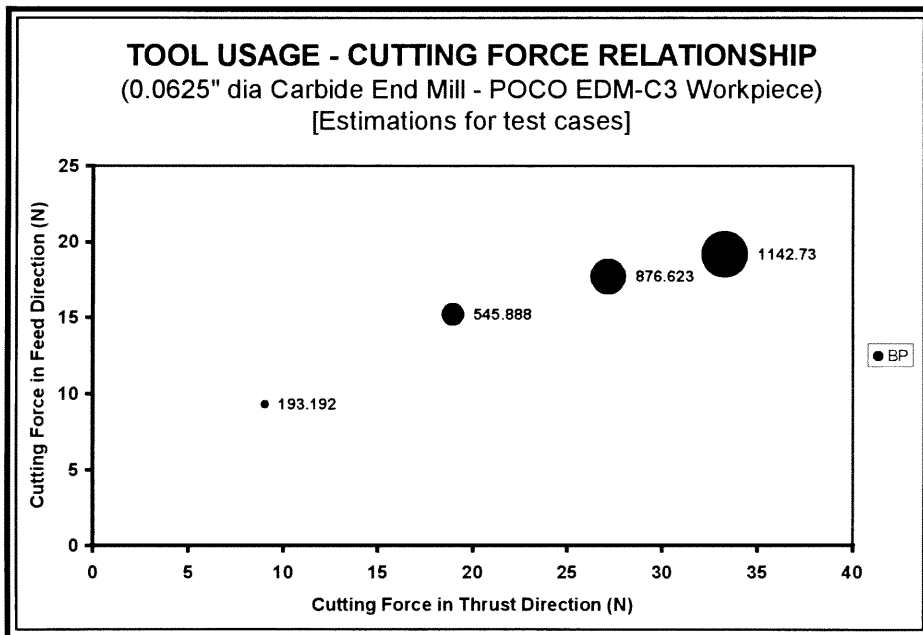Figure 43.c. Estimated Results of the Training Cases with SEPVAR PNN
for 0.030" Tool

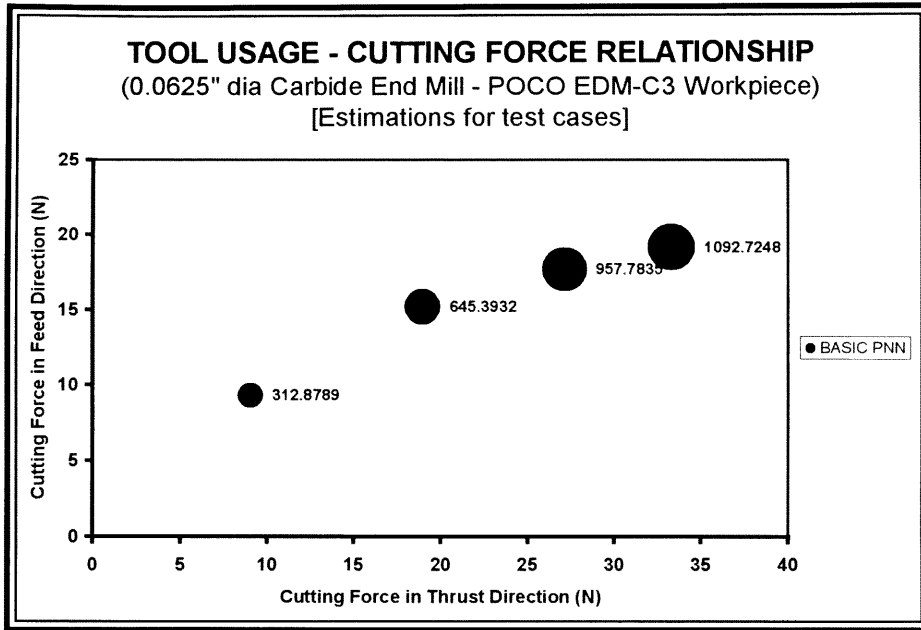Figure 44.a. Estimated Results of the Test Cases with Analog BP NN
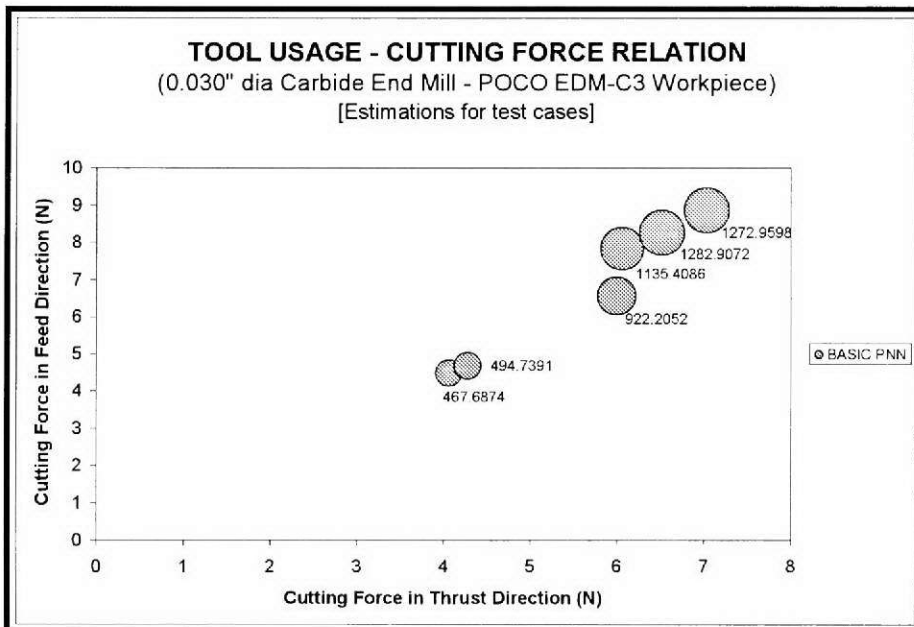
for 0.030" Tool

Figure 44.b. Estimated Results of the Test Cases with BASIC PNN

for 0.030" Tool
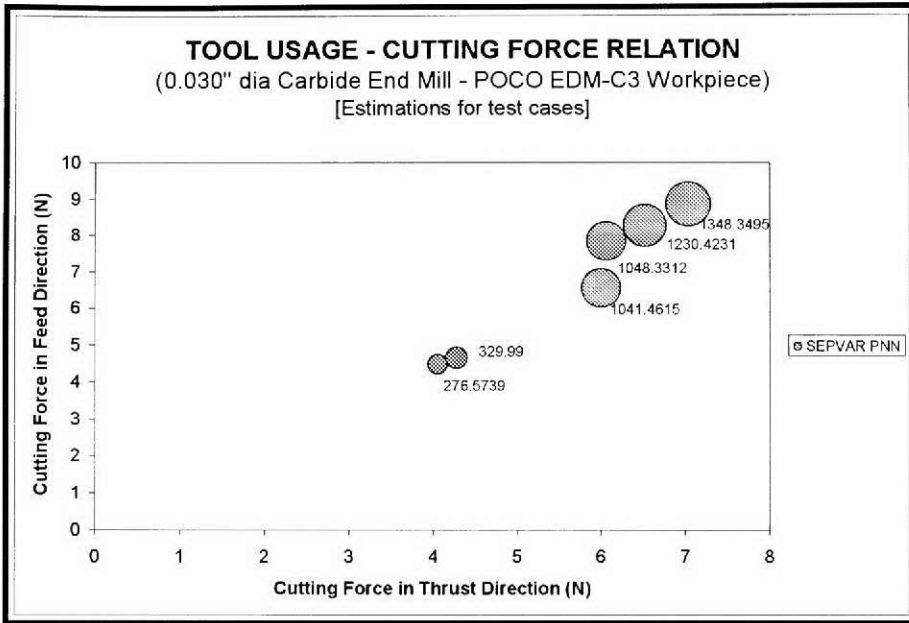
Figure 44.c.   Estimated Results of the Test Cases with SEPVAR PNN

for 0.030" Tool

Figure 45.a.   Estimation Accuracy Comparison of the Three Different Neural Network

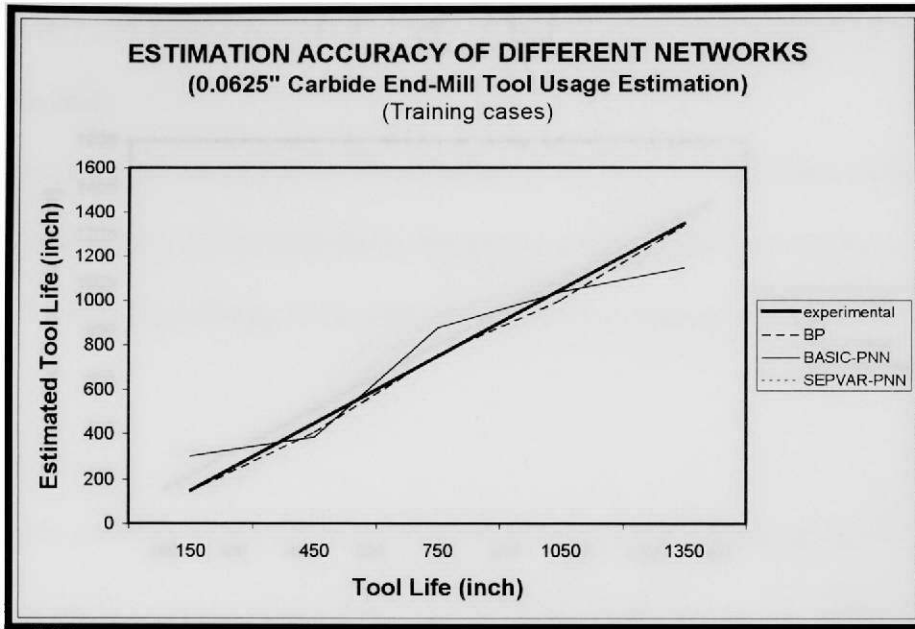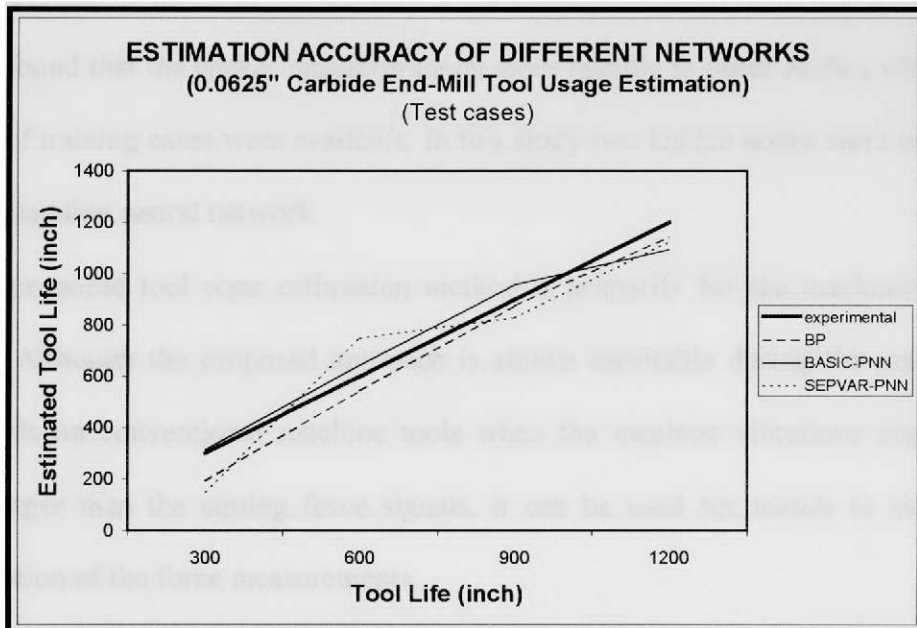with Test Cases Cutting Force Data (0.030" Tool)

Figure 45.b. Estimation Accuracy Comparison of the Three Different Neural Network with Training Cases Cutting Force Data (0030" Tool)
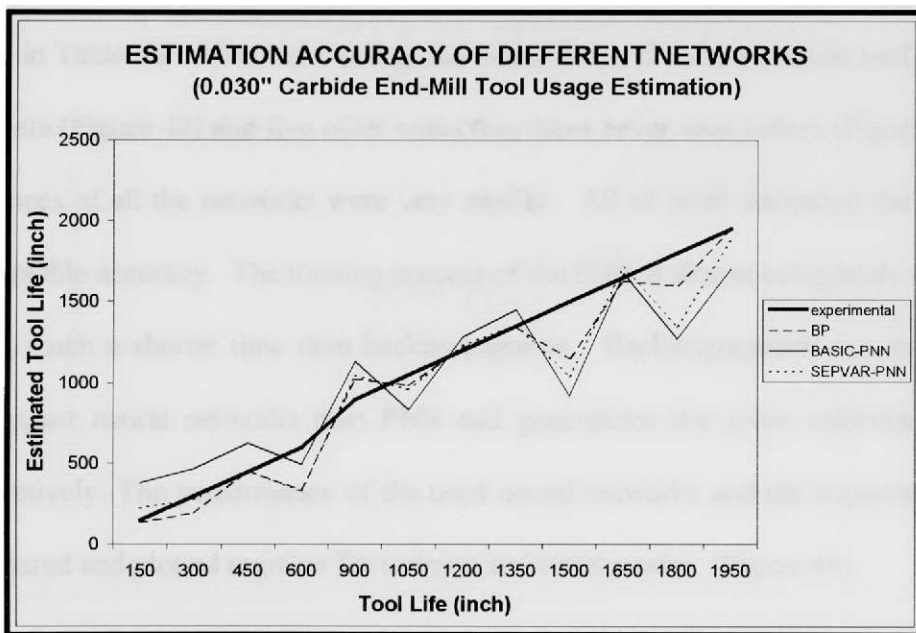
Figure 45.c. Estimation Accuracy of the Three NN for the 0.030" Tool Life

Aluminum:

N^{2}PTI was used to monitor the tool wear during the end milling of the aluminum workpiece. A 1/32" carbide tool was used to collect the experimental data. The spindle speed was 45,000 rpm. The tool was worn by cutting Aluminum workpiece material with a 5 inch/min feed rate and 0.015 inch depth of cut.

The experimentally observed cutting force variation readings are presented in Figure 46 by using bubble diagrams. The size of the bubble corresponds to the tool life. The observed thrust and feed direction force variations are shown on the X and Y axes, respectively. The diagram showed that both of the cutting force variations increased while the tool wore out. Six cases were given to three different neural networks for training. One of the networks was a backpropagation type neural network and the other two were Probabilistic Neural Networks (PNN). The BASIC PNN used single sigma for both inputs. The SEPVAR used different sigma for each input. The final setup used for training is presented in Table 16. After the training, the neural networks estimated the tool life of the training data (Figure 47) and five other cases they have never seen before (Figure 48). The performances of all the networks were very similar. All of them estimated the test cases with acceptable accuracy. The training process of the PNN is almost completely automated and takes much a shorter time than backpropagation. Backpropagation can create much more compact neural networks than PNN and generalizes the given information much more effectively. The performance of the used neural networks and the experimental data was compared and plotted together for training and testing cases. (Figure 49)
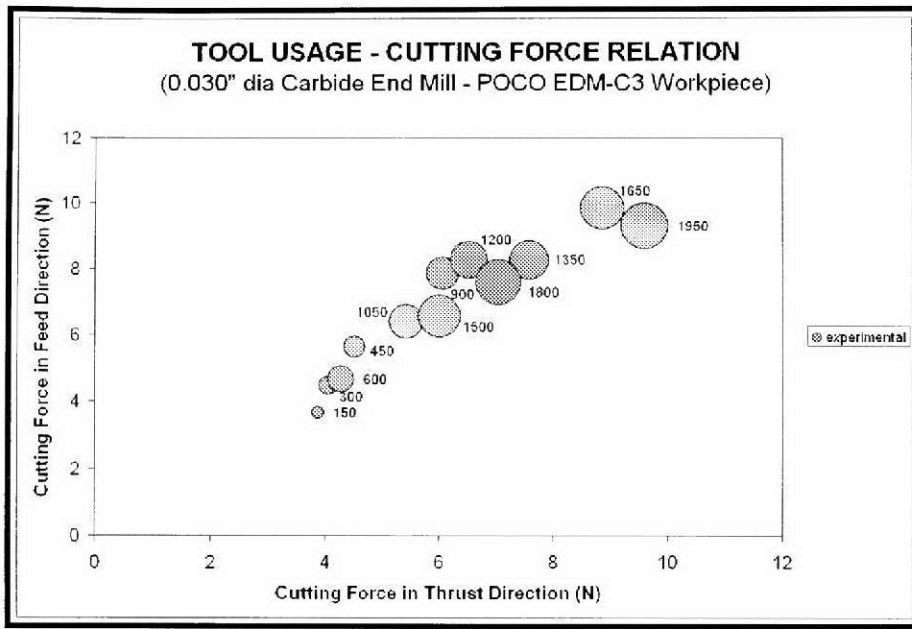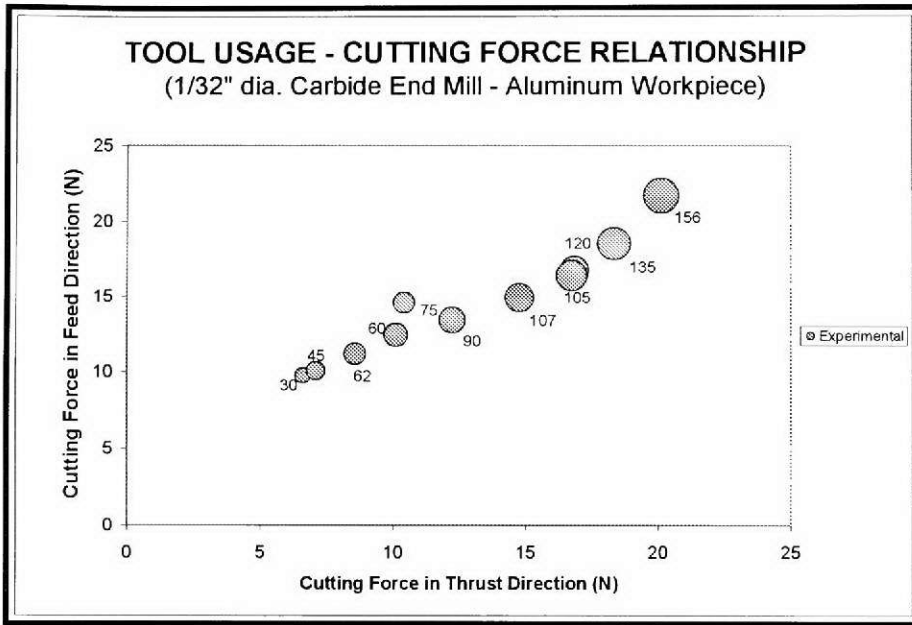
Figure 46.   Tool Usage and Cutting Force Relation for Aluminum – Experimental Results
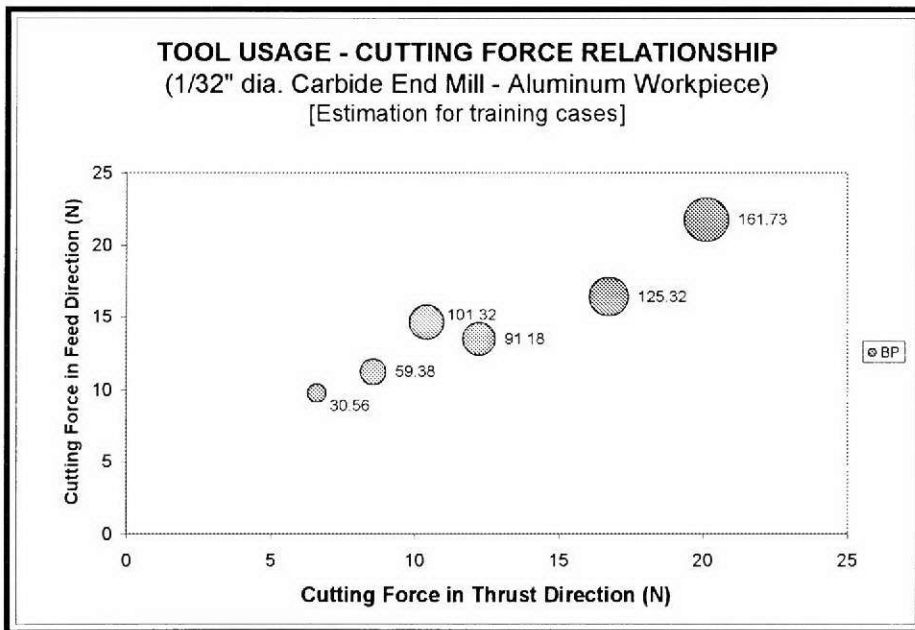
Figure 47.a.   Estimated Results of the Training Cases with Analog BP NN for Aluminum
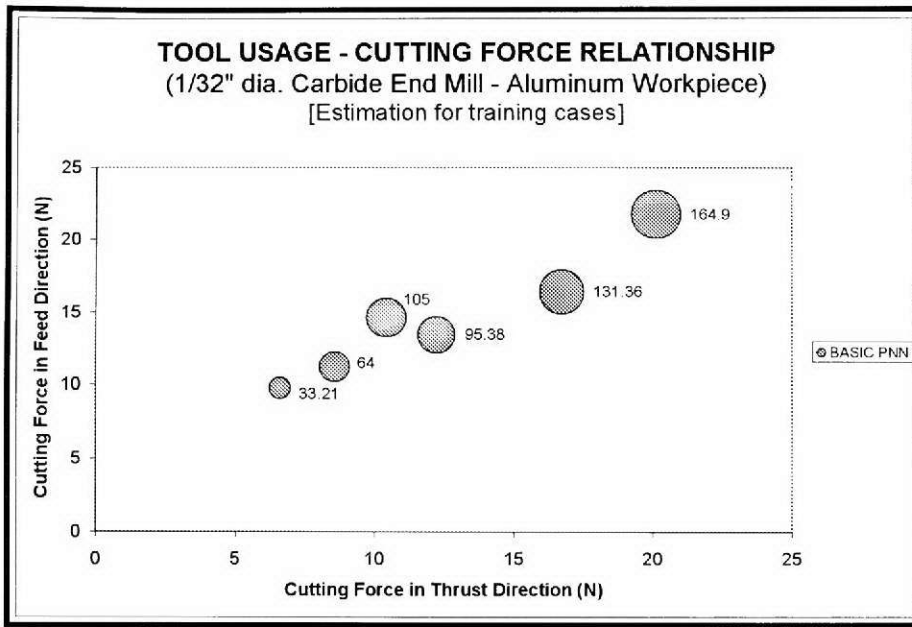
Figure 47.b.   Estimated Results of the Training Cases with PNN BASIC for Aluminum
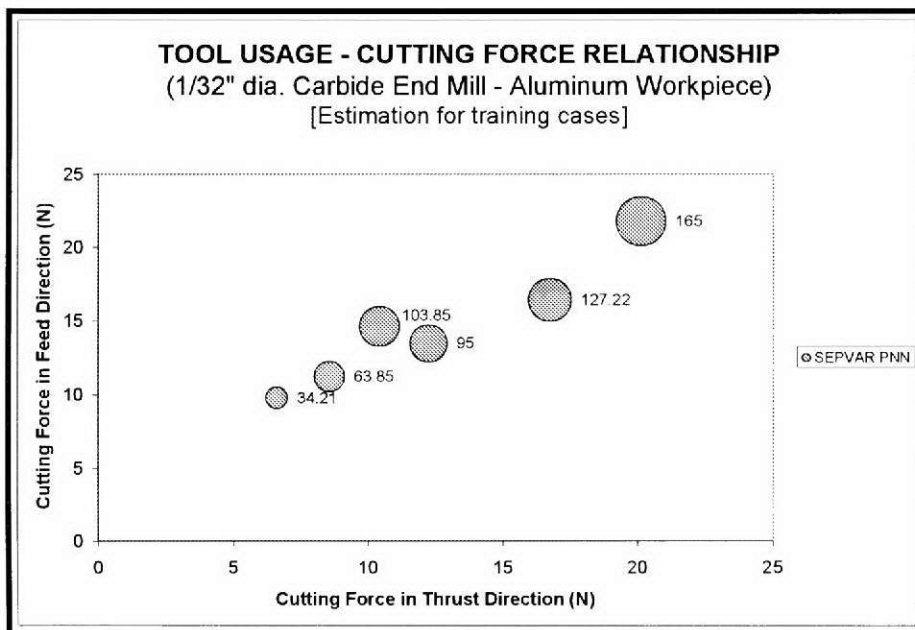
Figure 47.c.   Estimated Results of the Training Cases with PNN SEPVAR for Aluminum
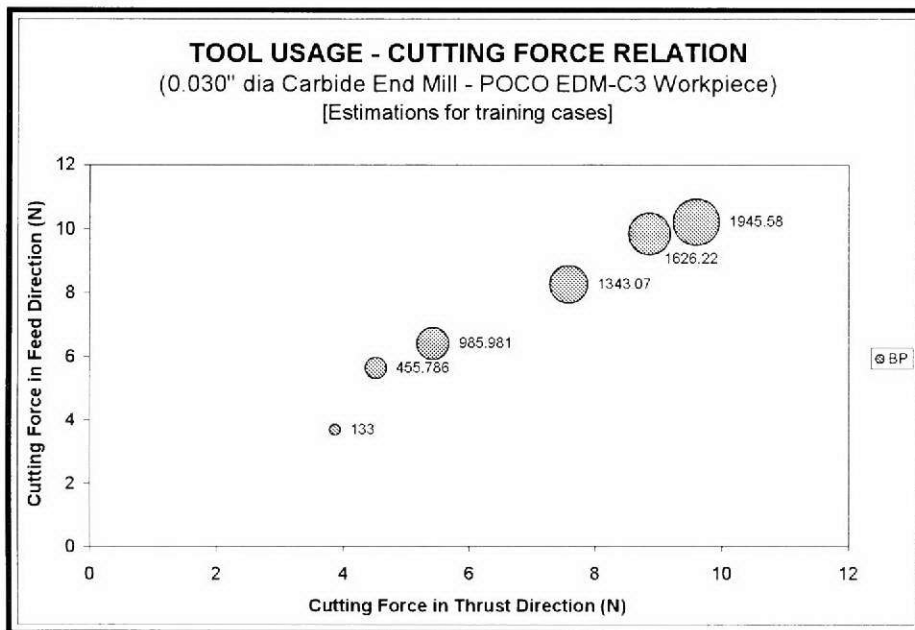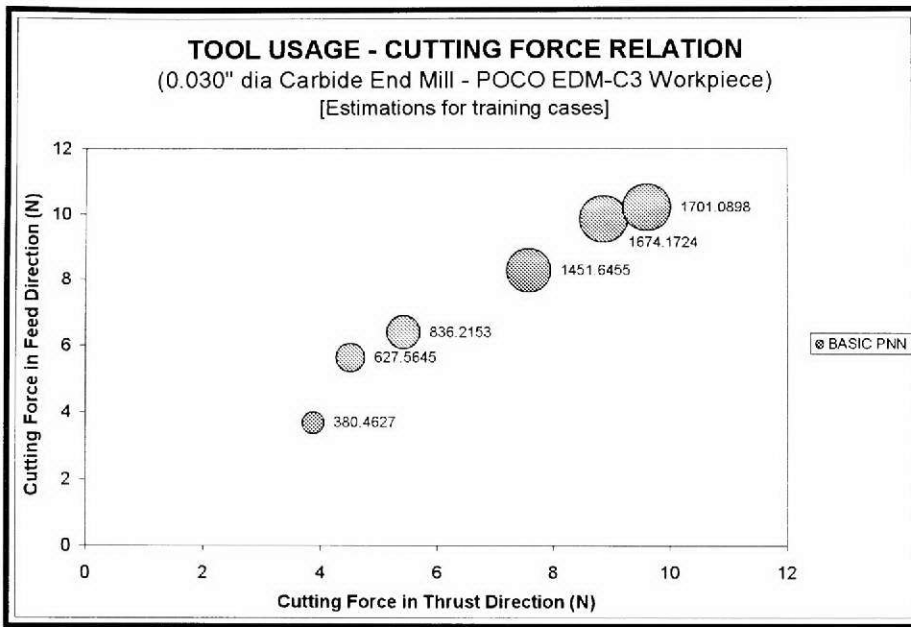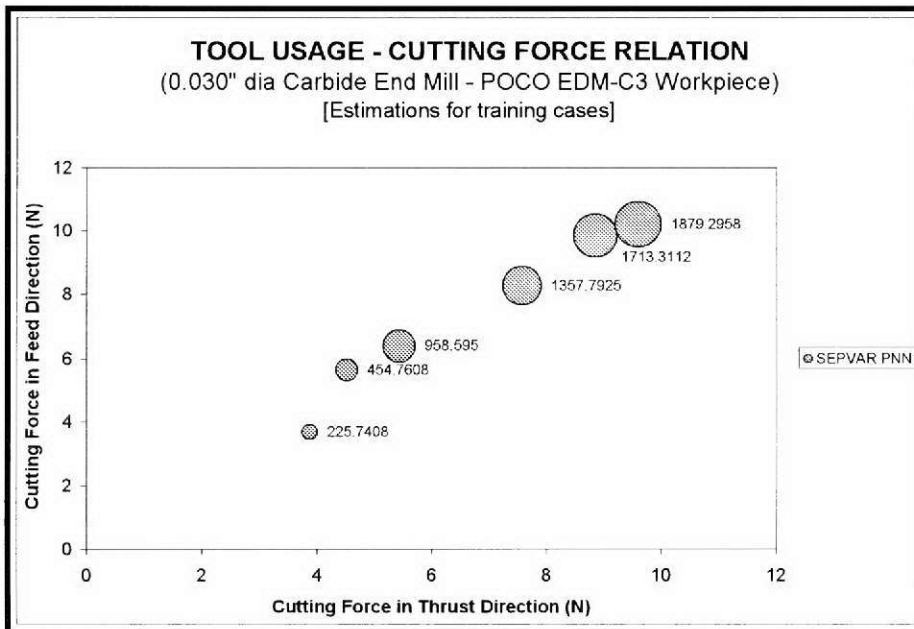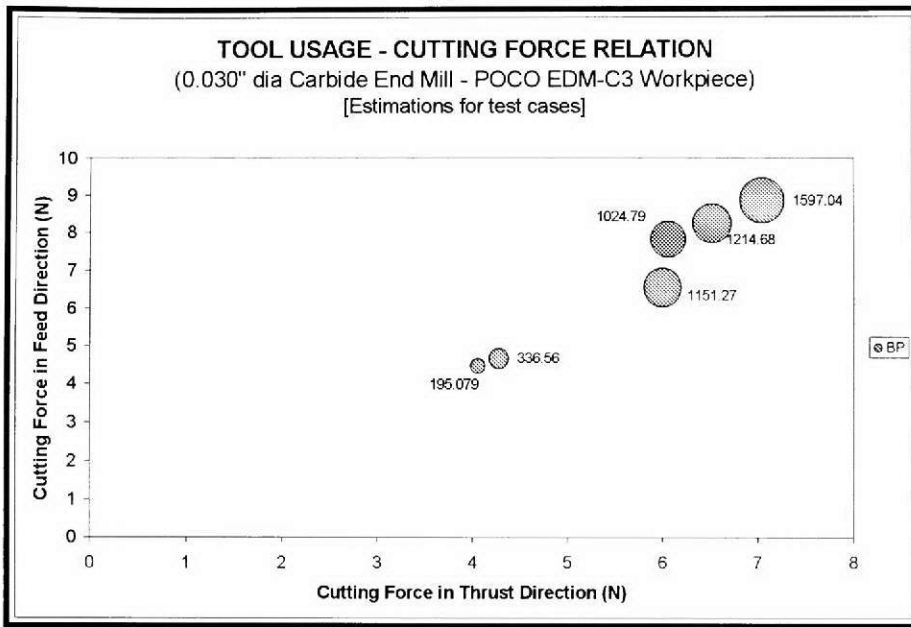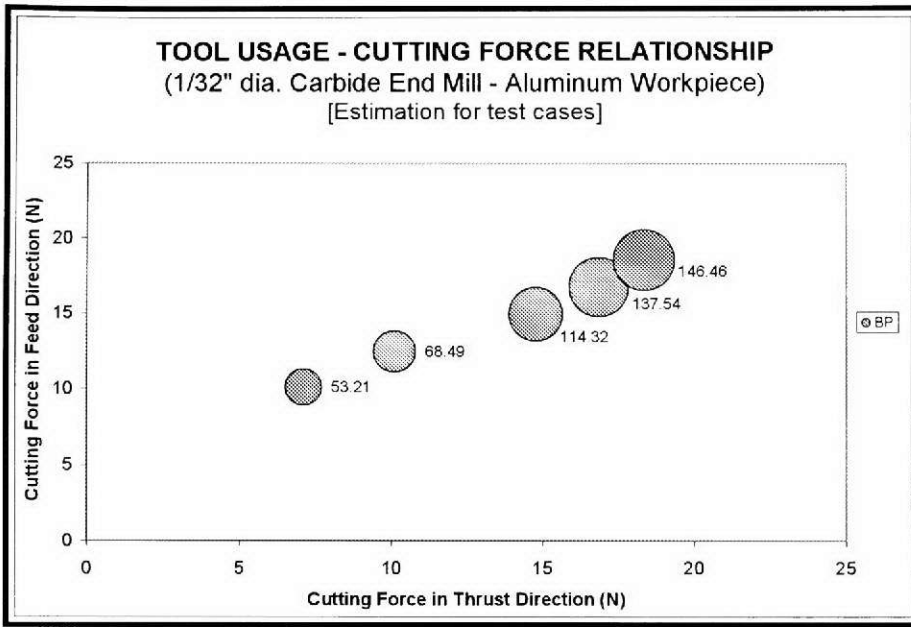
Figure 48.a.   Estimated Results of the Test Cases with Analog BP NN for Aluminum
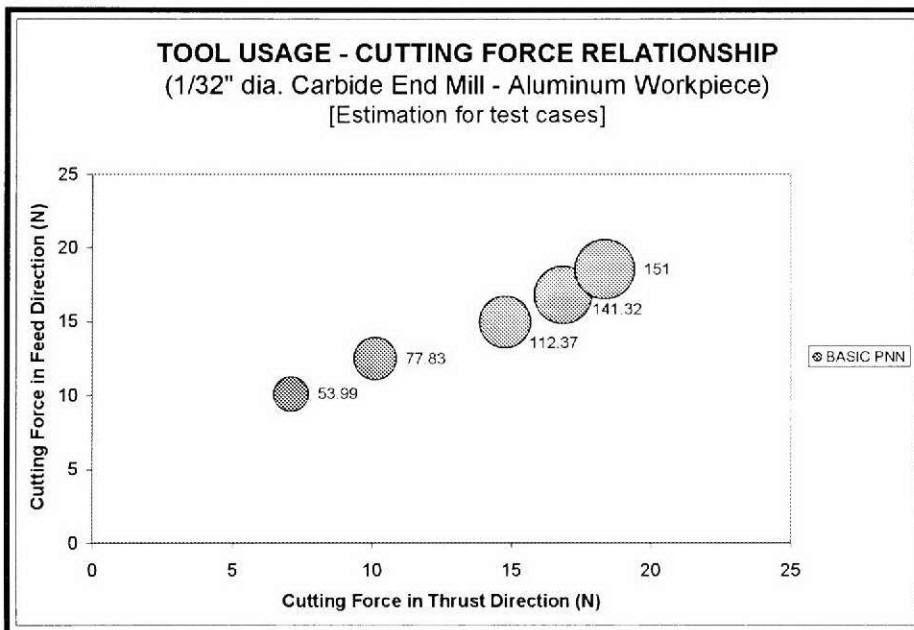
Figure 48.b.   Estimated Results of the Test Cases with PNN BASIC for Aluminum
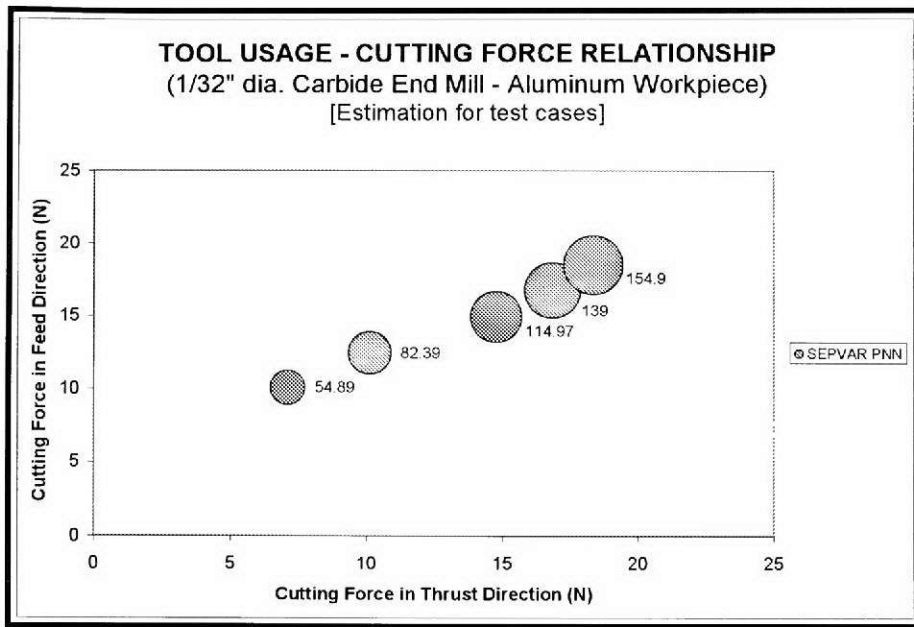
Figure 48.c.   Estimated Results of the Test Cases with PNN SEPVAR for Aluminum

Table 15.   Comparison of the Experimental Data and Neural Network Estimation Data

X Direction Force	Y Direction Force	Experimental Tool Life	Analog BP Estimation	Basic PNN Estimation	Sepvar PNN Estimation
6.6	9.78	30	30.56	33.21	34.21
7.1	10.11	45	53.21	53.99	54.89
10.42	14.62	60	101.32	105	103.85
8.56	11.23	62	59.38	64	63.85
10.11	12.5	75	68.49	77.83	82.39
12.23	13.47	90	91.18	95.38	95
16.86	16.78	105	137.54	141.32	139
14.78	14.96	107	114.32	112.37	114.97
16.74	16.41	120	125.32	131.36	127.22
18.35	18.54	135	146.46	151	154.9
20.13	21.75	156	161.73	164.9	165
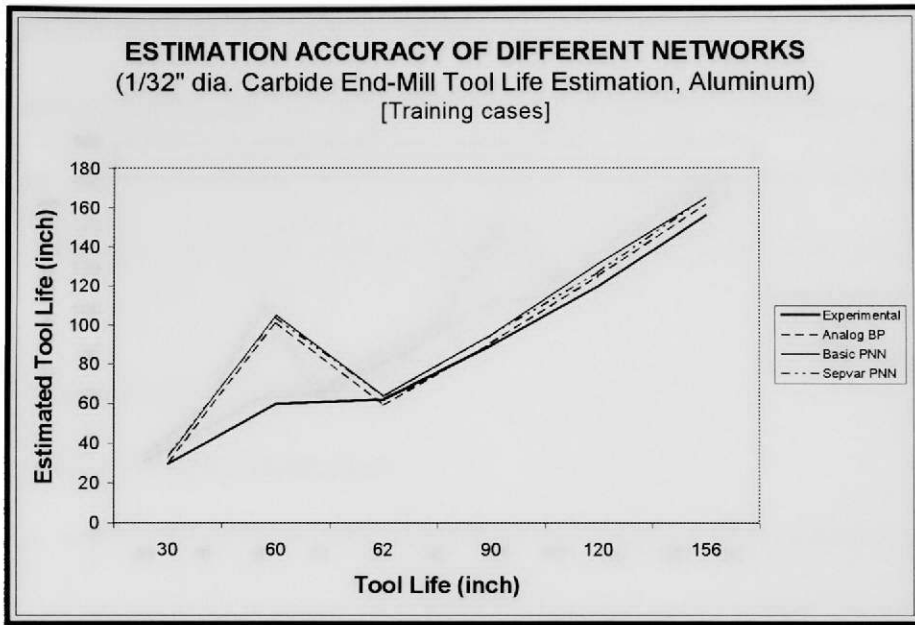
Figure 49.a.   Estimation Accuracy Comparison of the Three Different Neural Network

with Training Case Cutting Force Data
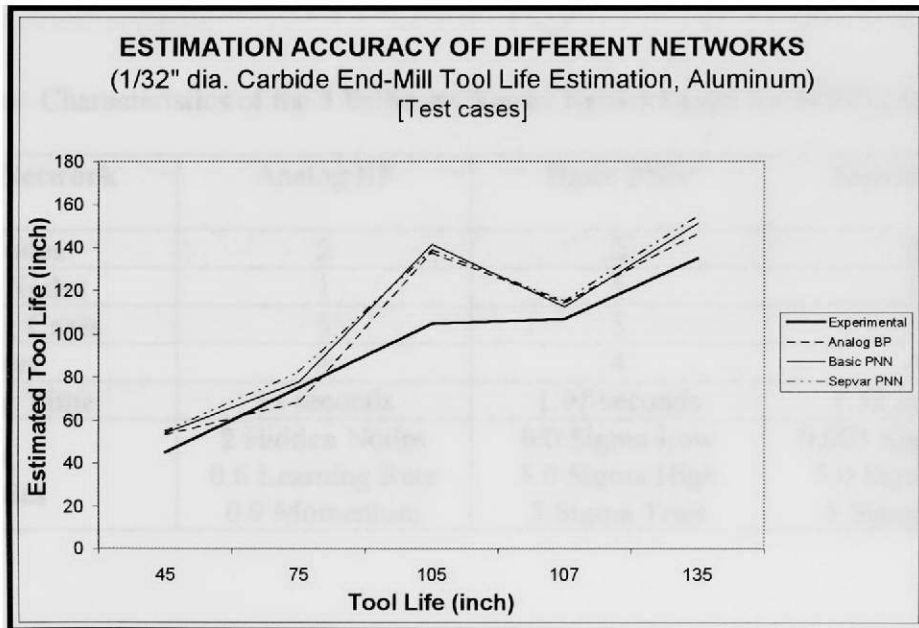
Figure 49.b.   Estimation Accuracy Comparison of the Three Different Neural Network

with Training Case Cutting Force Data
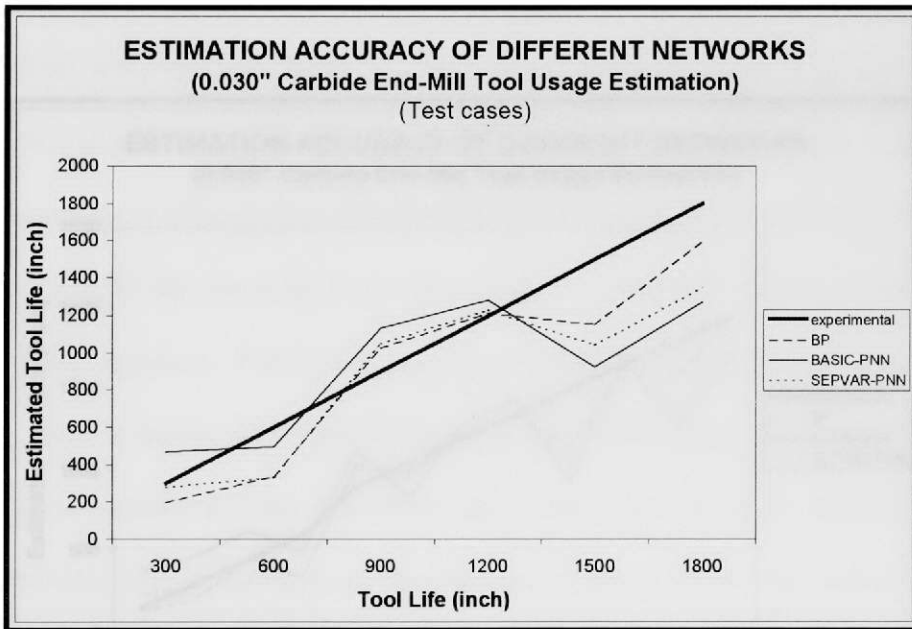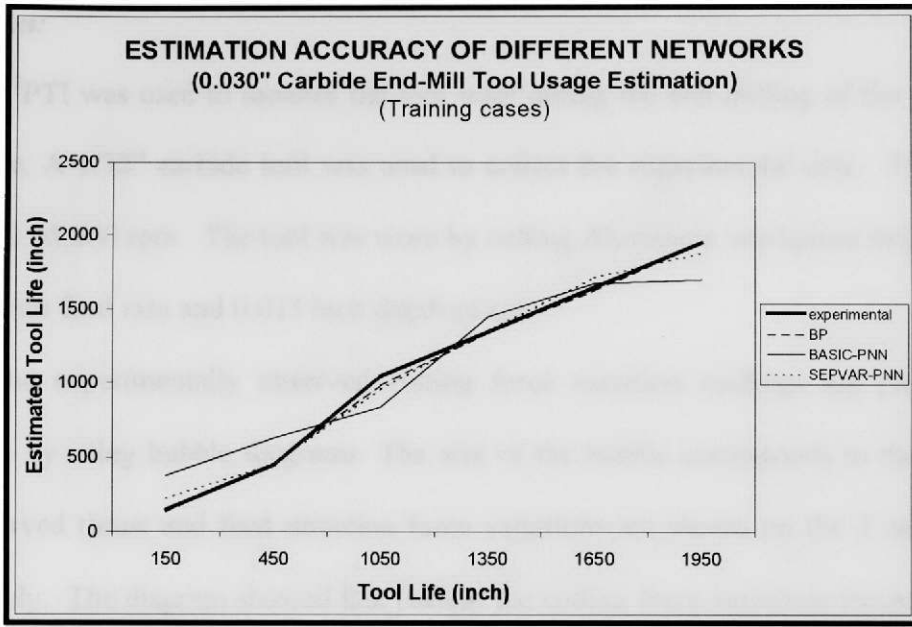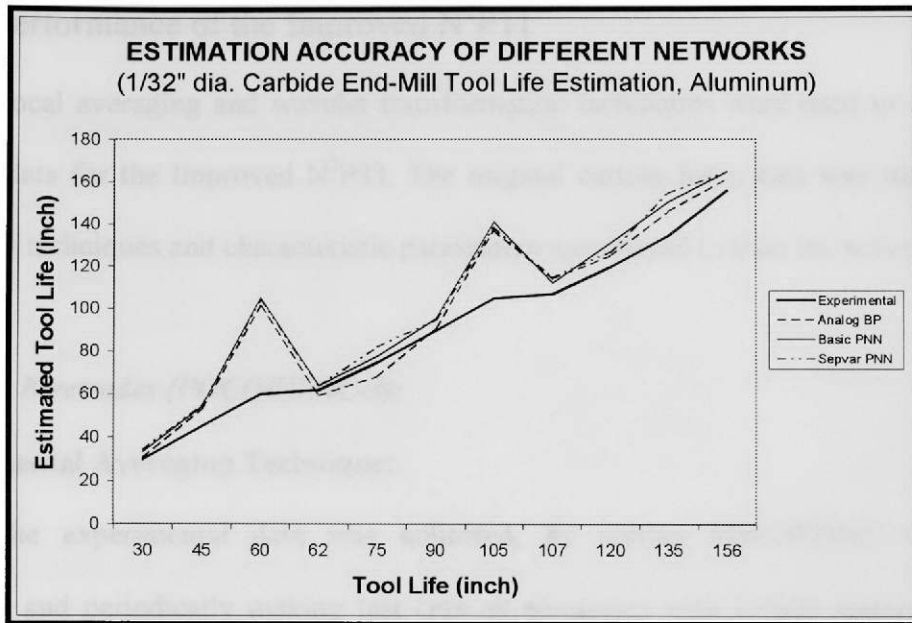
Figure 49.c. Estimation Accuracy Comparison of the Three Different Neural Network for

Tool Life

Table 16. Characteristics of the 3 Different Neural Network used for N^2PTI (Aluminum)

Neural Network	Analog BP	Basic PNN	Sepvar PNN
Input Nodes	2	2	2
Output Nodes	1	1	1
Training Cases	5	5	5
Test Cases	4	4	4
Training Time	13 seconds	1.91 seconds	1.52 seconds
Network Proprieties	2 Hidden Nodes 0.6 Learning Rate 0.9 Momentum	0.0 Sigma Low 5.0 Sigma High 5 Sigma Tries	0.003 Sigma Low 5.0 Sigma High 5 Sigma Tries

V.3. Performance of the Improved N^2PTI

Local averaging and wavelet transformation techniques were used to obtain the training data for the Improved N^2PTI. The original cutting force data was studied with these two techniques and characteristic parameters were found to train the networks.

Graphite Electrodes (POCOEDMC-3):

- **Segmental Averaging Technique:**

The experimental data was collected, by cutting POCOEDMC-3 graphite electrode and periodically making test cuts on aluminum with 0.0625 inches diameter carbide end-mill. The spindle speed for the experiment was 15,000 rpm. Data was collected with 20 μs sampling. In this case, there are 200 data points in each revolution. With the local averaging technique, for each case, 20 input values were presented to the Neural Network training.

The neural network was trained with 20 input nodes and 1 output node. The output node was tool life obtained during the wear analysis for POCOEDMC-3. The network was trained on 40 cases and tested on 30 different cases. Backpropagation and Probabilistic neural networks were used. Analog BP, Basic PNN and Sepvar PNN were trained with the normalized data. The final settings of the NN are listed in Table 17.

Table 17. Characteristics of the 3 Different Neural Network used for Improved N^2PTI (Segmental Averaging)

Neural Network	Analog BP	Basic PNN	Sepvar PNN
Input Nodes	20	20	20
Output Nodes	1	1	1
Training Cases	40	40	40
Test Cases	30	30	30
Training Time	121.56 seconds	12.3 seconds	11.4 seconds
Network Proprieties	10 Hidden Nodes 0.6 Learning Rate 0.9 Momentum	0.0 Sigma Low 5.0 Sigma High 5 Sigma Tries	0.003 Sigma Low 5.0 Sigma High 5 Sigma Tries

The results obtained after the training is represented below. Table 18 shows the estimated values for the training cases and Table 19 shows the testing cases.

The best estimations were obtained with Analog BP and results for each case are presented in Figure 50.

The improved N^2PTI gave less accurate estimation than the N^2PTI, however the new approach eliminated the influence of the depth of cut by the normalization of the data. The estimation results were still in the acceptable range and error of the estimation is around 10 to 15 % approximately.

Table 18. Estimation for the Training data (POCOEMDC-3) after the training of 3 NN

(Segmental Averaging Technique)

	Real Data	Analog BP	Basic PNN	Sepvar PNN	Analog Error %	Basic Error %	Sepvar Error %
Case 1	450	478.71	230.12	300.25	6.38	48.86	33.28
Case 2	450	475.54	200.73	304.22	5.68	55.39	32.40
Case 3	450	491.21	220	310.78	9.16	51.11	30.94
Case 4	450	478.23	214.92	313.32	6.27	52.24	30.37
Case 5	450	499.12	245.67	304.57	10.92	45.41	32.32
Case 6	450	474.32	267.75	311	5.40	40.50	30.89
Case 7	450	512.76	289.43	313.43	13.95	35.68	30.35
Case 8	450	501.28	287.84	321.15	11.40	36.04	28.63
Case 9	450	503.89	301.12	319.43	11.98	33.08	29.02
Case 10	450	489.72	299.54	317.43	8.83	33.44	29.46
Case 1	750	812.33	999.76	875	8.31	33.30	16.67
Case 2	750	801.21	998	875.36	6.83	33.07	16.71
Case 3	750	799.18	998.15	879.12	6.56	33.09	17.22
Case 4	750	784.82	995.32	877.34	4.64	32.71	16.98
Case 5	750	802.36	995.46	881.23	6.98	32.73	17.50
Case 6	750	811.2	989.01	885	8.16	31.87	18.00
Case 7	750	803.74	987.32	882.9	7.17	31.64	17.72
Case 8	750	788.33	985.43	884.38	5.11	31.39	17.92
Case 9	750	793.21	982.32	890	5.76	30.98	18.67
Case 10	750	806.85	980.26	885.43	7.58	30.70	18.06
Case 1	1050	905.37	1154.78	1190.54	13.77	9.98	13.38
Case 2	1050	907.89	1155	1196.47	13.53	10.00	13.95
Case 3	1050	905.38	1158.35	1195.32	13.77	10.32	13.84
Case 4	1050	910.77	1159.43	1189.34	13.26	10.42	13.27
Case 5	1050	930.23	1154.32	1199.65	11.41	9.94	14.25
Case 6	1050	927.45	1160	1195.39	11.67	10.48	13.85
Case 7	1050	932.12	1158.93	1200	11.23	10.37	14.29
Case 8	1050	940.16	1161.35	1201.12	10.46	10.60	14.39
Case 9	1050	935.69	1158.11	1194.21	10.89	10.30	13.73
Case 10	1050	927.91	1154.34	1200.43	11.63	9.94	14.33
Case 1	1350	1391.21	1478.95	1423.54	3.05	9.55	5.45
Case 2	1350	1400.12	1480	1434.55	3.71	9.63	6.26
Case 3	1350	1364.32	1487.32	1430.26	1.06	10.17	5.95
Case 4	1350	1373.98	1475.55	1427.59	1.78	9.30	5.75
Case 5	1350	1343.56	1477.53	1435.21	0.48	9.45	6.31
Case 6	1350	1366.37	1485.44	1439	1.21	10.03	6.59
Case 7	1350	1400	1489.59	1428.3	3.70	10.34	5.80
Case 8	1350	1458.74	1490.78	1425	8.05	10.43	5.56
Case 9	1350	1402.21	1492.96	1422	3.87	10.59	5.33
Case 10	1350	1383.73	1489	1423.45	2.50	10.30	5.44

Table 19. Estimation for the Testing data (POCOEDMC-3) after the training of 3 NN
(Segmental Averaging Technique)

	Real Data	Analog BP	Basic PNN	Sepvar PNN	Analog Error %	Basic Error %	Sepvar Error %
Case 1	600	720.62	890.45	910.15	20.10	48.41	51.69
Case 2	600	719.34	885	900.13	19.89	47.50	50.02
Case 3	600	715.63	887.59	902.44	19.27	47.93	50.41
Case 4	600	713.23	891.26	905	18.87	48.54	50.83
Case 5	600	712.11	895.27	902.89	18.69	49.21	50.48
Case 6	600	711	884.43	899.18	18.50	47.41	49.86
Case 7	600	710.96	883.17	893.24	18.49	47.20	48.87
Case 8	600	709.99	885.38	892.32	18.33	47.56	48.72
Case 9	600	710.55	890	897.93	18.43	48.33	49.66
Case 10	600	711.67	887.77	899	18.61	47.96	49.83
Case 1	900	1055	1234.32	1225.32	17.22	37.15	36.15
Case 2	900	1057.21	1230.11	1229.67	17.47	36.68	36.63
Case 3	900	1048.19	1229.93	1230	16.47	36.66	36.67
Case 4	900	1045.93	1227	1227.88	16.21	36.33	36.43
Case 5	900	1039.19	1229.03	1226.04	15.47	36.56	36.23
Case 6	900	1041	1230	1222	15.67	36.67	35.78
Case 7	900	1037.55	1228.07	1224.06	15.28	36.45	36.01
Case 8	900	1039.93	1229	1223.93	15.55	36.56	35.99
Case 9	900	1042.68	1224.54	1228.67	15.85	36.06	36.52
Case 10	900	1035.12	1125.8	1223.06	15.01	25.09	35.90
Case 1	1200	1368.32	1550.46	1578.75	14.03	29.21	31.56
Case 2	1200	1365	1547	1573.9	13.75	28.92	31.16
Case 3	1200	1367.18	1544.92	1570.34	13.93	28.74	30.86
Case 4	1200	1362.39	1548.39	1569.32	13.53	29.03	30.78
Case 5	1200	1359.41	1547.1	1568.4	13.28	28.93	30.70
Case 6	1200	1370.32	1545	1569	14.19	28.75	30.75
Case 7	1200	1373.95	1543.06	1571.23	14.50	28.59	30.94
Case 8	1200	1364.32	1544.43	1569.03	13.69	28.70	30.75
Case 9	1200	1363.89	1547.9	1573.44	13.66	28.99	31.12
Case 10	1200	1366.77	1546	1568.32	13.90	28.83	30.69
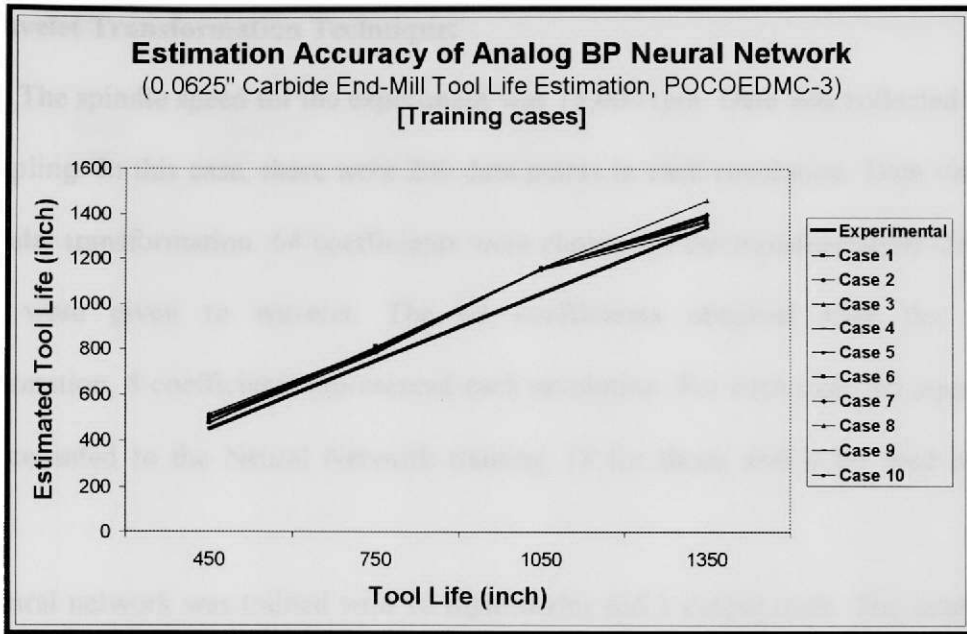
Figure 50.a. Estimation Accuracy of Analog BP for Training Cases with Improved N^2PTI

(Segmental Averaging)
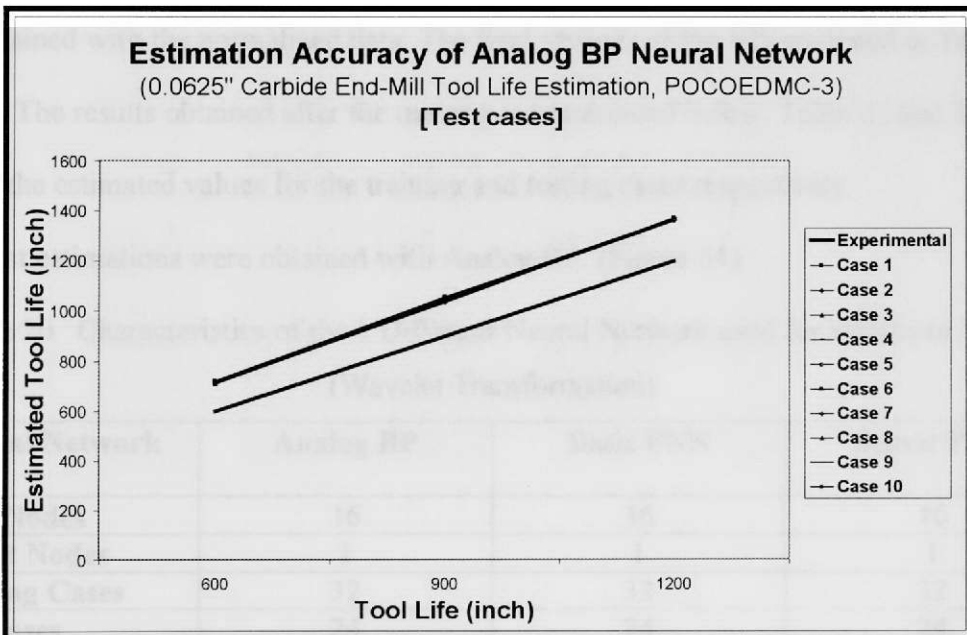
Figure 50.b. Estimation Accuracy of Analog BP for Test Cases with Improved N^2PTI

(Segmental Averaging)

- **Wavelet Transformation Technique:**

The spindle speed for the experiment was 15,000 rpm. Data was collected with 20 μs sampling. In this case, there were 200 data points in each revolution. Data was given to wavelet transformation. 64 coefficients were chosen for the transformation. 2048 data points were given to wavelet. The 64 coefficients obtained after the wavelet transformation, 8 coefficients represented each revolution. For each case, 16 input values were presented to the Neural Network training. (8 for thrust and 8 for feed direction force)

The neural network was trained with 16 input nodes and 1 output node. The output node was the tool life obtained during the wear analysis for POCOEDMC-3. The network was trained on 32 cases and tested on 24 different cases. The use of Backpropagation and Probabilistic neural networks was evaluated. Analog BP, Basic PNN and Sepvar PNN were trained with the normalized data. The final settings of the NN are listed in Table 20.

The results obtained after the training is represented below. Table 21 and Table 22 shows the estimated values for the training and testing cases respectively.

The best estimations were obtained with Analog BP. (Figure 51)

Table 20. Characteristics of the 3 Different Neural Network used for Improved N^2PTI (Wavelet Transformation)

Neural Network	Analog BP	Basic PNN	Sepvar PNN
Input Nodes	16	16	16
Output Nodes	1	1	1
Training Cases	32	32	32
Test Cases	24	24	24
Training Time	156.21 seconds	15.35 seconds	14.21 seconds
Network Proprieties	8 Hidden Nodes 0.6 Learning Rate 0.9 Momentum	0.0 Sigma Low 5.0 Sigma High 5 Sigma Tires	0.003 Sigma Low 5.0 Sigma High 5 Sigma Tires

Table 21. Estimation for the Training data (POCOEMDC-3) after the training of 3 NN
(Wavelet Transformation Technique)

	Real Data	Analog BP	Basic PNN	Sepvar PNN	Analog Error %	Basic Error %	Sepvar Error %
Case 1	450.00	402.34	640.32	303.43	10.59	42.29	32.57
Case 2	450.00	410.24	650.23	305.43	8.84	44.50	32.13
Case 3	450.00	414.32	653.21	311.23	7.93	45.16	30.84
Case 4	450.00	411.31	673.21	315.78	8.60	49.60	29.83
Case 5	450.00	408.56	655.00	306.74	9.21	45.56	31.84
Case 6	450.00	408.37	651.19	311.23	9.25	44.71	30.84
Case 7	450.00	415.32	645.32	317.54	7.71	43.40	29.44
Case 8	450.00	412.75	641.32	325.32	8.28	42.52	27.71
Case 1	750.00	789.43	523.12	923.43	5.26	30.25	23.12
Case 2	750.00	775.00	527.43	928.54	3.33	29.68	23.81
Case 3	750.00	788.43	531.21	925.00	5.12	29.17	23.33
Case 4	750.00	798.32	521.24	927.18	6.44	30.50	23.62
Case 5	750.00	777.23	517.93	921.23	3.63	30.94	22.83
Case 6	750.00	796.43	515.16	934.61	6.19	31.31	24.61
Case 7	750.00	801.00	519.12	933.38	6.80	30.78	24.45
Case 8	750.00	799.96	511.53	924.18	6.66	31.80	23.22
Case 1	1050.00	1026.53	841.21	1469.29	2.24	19.88	39.93
Case 2	1050.00	1035.43	832.76	1453.21	1.39	20.69	38.40
Case 3	1050.00	1033.00	835.43	1455.00	1.62	20.44	38.57
Case 4	1050.00	1029.43	837.29	1437.54	1.96	20.26	36.91
Case 5	1050.00	1034.29	816.00	1447.31	1.50	22.29	37.84
Case 6	1050.00	1038.42	819.92	1448.92	1.10	21.91	37.99
Case 7	1050.00	1034.32	811.17	1447.21	1.49	22.75	37.83
Case 8	1050.00	1037.75	831.21	1444.32	1.17	20.84	37.55
Case 1	1350.00	1327.43	1768.32	901.43	1.67	30.99	33.23
Case 2	1350.00	1333.00	1775.74	906.53	1.26	31.54	32.85
Case 3	1350.00	1322.99	1750.39	911.21	2.00	29.66	32.50
Case 4	1350.00	1325.83	1758.36	917.54	1.79	30.25	32.03
Case 5	1350.00	1319.54	1755.00	915.00	2.26	30.00	32.22
Case 6	1350.00	1324.39	1753.26	919.31	1.90	29.87	31.90
Case 7	1350.00	1332.11	1751.13	912.32	1.33	29.71	32.42
Case 8	1350.00	1327.51	1746.48	914.36	1.67	29.37	32.27

Table 22. Estimation for the Testing data (POCOEMDC-3) after the training of 3 NN
(Wavelet Transformation Technique)

	Real Data	Analog BP	Basic PNN	Sepvar PNN	Analog Error %	Basic Error %	Sepvar Error %
Case 1	600	514.32	276.12	321.23	14.28	53.98	46.46
Case 2	600	515	261.16	321.67	14.17	56.47	46.39
Case 3	600	516.87	268.43	322	13.86	55.26	46.33
Case 4	600	526.43	269.39	329.54	12.26	55.10	45.08
Case 5	600	531.23	270	341.21	11.46	55.00	43.13
Case 6	600	525.21	275.25	333.37	12.47	54.13	44.44
Case 7	600	528.42	274.38	341.13	11.93	54.27	43.15
Case 8	600	529.17	273.53	319.39	11.81	54.41	46.77
Case 1	900	1005.78	1234.32	643.78	11.75	37.15	28.47
Case 2	900	1007.85	1233	650.12	11.98	37.00	27.76
Case 3	900	1015.76	1238.43	655	12.86	37.60	27.22
Case 4	900	1017	1242.12	658.91	13.00	38.01	26.79
Case 5	900	1013.13	1239.31	661.23	12.57	37.70	26.53
Case 6	900	1019.43	1235.35	662.49	13.27	37.26	26.39
Case 7	900	1000.94	1237.64	664.43	11.22	37.52	26.17
Case 8	900	1002.38	1241.42	665.02	11.38	37.94	26.11
Case 1	1200	1298.64	1689.31	1678	8.22	40.78	39.83
Case 2	1200	1300.12	1700.12	1673.42	8.34	41.68	39.45
Case 3	1200	1305.43	1696.43	1671.21	8.79	41.37	39.27
Case 4	1200	1304.32	1693.43	1675.32	8.69	41.12	39.61
Case 5	1200	1297.81	1695.01	1676.04	8.15	41.25	39.67
Case 6	1200	1295	1698.83	1678.18	7.92	41.57	39.85
Case 7	1200	1296.64	1689.34	1679.93	8.05	40.78	39.99
Case 8	1200	1298.11	1688.89	1678	8.18	40.74	39.83
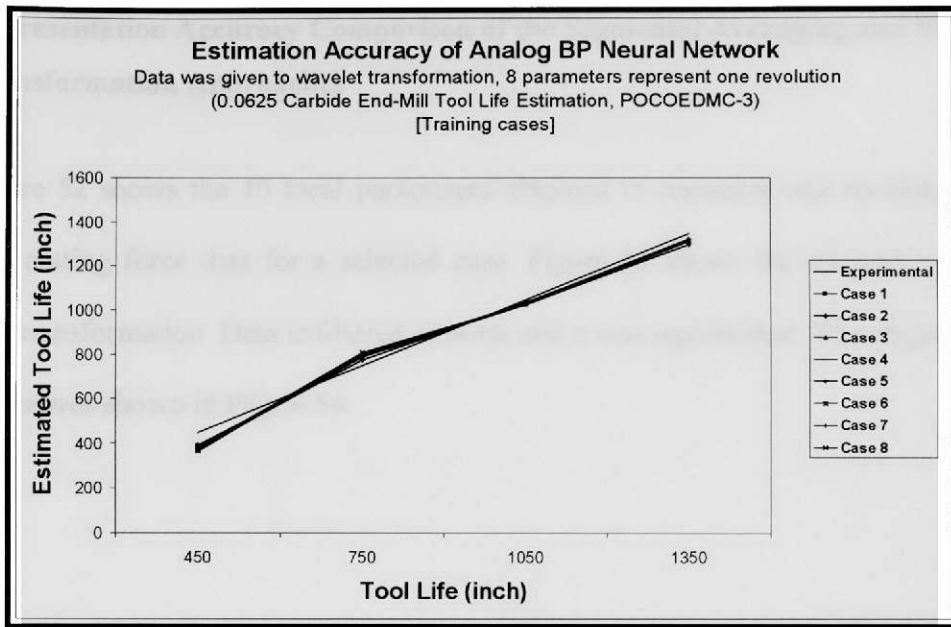
Figure 51.a. Estimation Accuracy of Analog BP for Training Cases with Improved N^2PTI

(Wavelet Transformation)
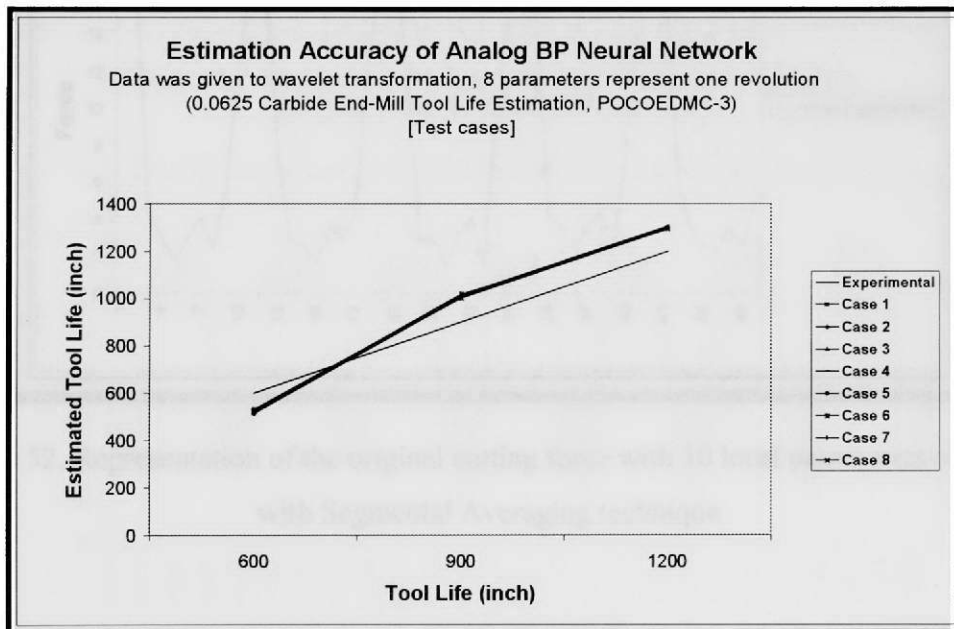
Figure 51.b. Estimation Accuracy of Analog BP for Testing Cases with Improved N^2PTI

(Wavelet Transformation)

- **Representation Accuracy Comparison of the Segmental Averaging and Wavelet Transformation Approaches**

Figure 52 shows the 10 local parameters obtained to represent one revolution of the original cutting force data for a selected case. Figure 53 shows the original signal after wavelet transformation. Data is filtered of noise and it was represented. The original cutting force data was shown in Figure 54.
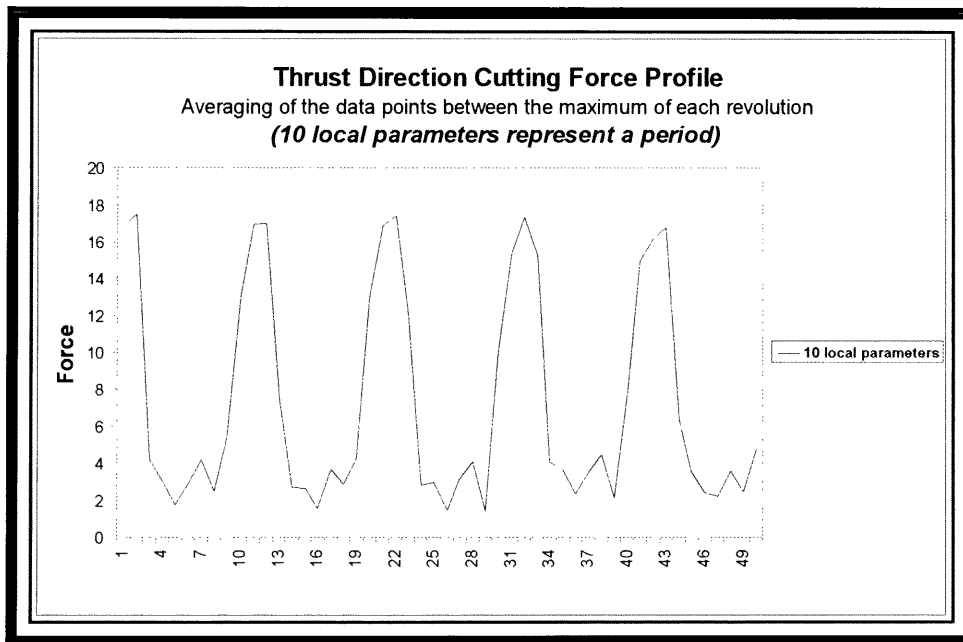
Figure 52. Representation of the original cutting force with 10 local parameters obtained with Segmental Averaging technique
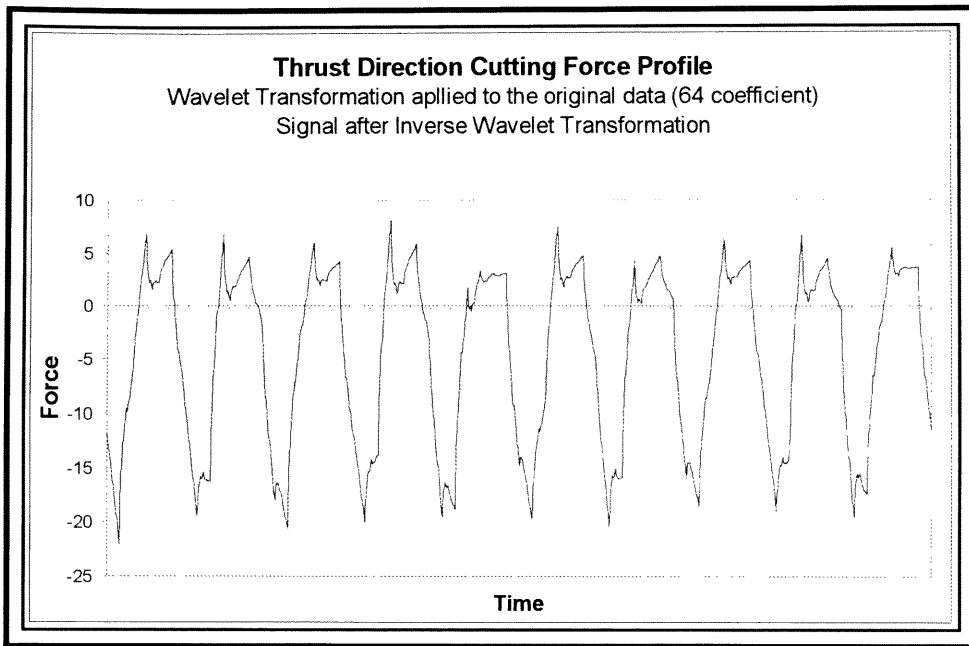
Figure 53. Representation of the original cutting force after wavelet transformation
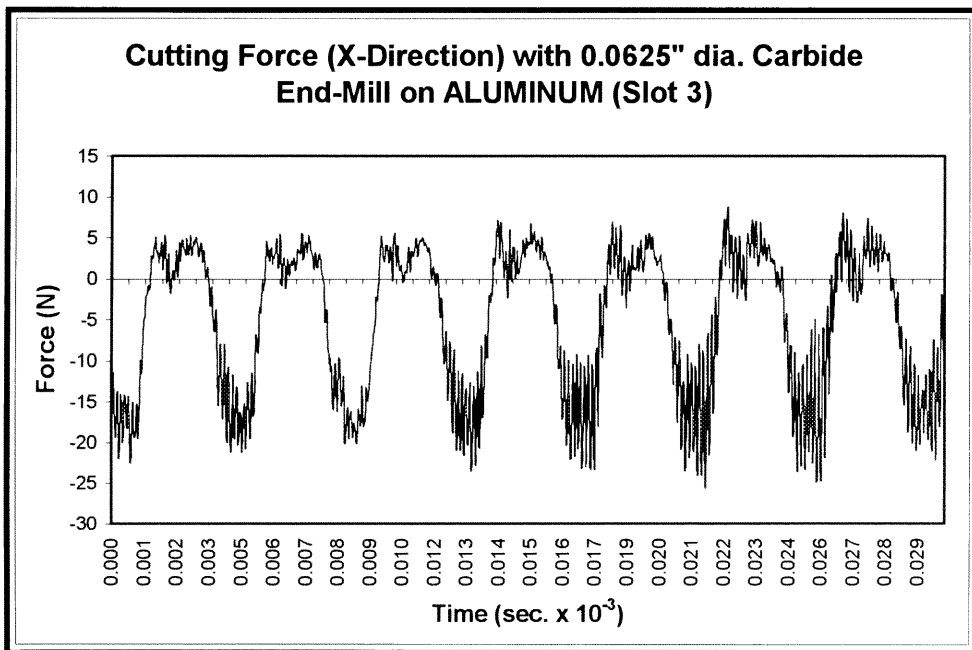
Figure 54. Experimental Cutting Force Data

111

Aluminum:

- **Segmental Averaging Technique:**

    Improved N^2PTI was also used to analyze the tool wear during the micro end-milling of the aluminum and POCOEDMC-3 workpiece. Normalization of the cutting force in thrust and feed direction made the N^2PTI more powerful. The effect of the depth of cut was eliminated with the normalization of the data. The spindle speed for the experiment was 45,000 rpm. Data was collected with 10 μs sampling. In this case, there are 130 data points in each revolution. For each case, 20 input values were presented to the Neural Network training.

Neural networks were trained with 20 input and 1 output. The 20 input consisted of 10 data, which were obtained with the averaging of the data points between the maximum of each period. 10 data point from thrust and 10 data point from feed direction cutting force were taken. The output node was the tool life obtained. 50 training cases and 40 testing cases were used. The characteristics of the networks used are listed in Table 23. The results obtained for the training and testing cases after the training of 3 different neural networks are presented in Table 24 and 25.

The optimal estimations were obtained with Analog BP and results are presented in Figure 55.

Table 23. Characteristics of the 3 Different Neural Network used for Improved N^2PTI (Segmental Averaging)

Neural Network	Analog BP	Basic PNN	Sepvar PNN
Input Nodes	20	20	20
Output Nodes	1	1	1
Training Cases	50	50	50
Test Cases	40	40	40
Training Time	151.52 seconds	17.8 seconds	14.6 seconds
Network Proprieties	10 Hidden Nodes 0.6 Learning Rate 0.9 Momentum	0.0 Sigma Low 5.0 Sigma High 5 Sigma Tries	0.003 Sigma Low 5.0 Sigma High 5 Sigma Tries

Table 24. Estimation for the Training data (Aluminum) after the training of 3 NN

(Segmental Averaging)

	Real Data	Analog BP	Basic PNN	Sepvar PNN	Analog Error %	Basic Error %	Sepvar Error %
Case 1	30	35.16	62.89	65.28	17.20	109.63	117.60
Case 2	30	35.51	63	63.23	18.37	110.00	110.77
Case 3	30	34.76	63.44	67.91	15.87	111.47	126.37
Case 4	30	35	65.23	69	16.67	117.43	130.00
Case 5	30	35.26	64.97	72.35	17.53	116.57	141.17
Case 6	30	34.99	66	75	16.63	120.00	150.00
Case 7	30	36.02	67.1	74.4	20.07	123.67	148.00
Case 8	30	35.64	67.14	72.9	18.80	123.80	143.00
Case 9	30	33	62.86	69.52	10.00	109.53	131.73
Case 10	30	35.85	68.01	64.21	19.50	126.70	114.03
Case 1	62	68.16	102.71	96.32	9.94	65.66	55.35
Case 2	62	70.34	105.32	99	13.45	69.87	59.68
Case 3	62	69	104.87	99.45	11.29	69.15	60.40
Case 4	62	71.21	107.42	99.23	14.85	73.26	60.05
Case 5	62	72.34	108.93	96.83	16.68	75.69	56.18
Case 6	62	73.32	105.97	98.5	18.26	70.92	58.87
Case 7	62	69.5	104.86	97	12.10	69.13	56.45
Case 8	62	68.75	103.3	95.34	10.89	66.61	53.77
Case 9	62	71.53	101.21	93	15.37	63.24	50.00
Case 10	62	70	102	94.18	12.90	64.52	51.90
Case 1	90	107.46	115.87	123.05	19.40	28.74	36.72
Case 2	90	107.21	118.43	128.92	19.12	31.59	43.24
Case 3	90	106.43	119.43	125	18.26	32.70	38.89
Case 4	90	105.84	117.75	127.4	17.60	30.83	41.56
Case 5	90	105.87	118	130.34	17.63	31.11	44.82
Case 6	90	106.53	115.78	131.05	18.37	28.64	45.61
Case 7	90	107.5	121.34	129.66	19.44	34.82	44.07
Case 8	90	103.65	120.84	126.43	15.17	34.27	40.48
Case 9	90	104.65	121.5	126.82	16.28	35.00	40.91
Case 10	90	105	119	125.1	16.67	32.22	39.00
Case 1	120	129.54	141.9	152.03	7.95	18.25	26.69
Case 2	120	124.54	145.86	149.54	3.78	21.55	24.62
Case 3	120	123.93	144.44	148.47	3.28	20.37	23.73
Case 4	120	122.3	143.38	145	1.92	19.48	20.83
Case 5	120	124.65	146.95	149.9	3.88	22.46	24.92
Case 6	120	126	145.3	148.36	5.00	21.08	23.63
Case 7	120	127.38	145	145.77	6.15	20.83	21.48
Case 8	120	125.55	143.1	151	4.63	19.25	25.83
Case 9	120	128	142.93	150.04	6.67	19.11	25.03
Case 10	120	125.04	141	150.5	4.20	17.50	25.42
Case 1	156	173.49	185.93	192	11.21	19.19	23.08
Case 2	156	175	191	198.54	12.18	22.44	27.27
Case 3	156	172.12	190.99	199	10.33	22.43	27.56
Case 4	156	169.32	193.26	194.65	8.54	23.88	24.78
Case 5	156	168.39	192.32	195.5	7.94	23.28	25.32
Case 6	156	171.2	189.43	195	9.74	21.43	25.00
Case 7	156	173	188.04	193.28	10.90	20.54	23.90

Table 25. Estimation for the Testing data (Aluminum) after the training of 3 NN
(Segmental Averaging)

|	Real Data	Analog BP	Basic PNN	Sepvar PNN	Analog Error %	Basic Error %	Sepvar Error %
Case 1	45	54.38	68.94	84.53	20.84	53.20	87.84
Case 2	45	55.15	70.34	90.21	22.56	56.31	100.47
Case 3	45	57.28	73	92.54	27.29	62.22	105.64
Case 4	45	58.54	71.24	93.32	30.09	58.31	107.38
Case 5	45	54.05	74.99	91.43	20.11	66.64	103.18
Case 6	45	53.99	74	87.54	19.98	64.44	94.53
Case 7	45	53.95	76.43	88	19.89	69.84	95.56
Case 8	45	55	75.43	83.65	22.22	67.62	85.89
Case 9	45	54.16	68.54	85.55	20.36	52.31	90.11
Case 10	45	53.06	71.05	83.5	17.91	57.89	85.56
Case 1	75	68	120.45	114.3	9.33	60.60	52.40
Case 2	75	65.32	125.04	115	12.91	66.72	53.33
Case 3	75	63.9	127.95	117.74	14.80	70.60	56.99
Case 4	75	65	128.37	118.43	13.33	71.16	57.91
Case 5	75	62.17	126.53	117.94	17.11	68.71	57.25
Case 6	75	60.83	126.2	114.32	18.89	68.27	52.43
Case 7	75	63.73	125.5	116.66	15.03	67.33	55.55
Case 8	75	64.94	122.31	117	13.41	63.08	56.00
Case 9	75	62.18	121.74	115.7	17.09	62.32	54.27
Case 10	75	66	124	113.99	12.00	65.33	51.99
Case 1	107	128	141.2	132.04	19.63	31.96	23.40
Case 2	107	130.26	143	135	21.74	33.64	26.17
Case 3	107	132.85	142.38	132.4	24.16	33.07	23.74
Case 4	107	133.25	145.83	136.32	24.53	36.29	27.40
Case 5	107	131	149.63	137.83	22.43	39.84	28.81
Case 6	107	133.73	148	135.53	24.98	38.32	26.66
Case 7	107	135.2	142.84	132	26.36	33.50	23.36
Case 8	107	133	144.06	134.45	24.30	34.64	25.65
Case 9	107	135.32	143.9	136.78	26.47	34.49	27.83
Case 10	107	132.63	145	135.3	23.95	35.51	26.45
Case 1	135	168.02	175.94	189.33	24.46	30.33	40.24
Case 2	135	165.32	177	191.21	22.46	31.11	41.64
Case 3	135	164.94	181.21	190	22.18	34.23	40.74
Case 4	135	163.26	182.32	187.17	20.93	35.05	38.64
Case 5	135	162.03	183.21	192.32	20.02	35.71	42.46
Case 6	135	165	184	190.86	22.22	36.30	41.38
Case 7	135	167.25	179.14	194	23.89	32.70	43.70
Case 8	135	166.24	179.99	193.32	23.14	33.33	43.20
Case 9	135	164.52	178.23	185.43	21.87	32.02	37.36
Case 10	135	167.17	181.19	188.85	23.83	34.21	39.89
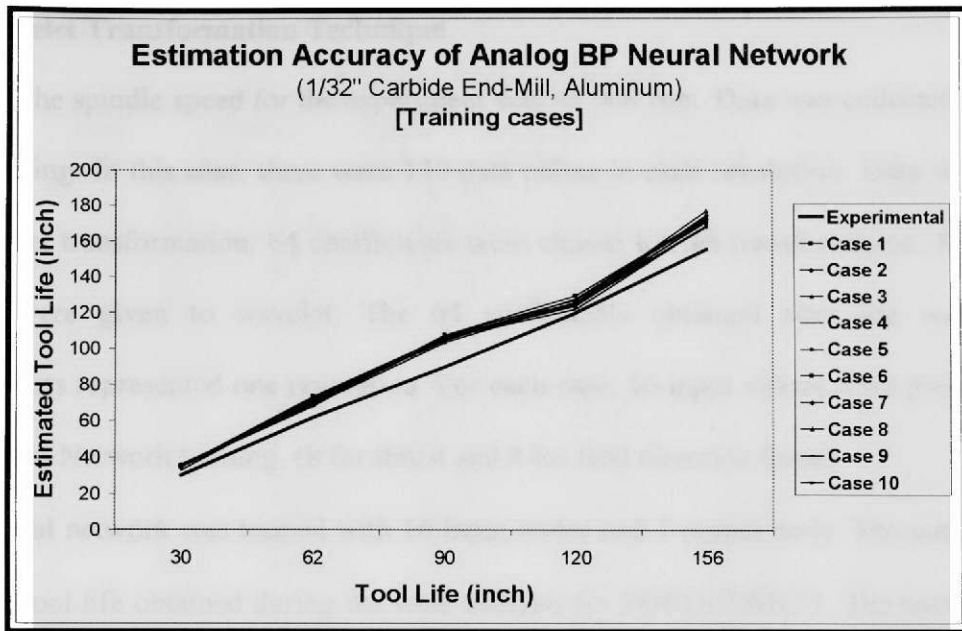
Figure 55.a. Estimation Accuracy of Analog BP for Training Cases with Improved N^2PTI
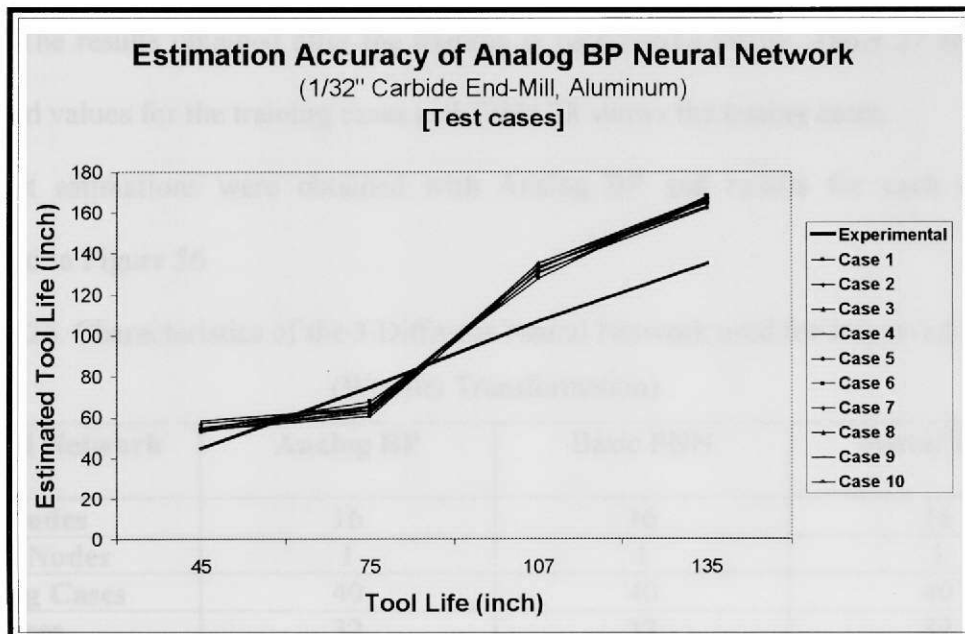
(Segmental Averaging)

Figure 55.b. Estimation Accuracy of Analog BP for Test Cases with Improved N^2PTI

(Segmental Averaging)

- **Wavelet Transformation Technique**

The spindle speed for the experiment was 45,000 rpm. Data was collected with 10 μs sampling. In this case, there were 130 data points in each revolution. Data was given to wavelet transformation. 64 coefficients were chosen for the transformation. 1024 data points were given to wavelet. The 64 coefficients obtained after the wavelet, 8 coefficients represented one revolution. For each case, 16 input values were presented to the Neural Network training. (8 for thrust and 8 for feed direction force)

The neural network was trained with 16 input nodes and 1 output node. The output node was the tool life obtained during the wear analysis for POCOEDMC-3. The network was trained for 40 training and 32 testing cases. Backpropagation and Probabilistic neural networks were evaluated. Analog BP, Basic PNN and Sepvar PNN were trained with the normalized data. The final settings of the NN are listed in Table 26.

The results obtained after the training is represented below. Table 27 shows the estimated values for the training cases and Table 28 shows the testing cases.

The best estimations were obtained with Analog BP and results for each case are presented in Figure 56.

Table 26. Characteristics of the 3 Different Neural Network used for Improved N^2PTI (Wavelet Transformation)

Neural Network	Analog BP	Basic PNN	Sepvar PNN
Input Nodes	16	16	16
Output Nodes	1	1	1
Training Cases	40	40	40
Test Cases	32	32	32
Training Time	173.18 seconds	14.17 seconds	13.96 seconds
Network Proprieties	8 Hidden Nodes 0.6 Learning Rate 0.9 Momentum	0.0 Sigma Low 5.0 Sigma High 5 Sigma Tires	0.003 Sigma Low 5.0 Sigma High 5 Sigma Tires

Table 27. Estimation for the Training data (Aluminum) after the training of 3 NN (Wavelet Transformation)

	Real Data	Analog BP	Basic PNN	Sepvar PNN	Analog Error %	Basic Error %	Sepvar Error %
Case 1	30	32.18	46.32	10.21	7.27	54.40	65.97
Case 2	30	32.94	45.00	11.21	9.80	50.00	62.63
Case 3	30	33.15	46.12	10.86	10.50	53.73	63.80
Case 4	30	32.85	46.78	10.03	9.50	55.93	66.57
Case 5	30	33.03	46.91	10.45	10.10	56.37	65.17
Case 6	30	33.12	48.37	10.57	10.40	61.23	64.77
Case 7	30	34.08	49.99	10.91	13.60	66.63	63.63
Case 8	30	33.13	48.03	10.38	10.43	60.10	65.40
Case 1	62	57.43	87.16	72.24	7.37	40.58	16.52
Case 2	62	55.01	87.93	74.25	11.27	41.82	19.76
Case 3	62	56.74	88.00	74.59	8.48	41.94	20.30
Case 4	62	55.93	88.18	74.42	9.79	42.23	20.04
Case 5	62	55.00	89.16	72.62	11.29	43.81	17.13
Case 6	62	55.21	87.38	73.88	10.95	40.94	19.15
Case 7	62	54.08	84.69	72.75	12.77	36.60	17.34
Case 8	62	54.86	85.55	71.51	11.52	37.98	15.33
Case 1	90	85.13	118.12	99.00	5.41	31.24	10.00
Case 2	90	84.38	119.91	96.69	6.24	33.23	7.43
Case 3	90	84.56	117.83	93.75	6.04	30.92	4.17
Case 4	90	83.91	120.34	95.55	6.77	33.71	6.17
Case 5	90	82.99	121.23	97.76	7.79	34.70	8.62
Case 6	90	83.00	121.00	98.29	7.78	34.44	9.21
Case 7	90	82.84	119.93	97.25	7.96	33.26	8.05
Case 8	90	82.04	120.04	94.82	8.84	33.38	5.36
Case 1	120	127.81	147.81	114.02	6.51	23.18	4.98
Case 2	120	125.93	143.38	112.16	4.94	19.48	6.54
Case 3	120	124.00	146.95	111.35	3.33	22.46	7.21
Case 4	120	126.84	147.93	108.75	5.70	23.28	9.38
Case 5	120	125.95	145.94	112.43	4.96	21.62	6.31
Case 6	120	125.75	151.21	111.27	4.79	26.01	7.28
Case 7	120	124.93	151.99	109.33	4.11	26.66	8.89
Case 8	120	124.78	149.93	113.25	3.98	24.94	5.63
Case 1	156	174.57	201.12	236.16	11.90	28.92	51.38
Case 2	156	174.93	204.43	244.20	12.13	31.04	56.54
Case 3	156	174.00	205.87	244.77	11.54	31.97	56.90
Case 4	156	173.06	207.93	239.42	10.94	33.29	53.47
Case 5	156	173.57	205.74	240.47	11.26	31.88	54.14
Case 6	156	174.01	209.21	239.85	11.54	34.11	53.75
Case 7	156	172.94	203.33	237.73	10.86	30.34	52.39
Case 8	156	172.99	209.42	239.16	10.89	34.24	53.31

Table 28. Estimation for the Testing data (Aluminum) after the training of 3 NN

(Wavelet Transformation)

|	Real Data	Analog BP	Basic PNN	Sepvar PNN	Analog Error %	Basic Error %	Sepvar Error %
Case 1	45	38.12	65.28	78.32	15.29	45.07	74.04
Case 2	45	38.29	63.23	79.92	14.91	40.51	77.60
Case 3	45	37.99	67.91	80.12	15.58	50.91	78.04
Case 4	45	39.94	69.00	83.32	11.24	53.33	85.16
Case 5	45	38.88	72.35	91.43	13.60	60.78	103.18
Case 6	45	37.84	75.00	87.54	15.91	66.67	94.53
Case 7	45	38.00	74.40	88.93	15.56	65.33	97.62
Case 8	45	38.27	72.90	87.43	14.96	62.00	94.29
Case 1	75	87.39	132.04	114.30	16.52	76.05	52.40
Case 2	75	88.00	135.00	114.82	17.33	80.00	53.09
Case 3	75	86.99	132.40	117.74	15.99	76.53	56.99
Case 4	75	86.53	136.32	118.43	15.37	81.76	57.91
Case 5	75	86.17	137.83	117.94	14.89	83.77	57.25
Case 6	75	85.94	135.53	126.22	14.59	80.71	68.29
Case 7	75	83.16	132.00	116.66	10.88	76.00	55.55
Case 8	75	84.00	134.45	118.46	12.00	79.27	57.95
Case 1	107	125.27	141.20	194.34	17.07	31.96	81.63
Case 2	107	126.99	143.00	191.21	18.68	33.64	78.70
Case 3	107	126.75	142.38	190.00	18.46	33.07	77.57
Case 4	107	127.00	145.83	187.17	18.69	36.29	74.93
Case 5	107	126.15	149.63	192.32	17.90	39.84	79.74
Case 6	107	125.94	148.00	190.86	17.70	38.32	78.37
Case 7	107	125.76	142.84	194.00	17.53	33.50	81.31
Case 8	107	126.38	144.06	193.32	18.11	34.64	80.67
Case 1	135	157.19	175.94	268.92	16.44	30.33	99.20
Case 2	135	155.00	177.00	261.39	14.81	31.11	93.62
Case 3	135	156.16	181.21	261.94	15.67	34.23	94.03
Case 4	135	156.00	182.32	259.11	15.56	35.05	91.93
Case 5	135	158.13	183.21	267.81	17.13	35.71	98.38
Case 6	135	156.39	184.00	265.03	15.84	36.30	96.32
Case 7	135	155.99	179.14	266.00	15.55	32.70	97.04
Case 8	135	157.17	179.99	268.18	16.42	33.33	98.65
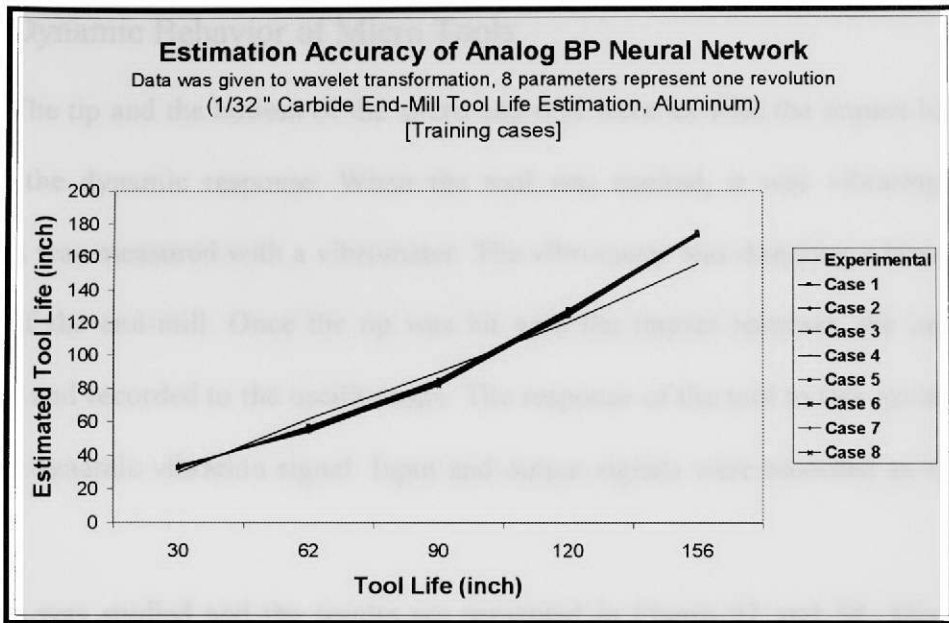
Figure 56.a. Estimation Accuracy of Analog BP for Training Cases with Improved N^2PTI
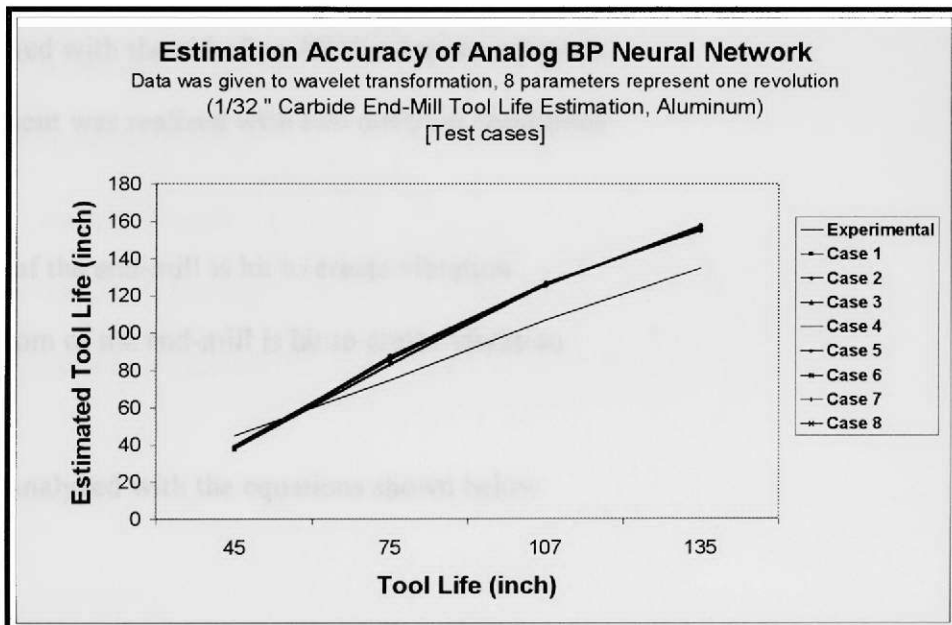
(Wavelet Transformation)

Figure 56.b. Estimation Accuracy of Analog BP for Test Cases with Improved N^2PTI

(Wavelet Transformation)

V.4. Dynamic Behavior of Micro Tools

The tip and the bottom of the micro end-mill were hit with the impact hammer to analyze the dynamic response. When the tool was excited, it was vibrating and the vibration was measured with a vibrometer. The vibrometer was directing a laser beam to the tip of the end-mill. Once the tip was hit with the impact hammer, the impact was digitized and recorded to the oscilloscope. The response of the tool to this excitation was a typical dynamic vibration signal. Input and output signals were recorded as 4,000 data points.

The data was studied and the results are presented in Figure 57 and 58. The dynamic characteristics of the end-mills were calculated from the variation of the output signal amplitude versus time. The natural-angular frequency and the damping factor of the tools were calculated analytically and numerically. Transfer function of the system was established with the aid of an ARV computer program.

Experiment was realized with two different conditions:

1. Tip of the end-mill is hit to create vibration
2. Bottom of the end-mill is hit to create vibration

Data is analyzed with the equations shown below:

$$y = y^* \cdot e^{-\zeta \cdot \omega_n \cdot t} \tag{5.4}$$

$$\zeta = -(1/\omega_n.t).\ln(y/y^*) \qquad (5.5)$$

$$\omega_n = 2.\pi.f_n \qquad (5.6)$$

$$t = n.1/f_n \qquad (5.7)$$

$$\zeta = -\ln(y/y^*)/2.\pi.n \qquad (5.8)$$

Where:

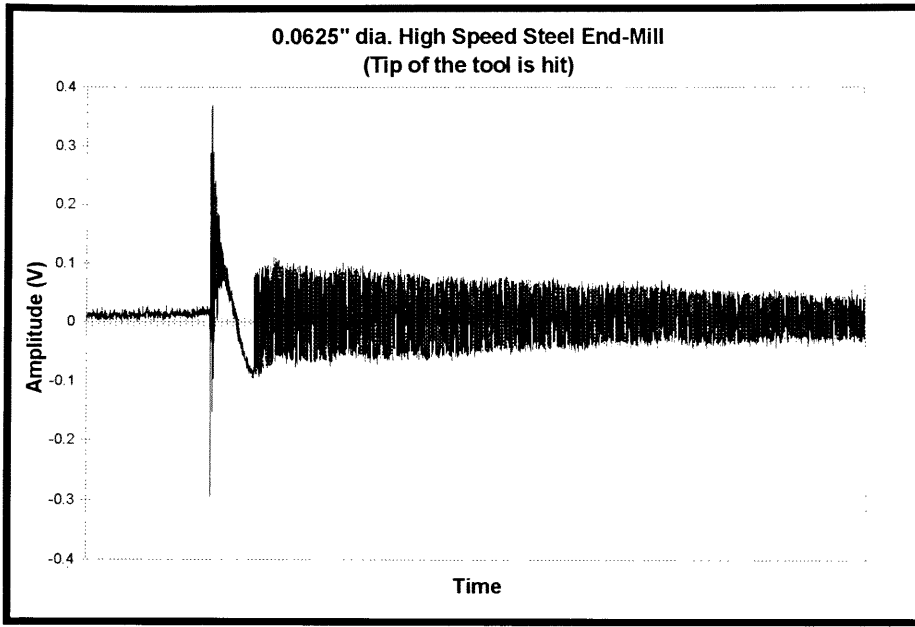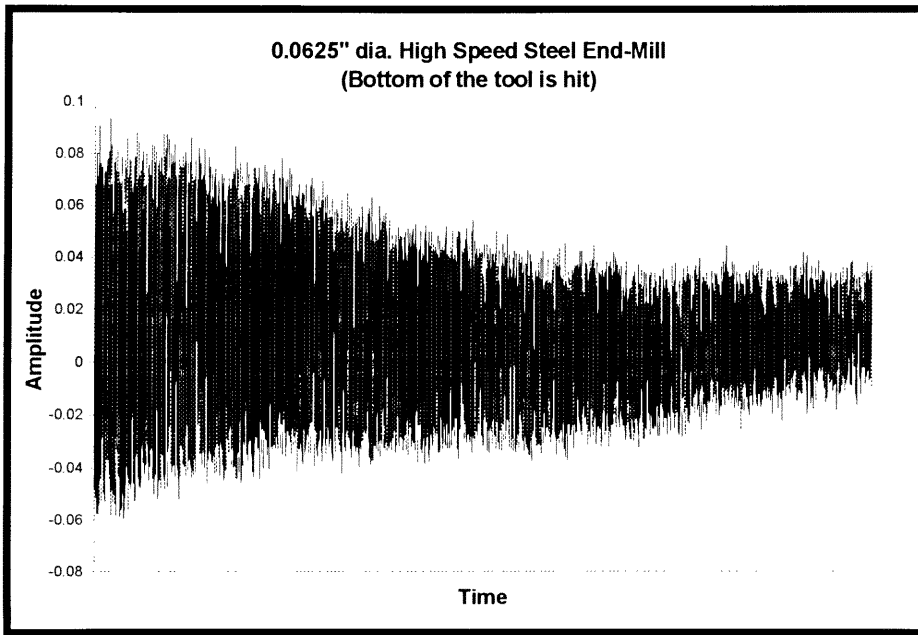|	
y	= Amplitude at time t
y^*	= Amplitude at time t_0
ζ	= Damping factor
ω_n	= Angular Frequency
f_n	= Natural Frequency
n	= Number of period

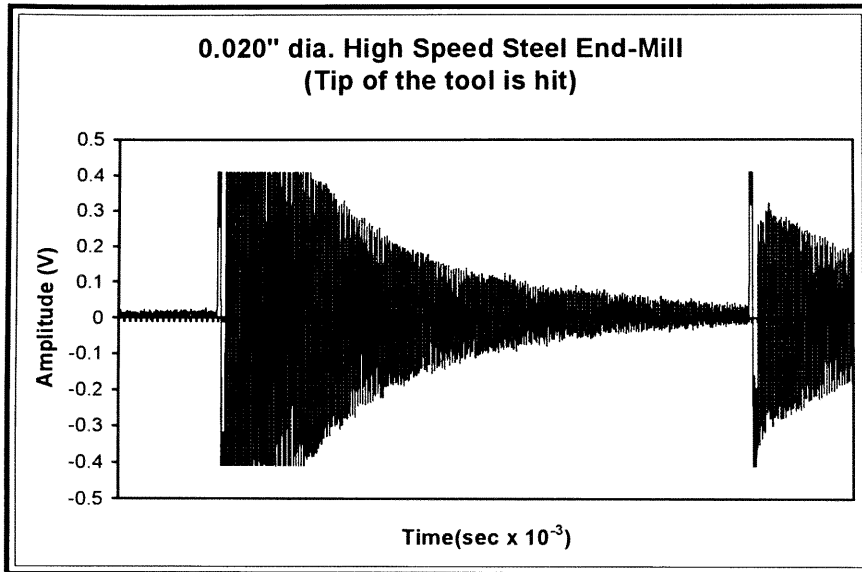$$\zeta = 2.39 \times 10^{-4} \qquad f_n = 23906 \text{ Hertz}$$

Figure 57.a.   0.0625" Diameter HSS End-Mill (Tip of the tool was hit)

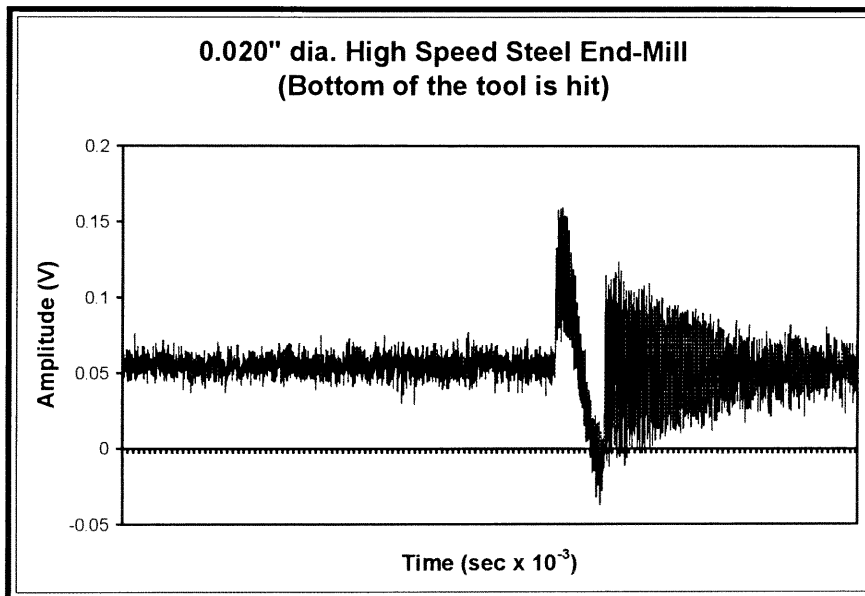$$\zeta = 1.92 \times 10^{-4} \qquad f_n = 23545 \text{ Hertz}$$

Figure 57.b.   0.0625" Diameter HSS End-Mill (Bottom of the tool was hit)

0.020" dia. High Speed Steel End-Mill
(Tip of the tool is hit)

$\zeta = 2.55 \times 10^{-3}$ $f_n = 8245$ Hertz

Figure 58.a.   0.020" Diameter (Tip of the tool was hit)

0.020" dia. High Speed Steel End-Mill
(Bottom of the tool is hit)

$\zeta = 2.07 \times 10^{-3}$ $f_n = 8470$ Hertz

Figure 58.b.   0.020" Diameter (Bottom of the tool was hit)

Results of these dynamic experiments showed that the natural frequency of the micro-tools used in the machinability and tool wear test was not critical because they were much bigger than the spindle frequency.

Experimental data fed to the ARV computer program. The results obtained for the natural frequency of the 0.0625 inches HSS micro end-mill are represented in Figure 59.
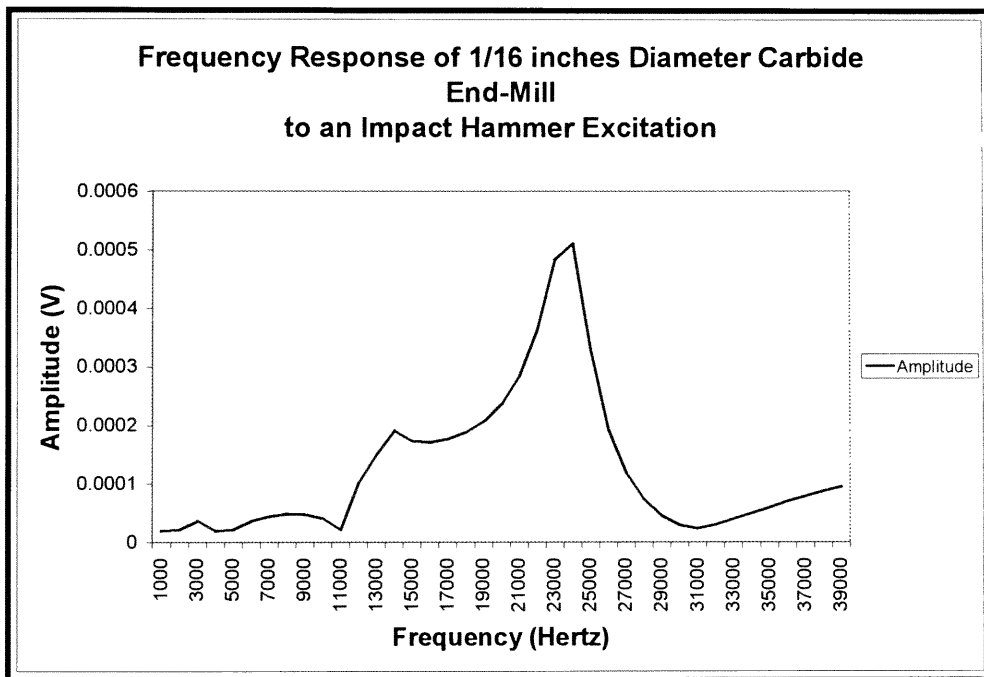

Figure 59. Frequency Response of the 1/16 inches Diameter Carbide End-Mill –ARV

Computer Program Output Results

V.5.   Static Behavior of Micro Tools

The same kind of micro tools used in the machinability experiments were used in this test. High speed steel (HSS) and Carbide 0.0625, 0.03125, 0.020 inches diameter two flutes end-mills were analyzed under the static loading conditions. The tool was attached to a Bridgeport Milling machine with an end-mill holder. The workpiece was clamped to the dynamometer. The dynamometer was tightened to a vise that is fixed on the X-Y table of the milling machine. A linear displacement sensor was clamped on the vise with respect to the tool holder. The sensor supposed to measure the linear table displacement during the experiment. The sensor with its signal conditioner was connected to a Nicolet 310 digital oscilloscope. The dynamometer was connected to a charge amplifier and to the oscilloscope also. Force and displacement data were collected and recorded. The main purpose of these experiments was to find out the stiffness of the micro-tools and use this data in cutting force displacement relationship. The new machinability method required the calculation of the maximum static bending force that can be applied to the tool. The results obtained for every tool – workpiece combinations are presented in the following figures.

0.020" HIGH SPEED STEEL END-MILL STIFFNESS WITH POCO 3 WORKPIECE
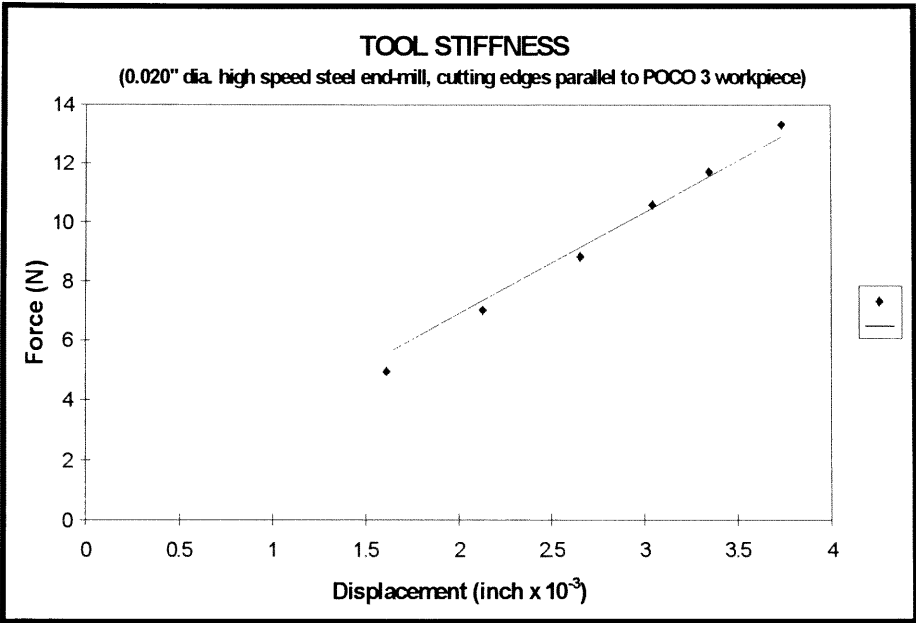

Figure 60.a. Cutting edges of the tool were parallel to the workpiece (slope = 3.44)
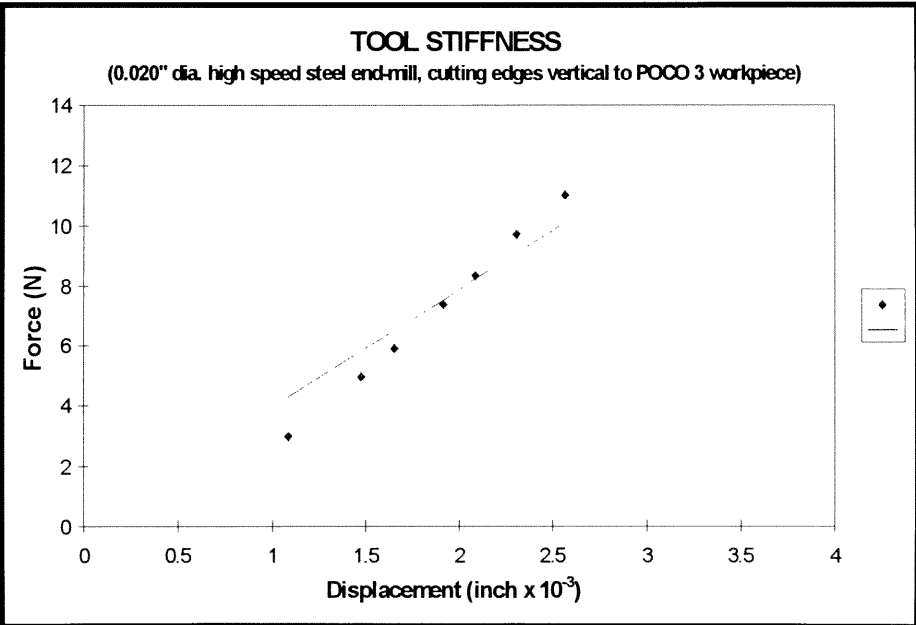

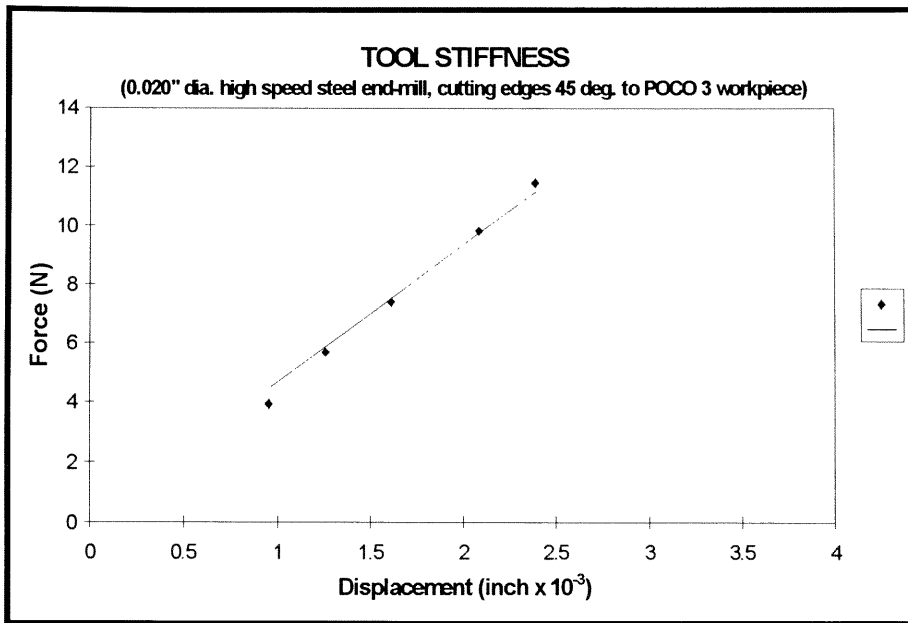Figure 60.b. Cutting edges of the tool were vertical to the workpiece (slope = 3.94)

Figure 60.c. Cutting edges of the tool were 45 degree to the workpiece (slope = 4.5)
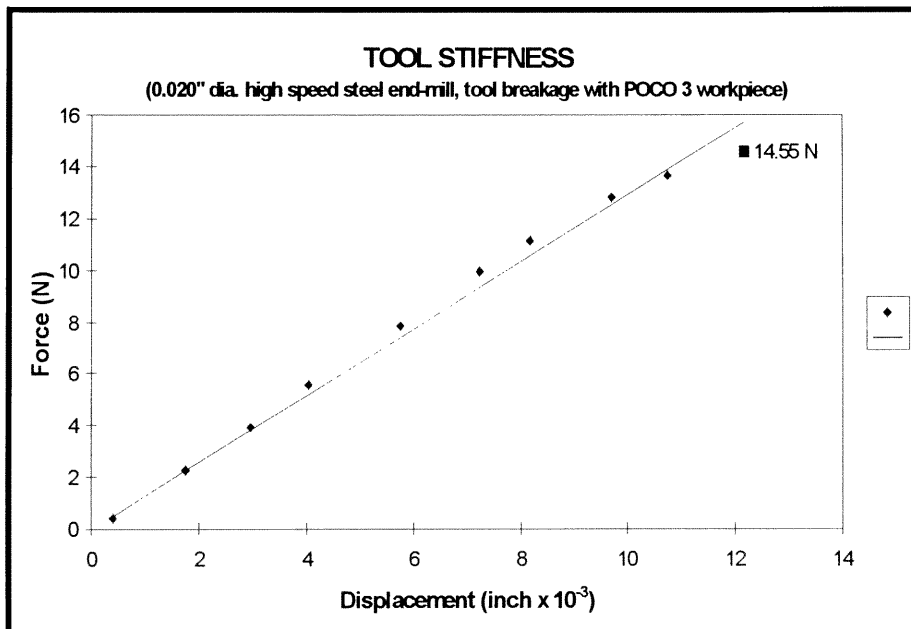

Figure 60.d. Tool breakage occurred at 14.55 N (slope = 1.3)

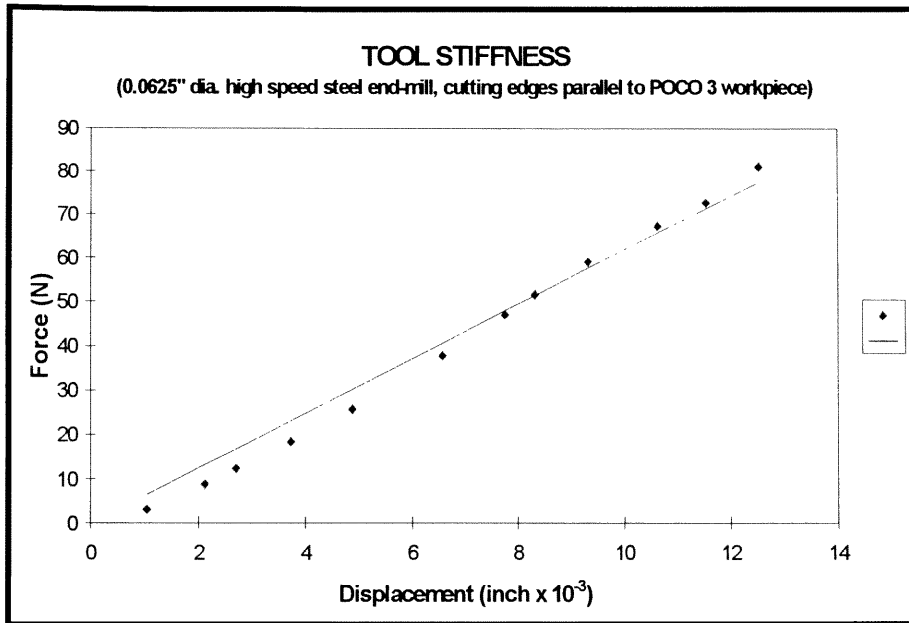# 0.0625" HIGH SPEED STEEL END-MILL STIFFNESS WITH POCO3 WORKPIECE

Figure 61.a. Cutting edges of the tool were parallel to the workpiece (slope = 6.20)
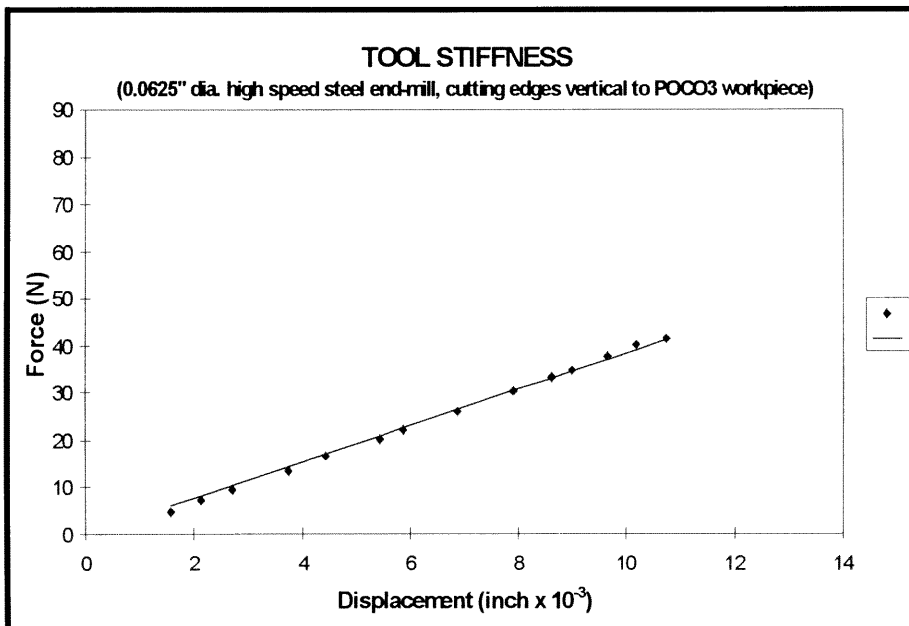

Figure 61.b. Cutting edges of the tool were vertical to the workpiece (slope = 3.95)
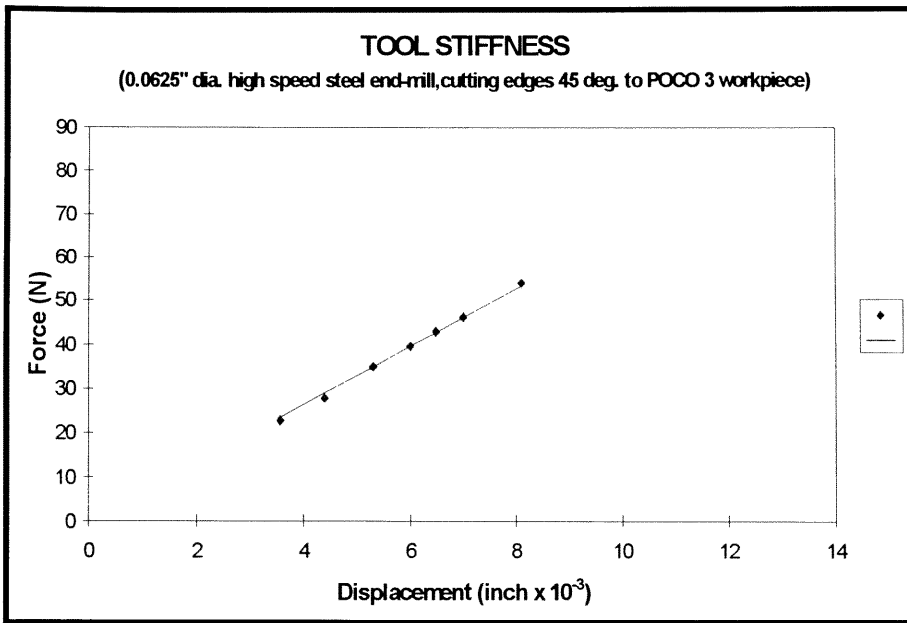
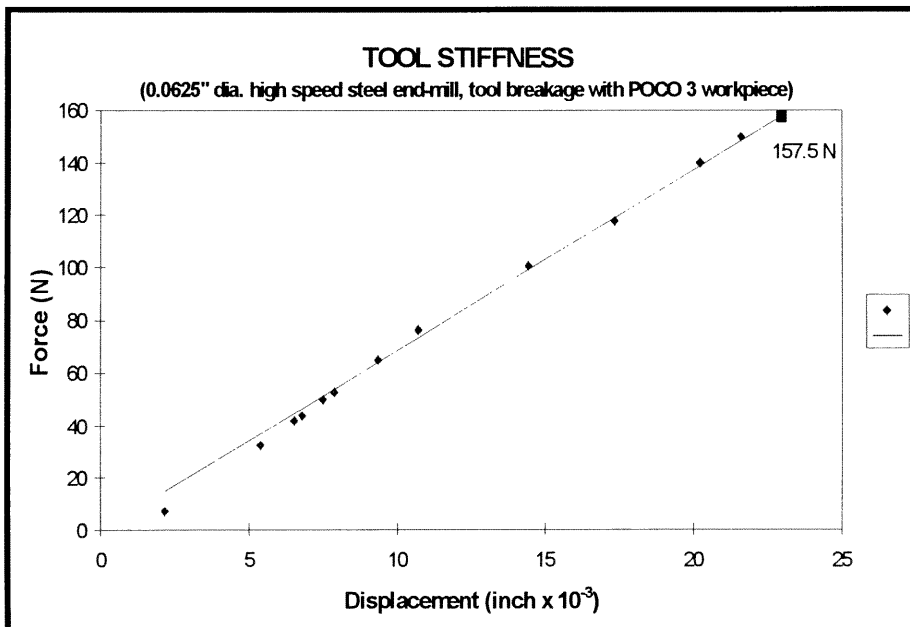Figure 61.c. Cutting edges of the tool were 45 degree to the workpiece (slope = 6.50)

Figure 61.d. Tool breakage occurred at 157.5 N (slope = 6.86)

0.020" CARBIDE END-MILL STIFFNESS WITH ALUMINUM WORKPIECE

Figure 62.a. Cutting edges of the tool were parallel to the workpiece (slope = 8.43)

Figure 62.b. Cutting edges of the tool were vertical to the workpiece (slope = 8.68)

Figure 62.c. Cutting edges of the tool were 45 degree to the workpiece (slope =10.04)

Figure 62.d. Tool breakage occurred at 36.1 N (slope = 9.75)

0.0625" CARBIDE END-MILL STIFFNESS WITH ALUMINUM WORKPIECE

TOOL STIFFNESS
(0.0625" dia. carbide end-mill, cutting edges parallel to ALUMINUM workpiece)

Figure 63.a. Cutting edges of the tool were parallel to the workpiece (slope = 19.6)

TOOL STIFFNESS
(0.0625" dia. carbide end-mill, cutting edges vertical to ALUMINUM workpiece)

Figure 63.b. Cutting edges of the tool were vertical to the workpiece (slope = 9.79)

Figure 63.c. Cutting edges of the tool were 45 degree to the workpiece (slope =13.89)

Figure 63.d. Tool breakage occurred at 122.09 N (slope = 17.83)

134

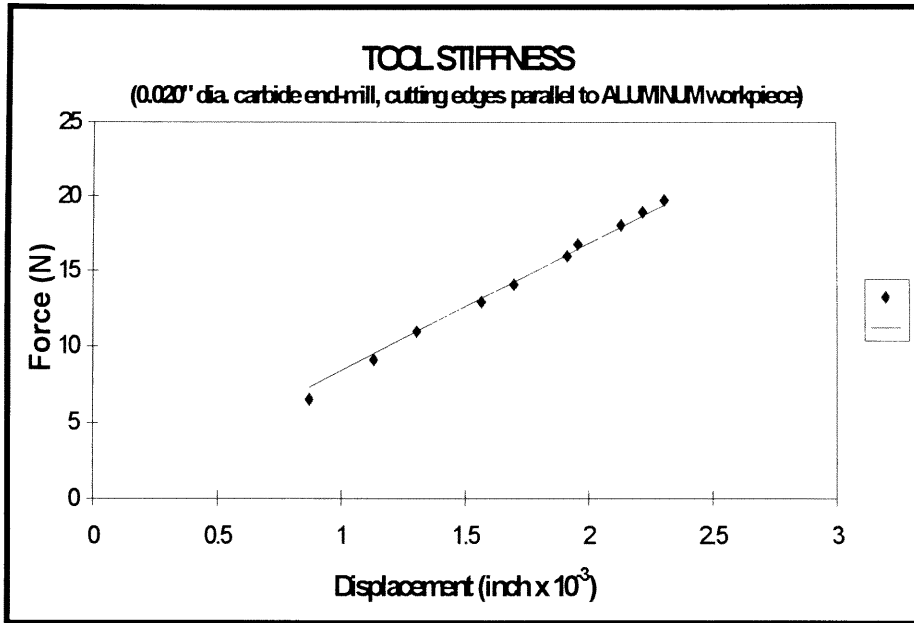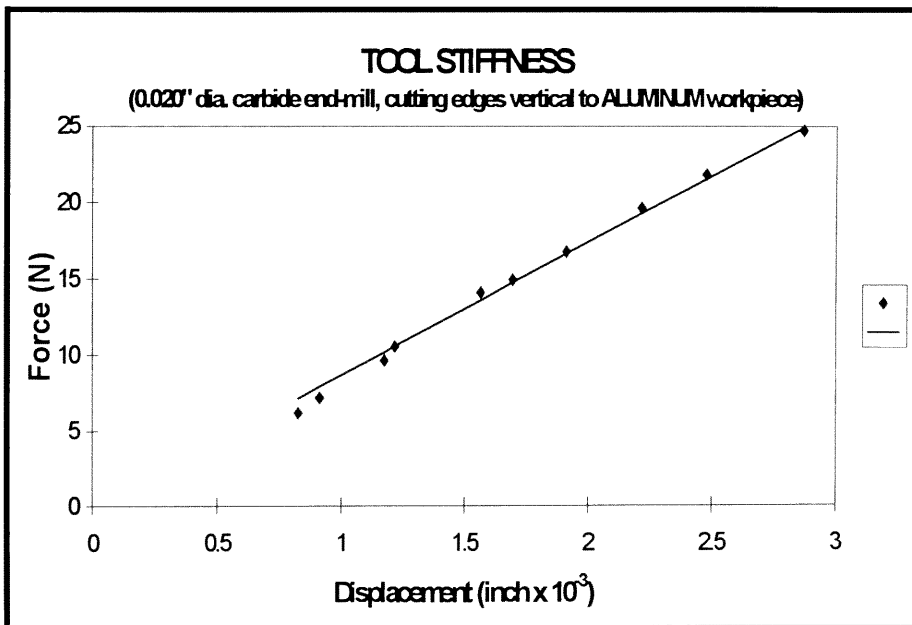# 0.020" HIGH SPEED STEEL END-MILL STIFFNESS WITH STEEL WORKPIECE

Figure 64.a. Cutting edges of the tool were parallel to the workpiece (slope = 1.41)

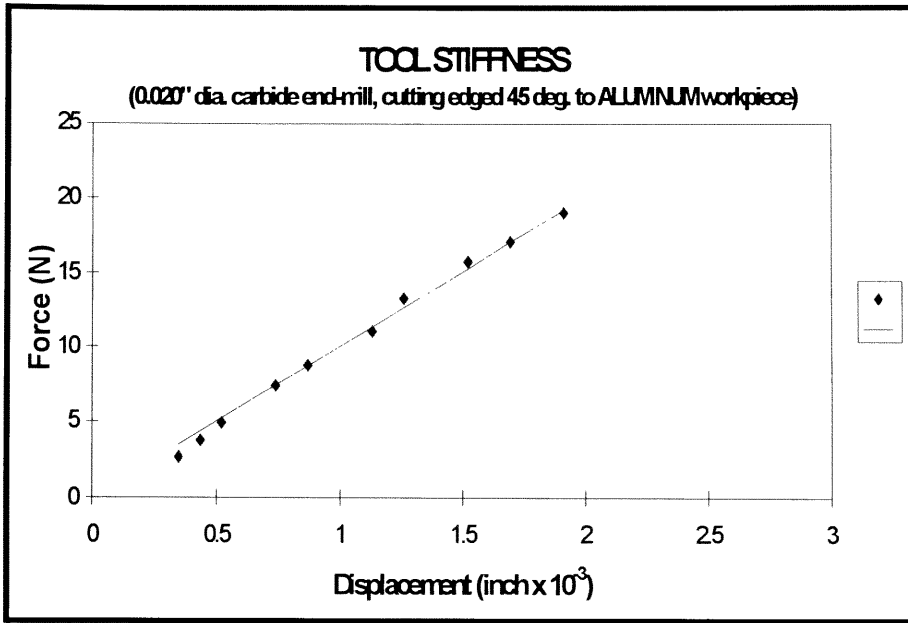Figure 64.b. Cutting edges of the tool were vertical to the workpiece (slope = 1.27)

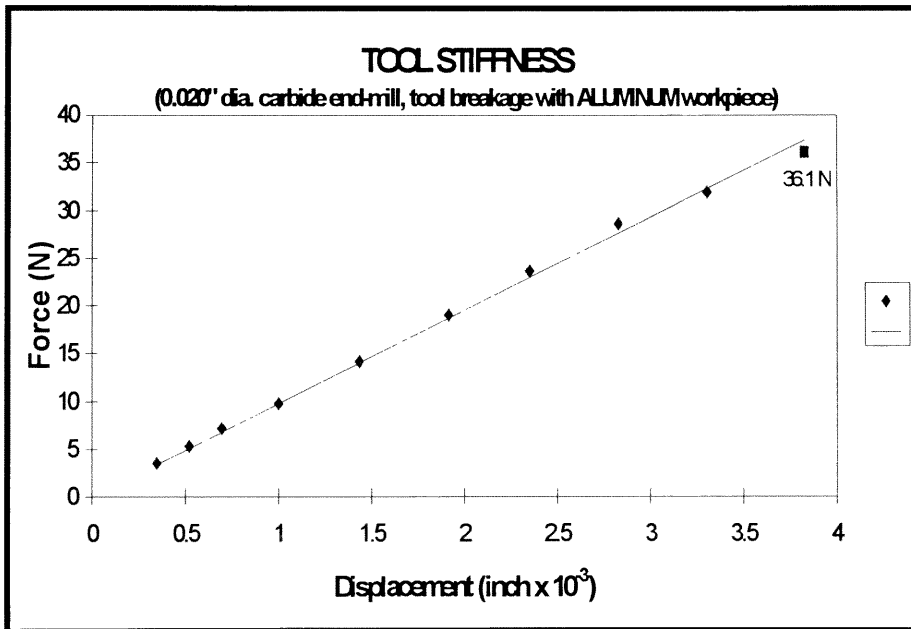Figure 64.c. Cutting edges of the tool were 45 degree to the workpiece (slope = 1.09)

Figure 64.d. Tool breakage occurred at 16.425 N (slope = 1.69)

136

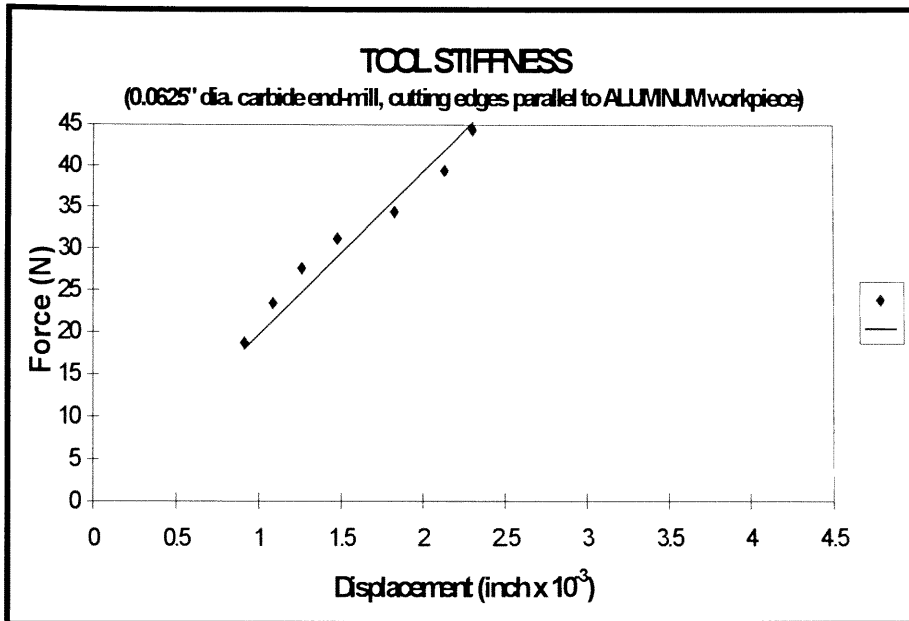# 0.020" CARBIDE END-MILL STIFFNESS WITH STEEL WORKPIECE

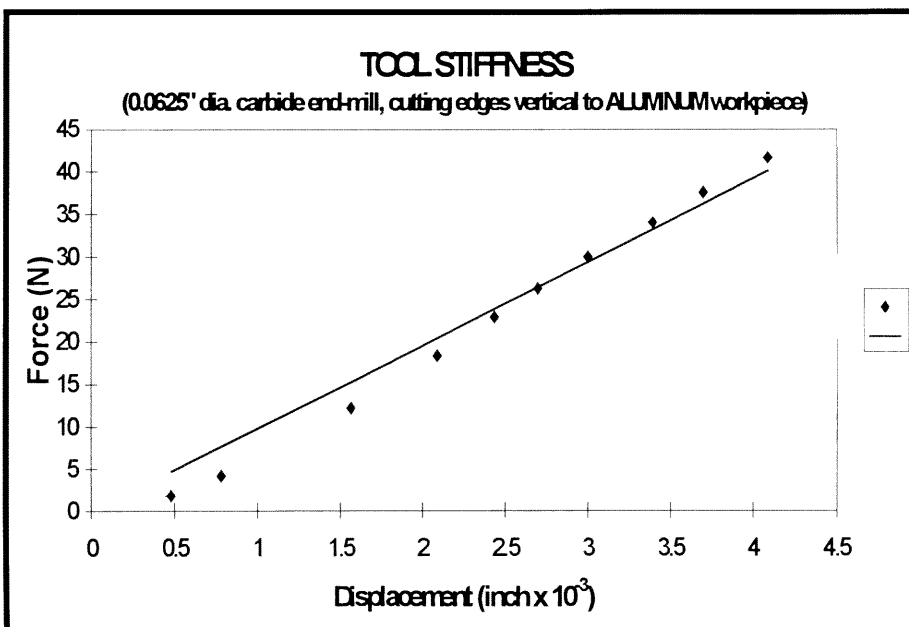Figure 65.a. Cutting edges of the tool were parallel to the workpiece (slope = 5.30)

Figure 65.b. Cutting edges of the tool were vertical to the workpiece (slope = 3.91)

Figure 65.c. Cutting edges of the tool were 45 degree to the workpiece (slope = 6.01)

Figure 65.d. Tool breakage occurred at 28.9 N (slope = 5.66)

0.0625" HIGH SPEED STEEL END-MILL STIFFNESS WITH STEEL WORKPIECE

Figure 66.a. Cutting edges of the tool were parallel to the workpiece (slope = 10.25)
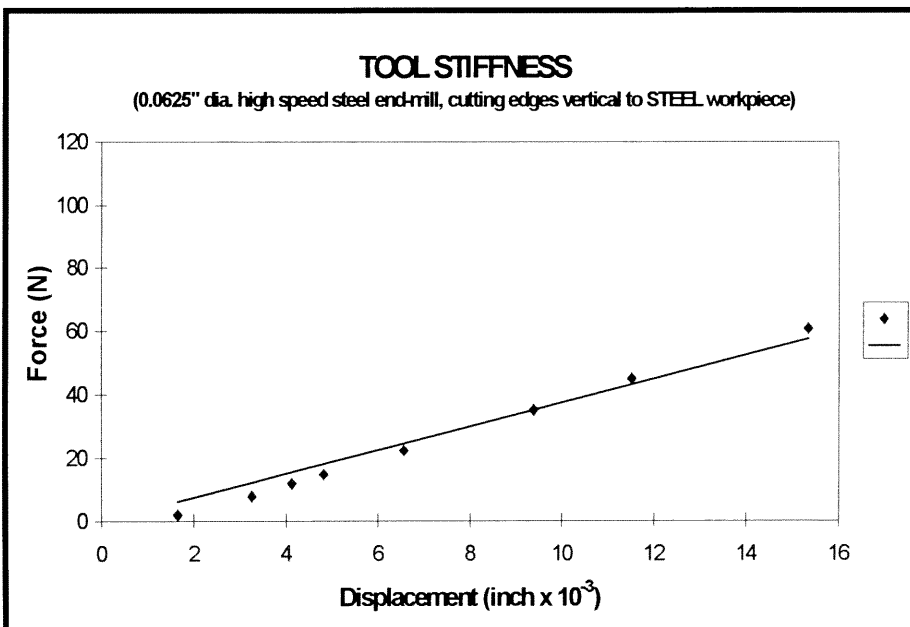
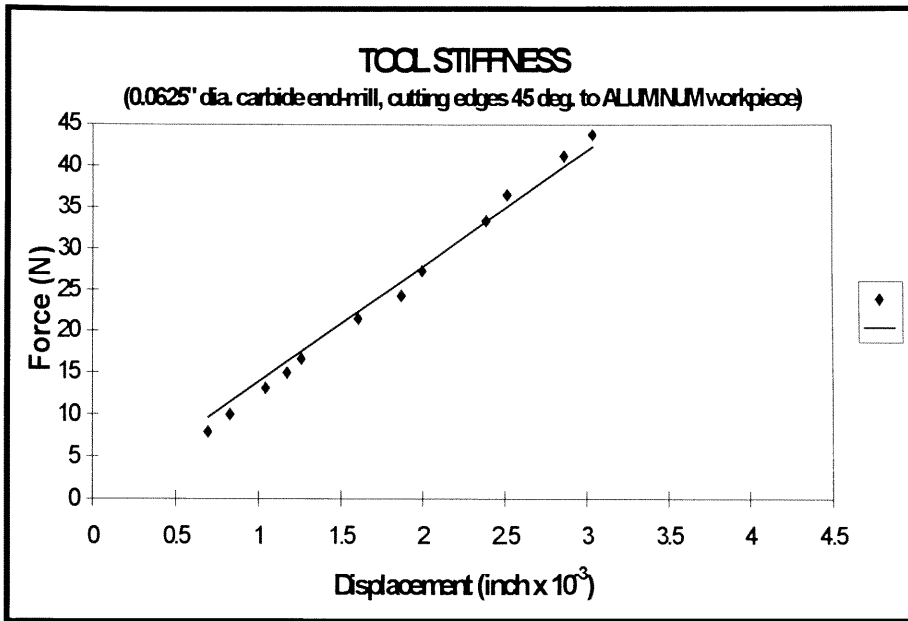Figure 66.b. Cutting edges of the tool were vertical to the workpiece (slope = 3.75)
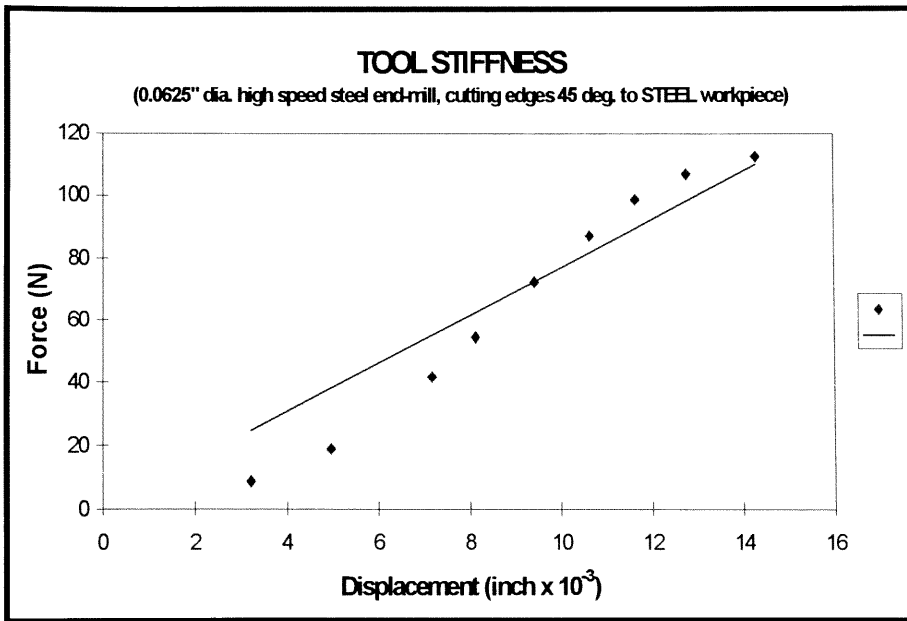
Figure 66.c. Cutting edges of the tool were 45 degree to the workpiece (slope = 7.69)
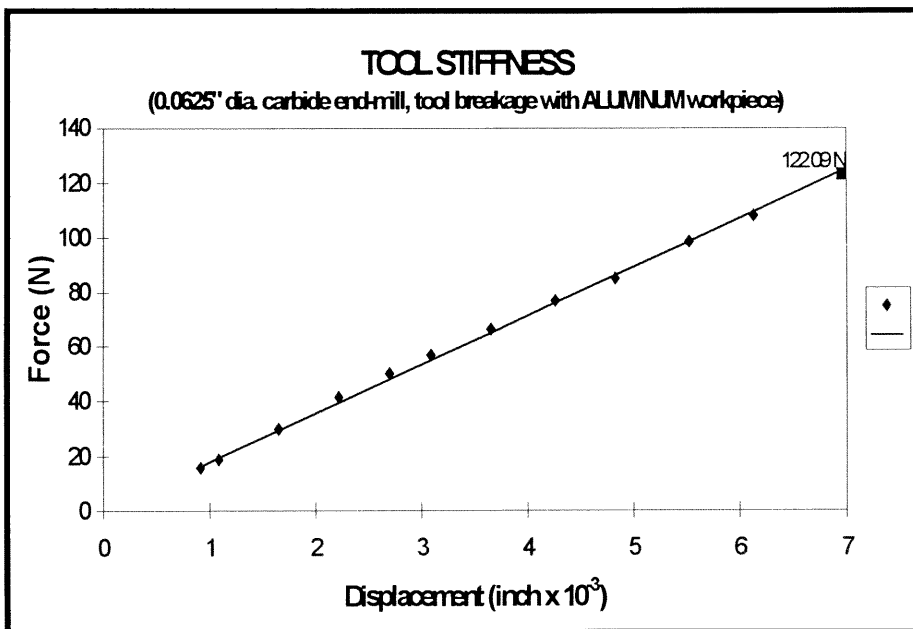
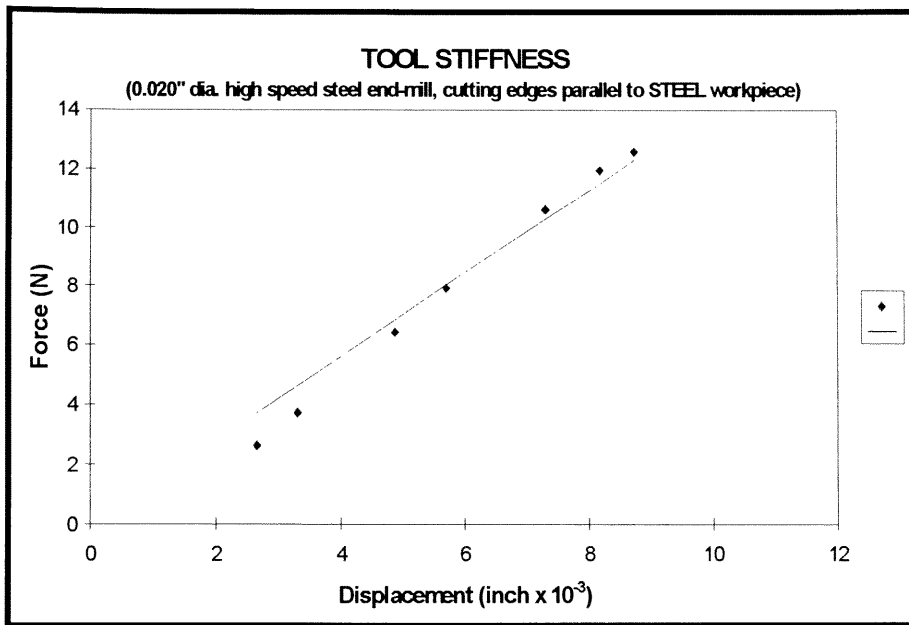# 0.0625" CARBIDE END-MILL STIFFNESS WITH STEEL WORKPIECE
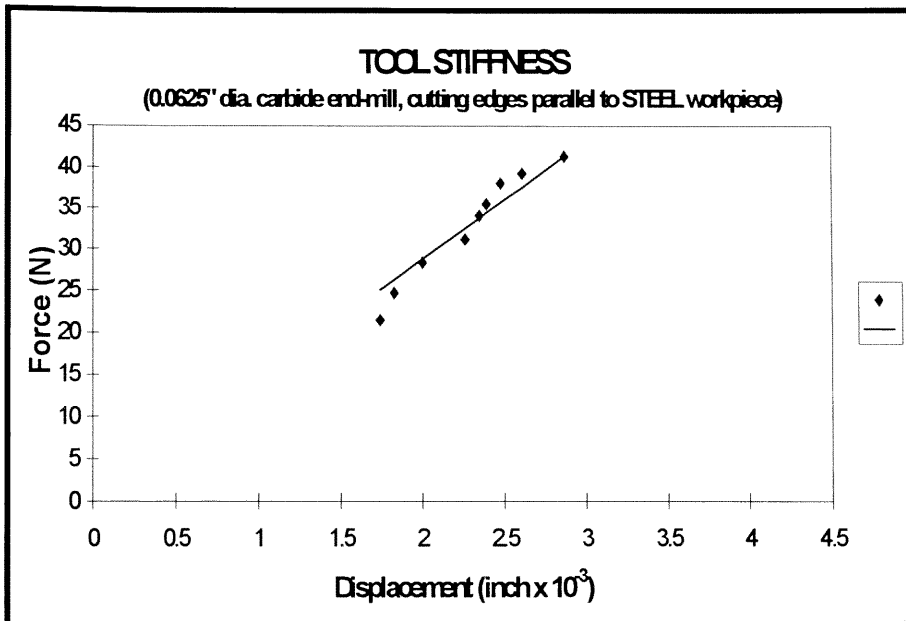
Figure 67.a. Cutting edges of the tool were parallel to the workpiece (slope = 14.40)
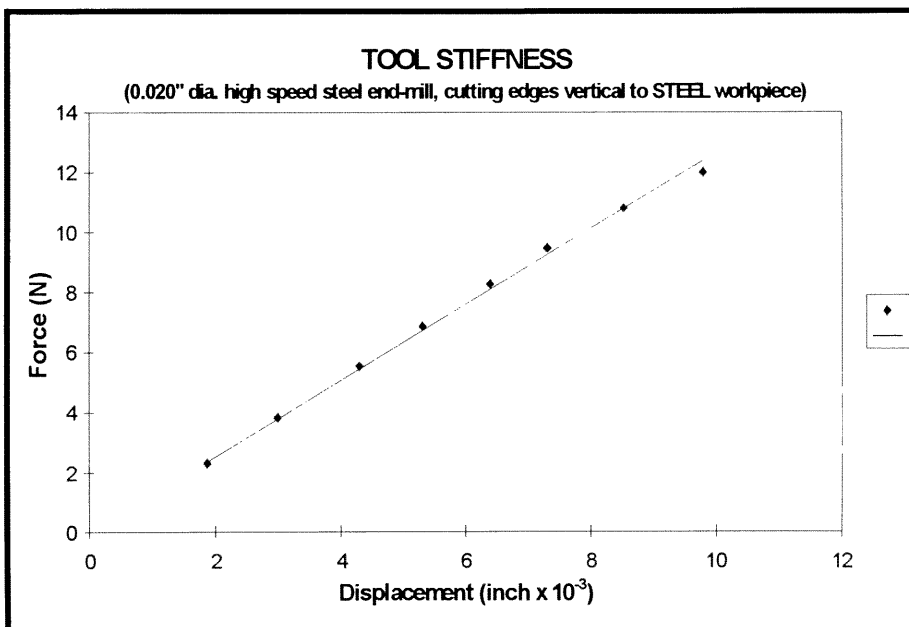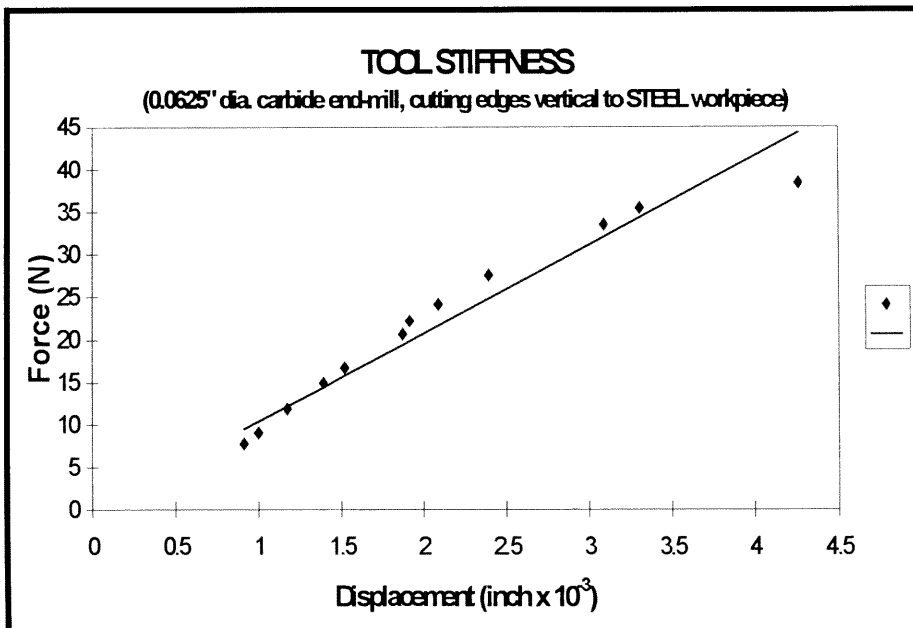

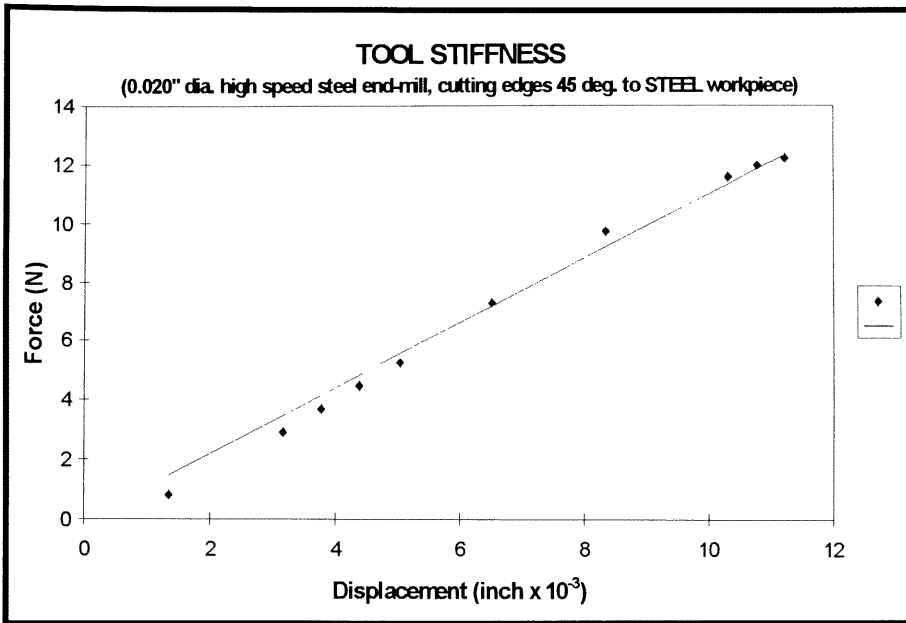Figure 67.b. Cutting edges of the tool were vertical to the workpiece (slope = 10.39)

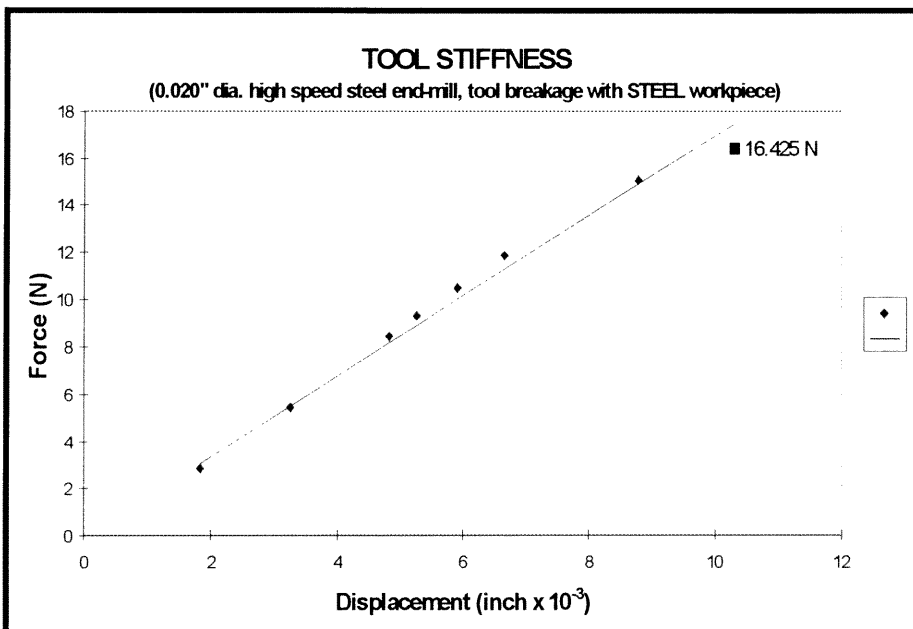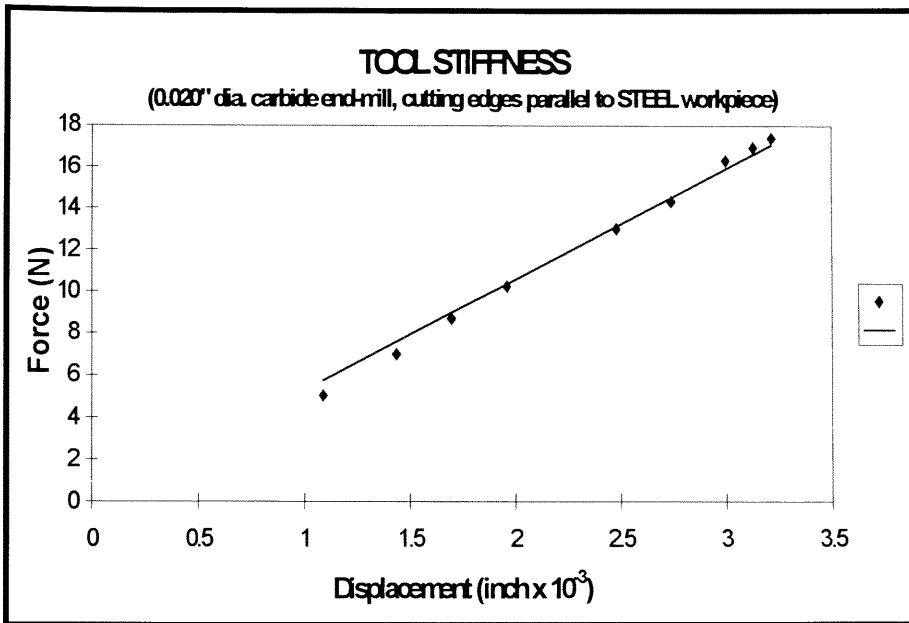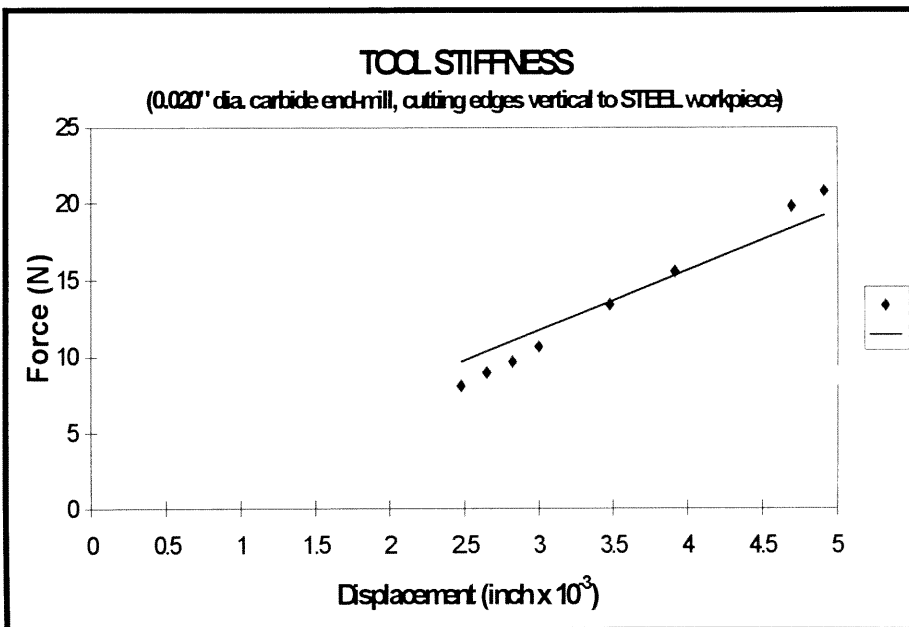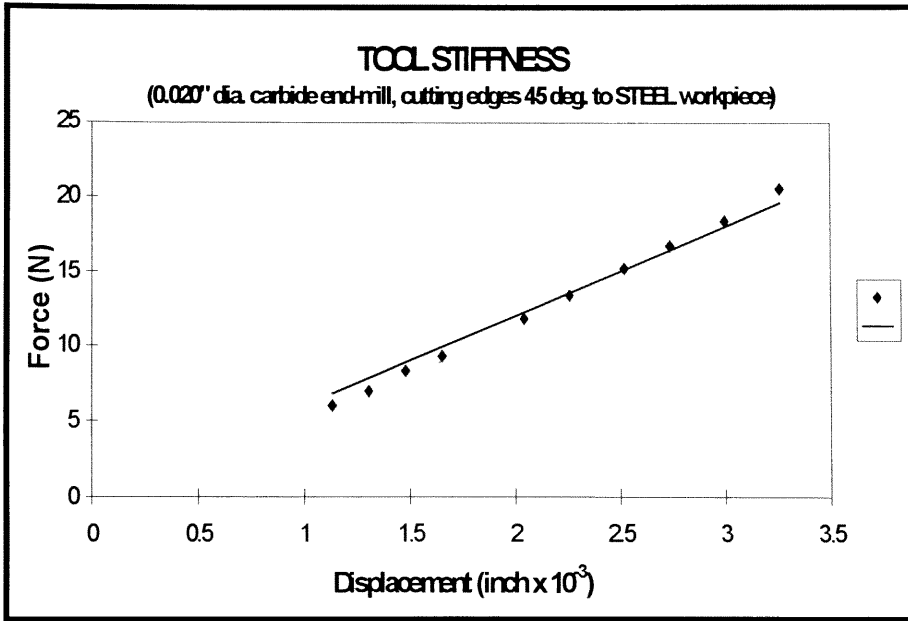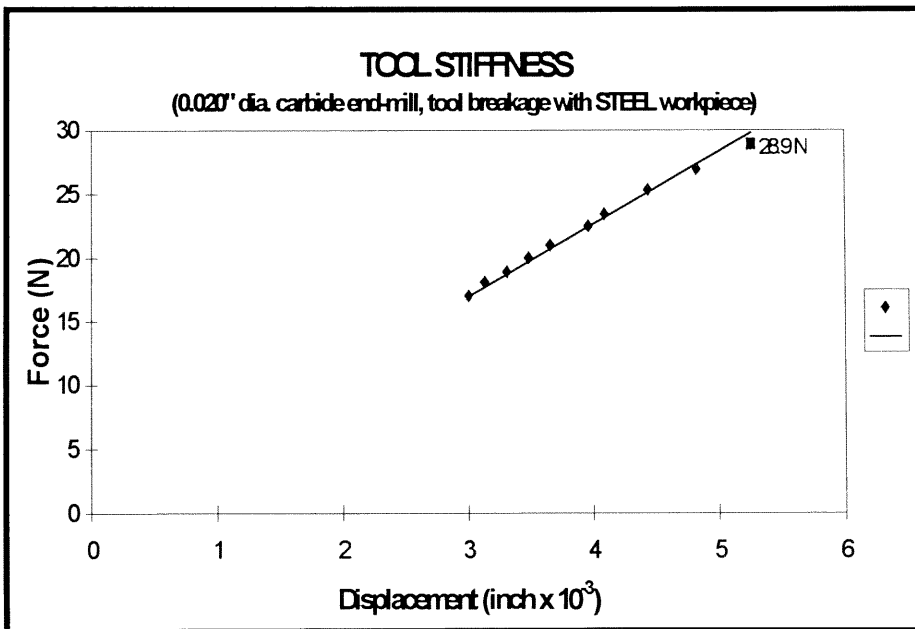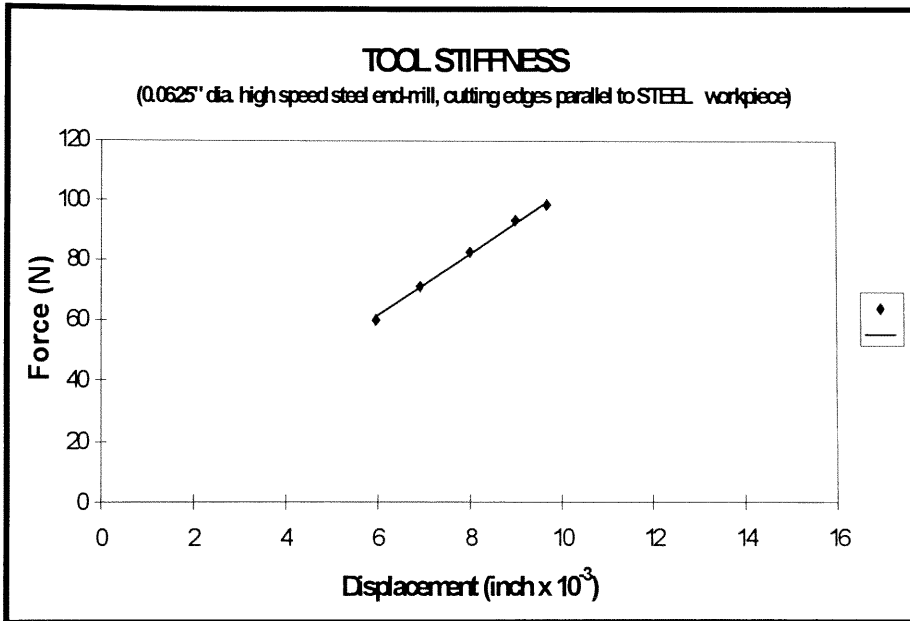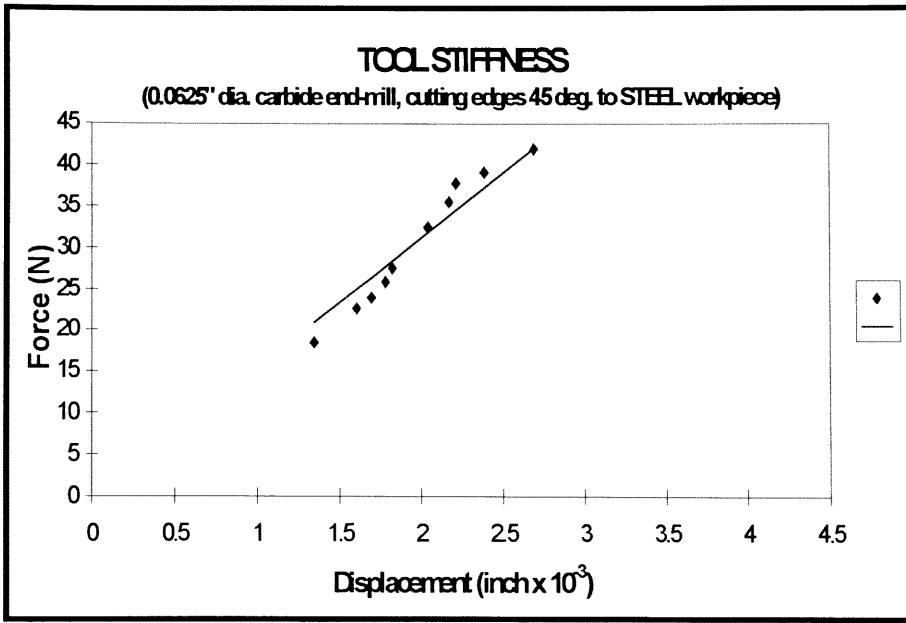Figure 67.c. Cutting edges of the tool were 45 degree to the workpiece (slope =15.57)
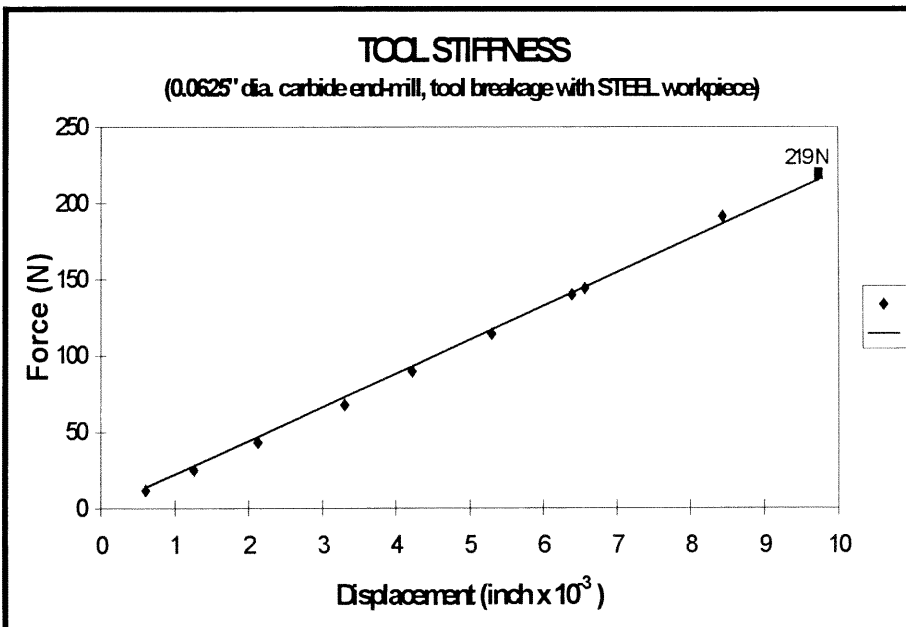
Figure 67.d. Tool breakage occurred at 219 N (slope = 22.1)

Chapter VI

Conclusion

Micro machining have been widely used in biomedical, aerospace and consumer product manufacturing. In this study, the characteristics of cutting forces and micro-tool structures were studied to develop low cost machinability and tool life evaluation methods.

The new machinability method is developed to evaluate the optimal cutting conditions to avoid premature tool breakage during micro end milling. The developed method repeats the machining tests with different cutting conditions until the targeted cutting force variation is obtained. The developed machinability method was applied during the micro machining of graphite electrodes (POCO-3, POCOEDMC-3), aluminum and steel (NAK 55). The new method required less experiment than the conventional machinability tests and tool life was at the acceptable levels.

The optimal cutting conditions were used during the evaluation of the tool wear. Cutting force amplitude variation during the micro machining of the workpiece was monitored at the different stages of tool life. As the tool wears out, the thrust and feed direction cutting forces had the tendency to increase. The cutting force amplitude increased 350% for POCOEDMC-3 after 1350 inches of cutting and 300% for aluminum after 155 inches of cutting. The recorded data was used to develop a new tool wear estimation method by using new neural networks. The Neural Network Based Periodic Tool Inspector (N^2PTI) estimated the tool wear with an acceptable accuracy for both POCOEDMC-3 and aluminum workpieces. To select the best paradigm accuracy, 3

143

different neural networks [Backpropagation neural network (Analog BP) and probabilistic neural network (Basic PNN, Sepvar PNN were evaluated.

Analog BP neural network took more time for training, however, the estimations were more accurate (4 to 5% while PNN had 8 to 9%) than the PNN neural networks. The proposed N^2PTI could only estimate the tool wear, if the spindle speed, feed rate and depth of cut are constant. To improve the N^2PTI, the effect of the depth of cut was eliminated by normalizing the thrust and feed direction cutting forces. The normalized data were used to train Analog BP, Basic and Sepvar PNN. The results were less accurate than the previous case study without normalization, but still estimations were in an acceptable error range. (10 to 13% for POCOEMDC-3 and 12-15% for Aluminum) Elimination of the constant depth of cut requirement allows on-line monitoring of micro machining of graphite electrodes and aluminum workpieces.

The elasticity and the critical static bending force (which breaks the tool) of Carbide and HSS end-mills were tested. The deflection and the critical bending force that breaks the micro end-mill were found. Carbide end-mills showed a brittle behavior. HSS tools are more ductile and their stiffness was higher. The carbide tools were 2 times more rigid than HSS tools (k=15.5 versus k=7.5 for 0.0625" tool) Also, carbide tools broke 1.5 times higher forces than the HSS tools. However, the deflection of HSS tools were 3 to 4 times bigger than the carbide tools. (16 inch$\times 10^{-3}$ versus 4.45 inch$\times 10^{-3}$ for 0.0625" tool)

Dynamic behavior of the micro tools was also studied to measure the natural frequency and the first natural frequencies were found at 23,000 HZ for 0.0625" HSS tools and 8,000 HZ for 0.020" HSS tools. The resonance problem was not critical at the commonly used spindle speeds.

To represent the characteristics of the cutting forces in more compact way, segmental averaging and wavelet transformation methods were used. 8 wavelet coefficients were representing the characteristics of one revolution for each cutting force more accurately than 10 segmental averages.

The performance of the Improved N^2PTI is outlined in Table 29 for POCOEEDMC-3 and in Table 30 for Aluminum.

The main objective of the study was to develop new methods to improve productivity and quality in industrial operations. The developed machinability analysis technique and N^2PTI can be easily used in industrial applications. Low hardware cost, simple and reliable algorithms are the main advantages of the proposed methods in real life applications.

Table 29. Performance of the N^2PTI – POCOEDMC-3

$N^2PTI - POCOEMDC-3$		Segmental Averaging		Wavelet Transformation	
Cases	Error %	Original Data	Normalized Data	Original Data	Normalized Data
Training (40 cases)	Average	6.5	7.25	4.5	6.7
	Minimum	1.4	2.15	1.1	1.95
	Maximum	12.6	14.3	9.5	13.8
Testing (30 cases)	Average	8.75	9.5	6.8	9.25
	Minimum	2.7	3	1.9	2.5
	Maximum	15.5	17.8	11.4	16.9

Table 30. Performance of the N^2PTI - Aluminum

$N^2PTI - Aluminum$		Segmental Averaging		Wavelet Transformation	
Cases	Error %	Original Data	Normalized Data	Original Data	Normalized Data
Training (50 cases)	Average	8.25	9.82	7.58	8.86
	Minimum	1.7	2.25	0.95	1.75
	Maximum	14.6	16.74	11.5	14.63
Testing (40 cases)	Average	9.65	10.25	8.64	9.82
	Minimum	3.3	3.78	2.27	3.07
	Maximum	16.65	18.25	15.07	17.95

REFERENCES

1.   J. Tlusty and P. MacNeil, "Dynamics of Cutting Forces in End Milling," *Annals of the CIRP*, v24, n1, 1975, pp.21-25.

2.   P.E. Gygax, "Dynamics of Single-Tooth Milling", Annals of CIRP, v28, n1, 1979, pp.65-70.

3.   F. Ismail and A. Bastami, "Improving Stability of Slender End Mills Against Chatter," Trans. of ASME, *Jour. of Eng. for Ind.*, Vol. 108, 1986, pp. 264-268.

4.   J. Tlusty and, F. Ismail, "Special Aspects of Chatter in Milling," *Jour. of Eng. for Ind.*, Trans. of the ASME, Vol. 105, 1983, pp. 24-32.

5.   W. A. Kline and R. E. DeVor, "The Effect of Cutter Run-out On Cutting Geometry and Forces in End Milling," *Int. Jour. of Mach. Tool Des. and Res.*, Vol. 23, 1983, pp. 123-148.

6.   J. W. Sutherland and R. E. DeVor, "An Improved Method for Cutting Force and Surface Error Prediction in Flexible End Milling Systems," ASME *Journal of Eng. for Ind.*, Vol. 108, 1986, pp. 269-27.

7.   T. I. Liu, "Automated Visual Inspection of Drill Wear," presented at the ASME Manufacturing International 90 Conference, Atlanta Georgia, 1990.

8.   S. Y. Liang and D. A. Dornfeld, "Tool Wear Detection Using Time Series Analysis of Acoustic Emission," Trans. of ASME, *Jour. of Eng. for Ind.*, Vol. 111, 1989, pp. 199-205.

9. Zheng, L., Luo, Z. B., Wu, Y., et al., "Research and Development on Synthetic Cutting Tool Monitoring with AE Signal," Transactions of NAMRI/SME, 1990, pp.360-365.

10. Koning, W., Kutzner K., Shehl, U., "Tool Monitoring of Small Drills With Acoustic Emission," *International Journal of Machine Tools Manufacture* Vol. 32, No. 4, pp. 487-493, Pergamon Press, Great Britain, 1992.

11. Vajpayee S., Sampath, A., "Acoustic Emission as an Indirect Parameter for Tools Monitoring," Proceedings of Manufacturing International '88, Symposium on Product and Process Design, Vol. 1, Atlanta, Georgia, 1988.

12. M. Liu, "Analytical modeling of acoustic emission for monitoring of peripheral milling process," *Inter. Journal of Mach. Tools & Manufacture*, Vol.31, No.4, 1991, p.589.

13. M. Liu, S.Y. Liang, "Monitoring of Peripheral Milling Using Acoustic Emission," Trans. of NAMRI/SME, 1990, pp.120-127.

14. Klaiber, J. R., Dornfeld, D. A., Liu, J. J., "Acoustic Emission Feedback for Diamond Turning," Transactions of NAMRI/SME, 1990, pp.113-119.

15. J.J. Liu, D.A. Dornfeld, "Monitoring of Micro-machining Process using Acoustic Emission," Trans. of NAMRI/SME, 1992, pp.189-195.

16. Diniz, A. E., Liu, J. J., Dornfeld, D. A., "Correlating Tool Life, Tool, Wear and Surface Roughness by Monitoring Acoustic Emission in Finish Turning," Wear No. 152, pp 395-407, 1992.

17. Hutton, D. V., "A Non-contact Acoustic Emission Sensing System For Rotating-Cutter Machining Process," Experimental Techniques, Nov/Dec, 1991

18. R.H. Osuri, S. Chatterjee, S. Chndrashekhar, "On-line condition monitoring of tool wear in end milling using acoustic emission," *International journal of production research,* Vol.29, No.7, 1991, p.1339.

19. Rangwala, S., Dornfeld, D., "A Study of Acoustic Emission Generated During Orthogonal Metal Cutting - 1:Energy Analysis," *International Journal of Mechanical Science* Vol. 33, No. 6 pp. 471-487, Pergamon Press, Great Britain, 1991.

20. Rangwala, D.A. Dornfeld, "A study of acoustic emission generated during orthogonal metal cutting-2: spectral analysis," *International journal of mechanical sciences,* V 33 n 6, 1991, p.489.

21. S.Y. Liang, D.A. Dornfeld, "Tool Wear Detection Using Time Series Analysis of Acoustic Emission", *Jour. of Eng. for Ind., Transactions of ASME,* Vol.111, No.3, 1986, pp.199-204.

22. E. Emel and E. Kannetey Assibu, Jr., "Characterization of Tool Wear and Breakage by Pattern Recognition Analysis of Acoustic Emission Signal," *Proc. of 14th NAMR Conf.,* 1986, pp. 266-272.

23. I.N. Tansel and C. McLaughlin, "Identification of Tool Breakage with Time Series Analysis in Milling Operations" *Control of Manufacturing Process,* Editors: K. Danai and S. Malkin, DSC-Vol.28, PED-Vol.52, ASME, 1991, pp. 59-65.

24. D.E. Rumelhart, G. Hilton and R.J. Williams, "Learning Internal Representations by Error Propagation, "Parallel Distributed Processing" *Explorations in the Microstructure of Cognition*, Vol.1, Ed. E. Rumelhart, J.L. McClelland, MIT Press, 1986.

25. D. Specht, "Probabilistic Neural Networks," *Neural Networks*, Vol. 3, 1990, pp. 109-118.

26. I.N. Tansel and C. McLaughlin, "Detection of Tool Breakage in Milling Opeartions-Neural Network Approach," *Int. Journal of Machine Tools Manufact.*, Vol. 33, n. 4, 1993, pp. 545-558.

27. I.N. Tansel and C. McLaughlin, "Detection of Tool Breakage in Milling Operations-Time Series Approach," *Int. Journal of Machine Tools Manufact.*, Vol. 33, n. 4, 1993, pp. 531-544.

28. I.N. Tansel, M.E. Trujillo, W.Y. Bao, T.T Arkan, "Detection of Tool Breakage in Micro-End-Milling Operations by Monitoring Acoustic Emission," Transaction of ASME, NAMRI, 1997, MR97-180.

29. I.Tansel, W.Y. Bao, T.T. Arkan, B. Shisler, M. McCool, and D Smith, "Neural Network Based Cutting Force Estimators for Micro-End-Milling Operations," to be presented at the Artificial Neural Networks In Engineering (ANNIE '97) and to be published at the "Smart Engineering System Design: Neural Networks, Fuzzy Logic, and Evolutionary Programming, edited by Drs. Dagli, Akay, Ersoy, Fernandez, and Smith, ASME Press, New York, 1997.

30. I.Tansel, W.Y. Bao, T.T. Arkan, B. Shisler, M. McCool, A. Jinks, and D. Smith, "Wear Estimation for Micro-Machining of Non-Metal Materials," to be presented at the Artificial Neural Networks In Engineering (ANNIE '97) and to be published at the "Smart Engineering System Design: Neural Networks, Fuzzy Logic, and Evolutionary Programming, edited by Drs. Dagli, Akay, Ersoy, Fernandez, and Smith, ASME Press, New York, 1997.

31. T.A. Carolan, D.P. Hand, J.S. Barton, "Assessment of Tool Wear in Milling Using Acoustic Emission Detected by a Fiber-Optic Interferometer," *Journal of Manufacturing Science and Engineering*, 1996, Vol. 118, Transaction of ASME.

32. J.C. Principe, T. Yoon, "A New Algorithm for the Detection of Tool Breakage in Milling," *Int. Journal of Machine Tools & Manufacturing,* Vol. 31, No. 4, pp. 443-454, Great Britain, 1991

33. R. Hecht-Nielsen, "Neuro-computing," Addison-Wesley, January 1991

34. "Fundamentals of Tool Design," Third Edition, SME Publication, David T. Reid, P. Administrator, 1991.

35. E.M. Trent, "Metal Cutting," 3rd Edition, Butterworth-Heinemann, 1991

36. M.C. Shaw, "Metal Cutting Principles," Oxford Series Advanced Manufacturing 3, 1986

37. Serope Kalpakjian, "Manufacturing Engineering and Technology", Addison-Wesley Publishing Company, 1989.

38. I.N. Tansel, Ghaleb A. Satar, "A Fast Procedure for the Identification of Complex Mode Shapes in the Time Domain".

39.   M.A. Cody, "The Fast Wavelet Transform," Dr. Dobb's Journal, April 1992, pp. 16-28

40.   I. Daubechies, "Orthonormal Bases of Wavelets with Finite Support-Connection with Discrete Filters," Wavelets, Edited by J.M. Combes, New York, 1989, pp. 38-67

41.   I. Daubechies, "The Wavelet Transform, Time-Frequency Localization and Signal Analysis," IEEE Transactions on Information Theory, Vol. 36, No. %, 1990, pp. 961-1005